UNIVERSITY OF UDINE

Department of Electrical Engineering, Mechanical and Management

PhD in Industrial Engineering and Information

CYCLE XXVI

PhD THESIS

APPLICATION OF FINITE ELEMENT METHOD TO THE DESIGN OF INNOVATIVE MECHANICAL DEVICES

Supervisor:

Professor Alessandro Gasparetto

By:

Seyed Amir Hossein Kiaeian Moosavi

To my mother and father

Special thanks to professor Gasparetto, supervisor of this thesis, for the great support.

CONTENTS

ABSTRACT

The research activity, carried out during the PhD course, focused on application of finite element method to the design of innovative devices.

In the first part of this thesis the fundamental formulation of finite element method is discussed. Then as the first part of the PhD course, the dynamic modelling of flexible link robots under large displacements and small deformations was studied and implemented. A dynamic model, based on Finite Element Method (FEM), was developed and implemented into a simulator running in a Matlab environment. Several flexible link robots, both 2D and 3D, have been simulated, and the results have been discussed.

In the second part of the PhD course, a thermo-mechanical analysis of fire door subjected to a fire was carried out. First, a fire door was subjected to standard fire tests to evaluate fire resistance. The thermal and structural response of the three-layer fire door exposed to high temperature was modelled using finite element software. The model included the necessary complication of the real door. Temperature dependency of the constituent materials was also considered in the modelling. Two different kinds of elements were used for modelling the door, namely solid and shell elements. The accuracy of the model was evaluated by a comparison between the response of the software simulator and the experimental data. The comparison between simulated and measured data confirms that the proposed approach can be a valid tool for a fire door design, allowing the development of customized solutions to ensure fire safety in structures.

CHAPTER 1

The Finite Element Method: Fundamental Description

The finite element method is a numerical method which is useful to achieve solutions to a large range of engineering cases such as electromagnetism, fluid flow, heat transfer, and stress analysis. The main purpose of this chapter is to introduce basic concepts in finite element formulation.

1.1 ENGINEERING PROBLEMS

Usually, engineering problems are mathematical models of physical situations Mathematical models are differential equations with a set of corresponding boundary and initial conditions The differential equations are derived by applying the fundamental laws and principles of mass, force, or energy. When possible, the exact solution of these equations renders detailed behavior of two parts: (1) a homogenous part and (2) a particular part. In each engineering problem, there are two groups of parameters that impress the way of the behavior of the system, first those parameters that provide information regarding the natural behavior of a given system. This set of parameters includes properties such as modulus of elasticity and viscosity.

The second set, those are parameters that produce disturbances in a system. These kinds of parameters are listed briefly in Table 1.1. Some examples of these types of parameters are temperature difference across a medium, external forces, moments and pressure difference in fluid flow.

The system characteristics dictate the natural behavior of a system, and they always appear in the homogenous part of the solution of a governing differential equation. In the other side, those parameters that cause the disturbances appear in the particular solution. The important matter is to figure out the role of these kinds of parameters in finite element modeling according their respective appearances in load or forcing matrices or conductance and stiffness matrices. The system characteristics will always show up in the stiffness matrix, conductance matrix or resistance matrix whereas the disturbance parameters will always appear in the load matrix.

1.2 NUMERICAL METHODS

There are many practical engineering problems for which cannot obtain exact solutions. This lack to receive an exact solution may be assigned to either the difficulties that arise from initial conditions and the boundary or the complex nature of governing differential equations. To deal with such problems, we resort to numerical approximations In contrast to analytical solutions, which show the precise behavior of a system at any point within the system, numerical solutions estimate exact solutions only at discrete points, called nodes. The first step of any numerical procedure is

discretization. Thus, this process divides the medium of interest into a number of small sub regions and nodes. There are two common classes of numerical method: (1) finite difference methods and (2) finite element methods. With finite difference methods, the differential equation is written for each one of the node, and the derivatives must be replaced by difference equations. These approach methods are easy to understand and employ in simple problems, they become difficult to apply to problems with complex geometries or complex boundary conditions. Also this situation is true for problems with nonisotropic material properties.

TABLE1.1 Parameters causing disturbances in various engineering systems

Problem Type	Examples of Parameters That Produce Disturbances in a System
Solid Mechanics	**External forces and moments; support excitation**
Heat Transfer	Temperature difference; heat input
Fluid Flow and Pipe Networks	Pressure difference; rate of flow
Electrical Network	Voltage difference

In contrast, the finite element method uses different formulation like, integral formulations rather than difference equations to create a system of algebraic equations. Moreover, an approximate continuous function is evaluated to represent the solution for each one of element. The optimal solution is then generated by assembling or connecting the individual solutions, appropriating continuity at the interelemental boundaries.

1.3 A BRIEF HISTORY OF THE FINTE ELEMENT METHOD AND ANSYS

The finite element method is a numerical procedure and applied to obtain solutions to a different kind of problems in engineering. Steady, linear, transient or nonlinear problems in stress analysis, fluid flow, and electromagnetism problems may method may be was started the early 1900s. In that year, some researcher approximated and modeled elastic continua using discrete equivalent elastic bars. However, the first person to develop the finite element method was However, Courant (1943). In the early 1940s, Courant published a paper and used piecewise polynomial interpolation in his research to investigate torsion problems.

The next step in the utilization of finite element methods was taken by Boeing in the 1950s. When Boeing, followed by others, used triangular stress elements by means of model airplane wings. Clough made the term "finite element" popular for the first time in 1960. During the 1960s, group of researcher and engineering began to apply the finite element method to different field of their research, such as: heat transfer and seepage flow

problems. Zienkiewicz and Cheung wrote the first book finite element method in 1967 and after that ANSYS was released in 1971.

ANSYS is as simulation software and contains over 100,000 lines code. The comprehensive general-purpose is finite element computer program. Also ANSYS have ability to performing static, dynamic, fluid flow, electromagnetism analyses and heat transfer. ANSYS is a very powerful and impressive engineering software. It is used to solve engineering fields problems. 20 years ago ANSYS has been a leading FEA program. The current version of ANSYS simulator has a completely incorporating Graphical User Interface (GUI), with multiple windows pull down menus and have a user friendly tool bar. Today ANSYS in use in many engineering fields, including aerospace, automotive, robotic, aerospace, and etc. By means of use ANSYS or any other "canned" FEA computer program, it is imperative one first fully understands the limitations of the finite element methods and underlying basic concepts of finite element.

User without a basic knowledge of the finite element methods will find the same predicament as a computer technician. They access to many impressive tools and instruments. Groups of person cannot fix a computer becausethey did not understand the inner workings of a computer!

1.4 Advantages of FEA

- Versatility: FEA is applicable to any field problem, such as heat transfer, stress analysis, magnetic fields, and so on.
- There is no geometric restriction: It can be applied the body or region with any shape.
- Boundary conditions and loading are not restricted (boundary conditions and loads may be applied to any portion of the body)
- Material properties may be change from one element to another (even within an element) and the material anisotropy is allowed.
- Different elements (behavior and mathematical descriptions) can be combined in a single FE model.
- An FE structure closely resembles the actual body or region to be analyzed.
- The approximation is easily improved by grading the mesh (mesh refinement).

In industry FEA is mostly used in the analysis and optimization phase to reduce the amount of prototype testing and to simulate designs that are not suitable for prototype testing. Computer simulation allows multiple "what-if" scenarios to be tested quickly and effectively. The example for the second reason is surgical implants, such as an artificial knee. On the other hand, the other reasons for preference of the FEM are cost savings,

time savings, reducing time to market, creating more reliable and better-quality designs.

1.5 PROBLEM SOLVING BY FEA

Solving a structural problem by FEA involves following steps

- Learning about the problem
- Preparing mathematical models
- Discretizing the model
- Having the computer do calculations
- Checking results

Generally an iteration required over these steps.

1.5.1 Learning about the Problem

It is important to understand the physics or nature of the problem and classify it. The first step in all research's solving a problem is to identify it. Therefore an engineer has to identify the problem asking the following questions.

- What are the more important physical phenomena involved?
- Is the problem time-independent or time dependent? (Static or dynamic?)
- Is nonlinearity involved? (Is iterative solution necessary or not?)
- What results are sought from analysis?
- What accuracy is required?

From answers it is decided that the necessary data and information to carry out an analysis, how the problem is modeled, and what method of solution is accepted.

Some problems are interdisciplinary nature. There are some couplings between the fields. If the fields interacts each other, it is called direct or mutual coupling. If one field influences the other, it is called indirect or sequential coupling. An example of direct coupling is flutter of an aircraft panel. The pressure produced by airflow on the panel deflects the panel and the deflection modifies the airflow and pressure Therefore structural displacement and air motion fields cannot be considered separately.

1.5.2 Preparing Mathematical Models

FEA is applied to the mathematical model. FEA is simulation, not reality. Even very accurate FEA may not match with physical reality if the mathematical model is inappropriate or inadequate.

Devise model problem for analysis,

- Understanding the physical nature of the problem. Because a model for analysis can be devised after the physical nature of the problem has been understood.
- Excluding superfluous detail but including all essential features. Unnecessary detail can be omitted. This must enable that the analysis of the model is not unnecessarily complicated. Decide what features are important to the purpose at hand. This provides us to obtain the results with sufficient accuracy.
- A geometric model becomes a mathematical model when its behavior is described, or approximated, by selected differential equations and boundary conditions.

Thus, we may ignore geometric irregularities, regard some loads as concentrated, say that some supports are fixed and idealize material as homogeneous, isotropic, and linearly elastic.

What theory or mathematical formulation describes behavior? Depending on the dimensions, loading, and boundary conditions of this idealization we may decide that behavior is described by beam theory, plate-bending theory, equations of plan elasticity, or some other analysis theory.

Modeling decisions are influenced by what information is sought, what accuracy is required, the anticipated expense of FEA, and its capabilities and limitations. Initial modeling decisions are provisional. It is likely that results of the FEA will suggest refinements, in geometry, in applicable theory, and so on.

1.5.3 Discretization

A mathematical model is discretized by dividing it into a mesh of finite elements. Thus a fully continuous field is represented by a piecewise continuous field. A continuum problem is one with an infinite number of unknowns. The FE discretization procedures reduce the problem to one of finite number of unknowns, Fig.1.1.

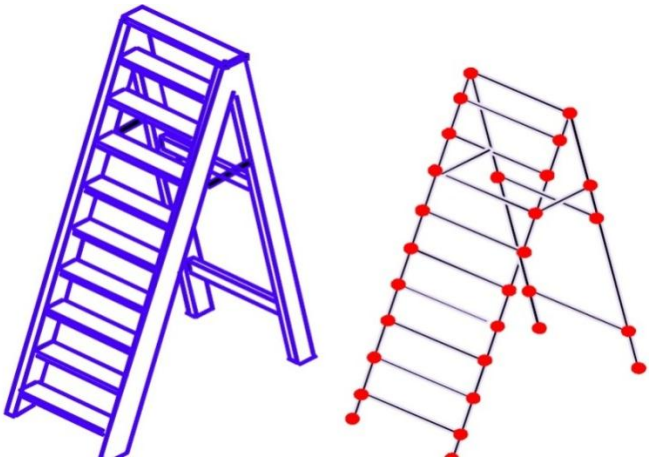

Figure1.1 Finite element model of a stair (from ANSYS presentation).

Discretization introduces another approximation. Relative to reality, two sources of error have now been introduced: modeling error and discretization error. Modeling error can be reduced by improving the model; discretization error can be reduced by using more elements. Numerical error is due to finite precision to represent date and the results manipulation.

The FEA is an approximation based on piecewise interpolation of filed quantity. By means of this FE method

- Solution region is divided into a finite number of sub regions (elements) of simple geometry (triangles, rectangles…)
- Key points are selected on the elements to serve as nodes, the nodes share values of the field quantity and may also share its one or more derivatives. The nodes are also locations where loads are applied and boundary conditions are imposed. The nodes usually lie on the element boundaries, but some elements have a few interior nodes.
- The unknown field variable is expressed in terms of interpolation functions within each element. The interpolation functions approximate (represent) the field variable in terms of the d. o. f. overa finite element. Polynomials are usually chosen as interpolation functions because differentiation and integration is easy with polynomials. The degree of polynomial depends on the number of unknowns at each node and certain compatibility and continuity requirements. Often function are chosen so that the field variable and its derivatives are continuous across adjoining element boundaries.

- Degrees of freedom (d. o. f.)Are independent quantities that govern the spatial variation of a field. In this way, the problem is stated in terms of these nodal values as new unknowns.
- Now, we can formulate the solution for individual elements. There are four different approaches to formulate the properties of individual elements: Direct approach, variational approach, weighted residuals approach, and energy balance approach.
- Stiffness and equivalent nodal loads for a typical element are determined using the mentioned above.
- The element properties are assembled to obtain the system equations.
- The equations are modified to account for the boundary conditions of the problem.
- The nodal displacements are obtained solving this simultaneous linear algebraic equation system. Once the nodal values (unknowns) are found, the interpolation functions define the field variable through the assemblage of elements. The nature of elements, and interpolation functions.
- Support reactions are determined at restrained nodes.

In continue, this chapter will explain first the method of weighted residuals and the Rayleigh Ritz method which furnish a basis for the finite-element method and then since we used one dimensional and two dimensional elements in the next chapters, the fundamental finite element formulation of these kinds of elements is discussed.

1.6 METHOD OF WEIGHTED RESIDUALS

Differential equations are ordinarily formulated so as to be satisfied for each point which connected to regions of interest [128]. The method of weighted residuals determinate the estimate solution $\bar{u}$ to a differential equation such that integral of the weighted rang result of the differential equation of the approximate function $\bar{u}$ over the region of interest is zero. This technique determines the estimate result which satisfies the differential equation of interest:

$$\begin{cases} L[u(x)] = f(x)(a \le x \le b) \\ BC(Boundary\ Conditions): u(a) = u_a, u(b) = u_b \end{cases} \tag{1.1}$$

Where L is a linear differential operator, $f(x)$ a function of x, and u_a and u_b the values of a function u(x) of interest at the endpoints, or the one-dimensional boundaries of the region D. Now, let us suppose an approximate solution to the function u be

$$\bar{u}(x) = \emptyset_0(x) + \sum_{i=1}^{n} a_i \emptyset_i(x) \tag{1.2}$$

Where $\emptyset_i$ are called trial functions (i=1,2,…,n) which are chosen arbitrarily as any function $\emptyset_0$(x) and a_i some parameters which are computed as to obtain a good "fit".

The substitution of $\bar{u}$ into Equation (1.1) makes the right-hand side non-zero but gives some error R:

$$L[\bar{u}(x) - f(x)] - f(x) = R \tag{1.3}$$

The method of weighted residuals determines $\bar{u}$ such that integral of the error R over the region of interest weighted by arbitrary functions $w_i(i = 1,2, \dots, n)$is zero, i.e., coefficients a_i in Equation (1.2) are determined so as to satisfy the following equation:

$$\int_D w_i R dv = 0 \tag{1.4}$$

Where D is the region considered.

1.6.1 SUB-DOMAIN METHOD (FINITE VOLUME METHOD)

By means of following weighting function brings about the sub- domain techniques or finite- volume techniques.

$$w_i(x) = \begin{cases} 1 & (for\ x\ \in D) \\ 0 & (for\ x\ \notin D) \end{cases} \tag{1.5}$$

Consider a boundary-value problem described by following one-dimensional differential equation:

$$\begin{cases} \dfrac{d^2u}{dx^2} - u = 0 \quad (0 \le x \le 1) \\ BC: u(0) = 0\ \ u(1) = 1 \end{cases} \tag{1.6}$$

The linear operator L[0] and the function f (x) in Equation (1.6) are defined as follows:

$$L[0] \equiv \frac{d^2(0)}{dx^2} \qquad f(x) \equiv u(x) \tag{1.7}$$

For simplicity, let us choose the power series of x as the trial functions $\emptyset_i, i.e.,$

$$\bar{u}(x) = \sum_{i=0}^{n+1} c_i x^i \tag{1.8}$$

For satisfying the required boundary conditions,

$$c_0 0, \sum_{i=1}^{n+1} c_i = 1 \tag{1.9}$$

$$\bar{u}(x) = x + \sum_{i=1}^{n} A_i (x^{i+1} - x) \tag{1.10}$$

If the second term of the right-hand side of Equation (1.10) is chosen as a first-order estimated solution

$$\bar{u}_1(x) = x + A_1 A_i (x^2 - x) \tag{1.11}$$

The error or residual is obtained as

$$R \equiv \frac{d^2\bar{u}}{dx^2} - \bar{u} = -A_1 x^2 + (A_1 - 1)x + 2A_1 \neq 0 \tag{1.12}$$

$$\int_0^1 w_i R dx = \int_0^1 1 - [A_1 x^2 + (A_1 - 1)x + 2A_1] dx = \frac{13}{6} A_1 - \frac{1}{2} = 0 \tag{1.13}$$

Accordingly, the first-order estimated solution is shown in below:

$$\bar{u}_1(x) = x + \frac{3}{13} x(x - 1) \tag{1.14}$$

Which agrees well with the exact result?

$$u(x) = \frac{e^x - e^{-x}}{e - e^{-1}} \tag{1.15}$$

As shown by the dashed and the solid lines in Figure 1.2

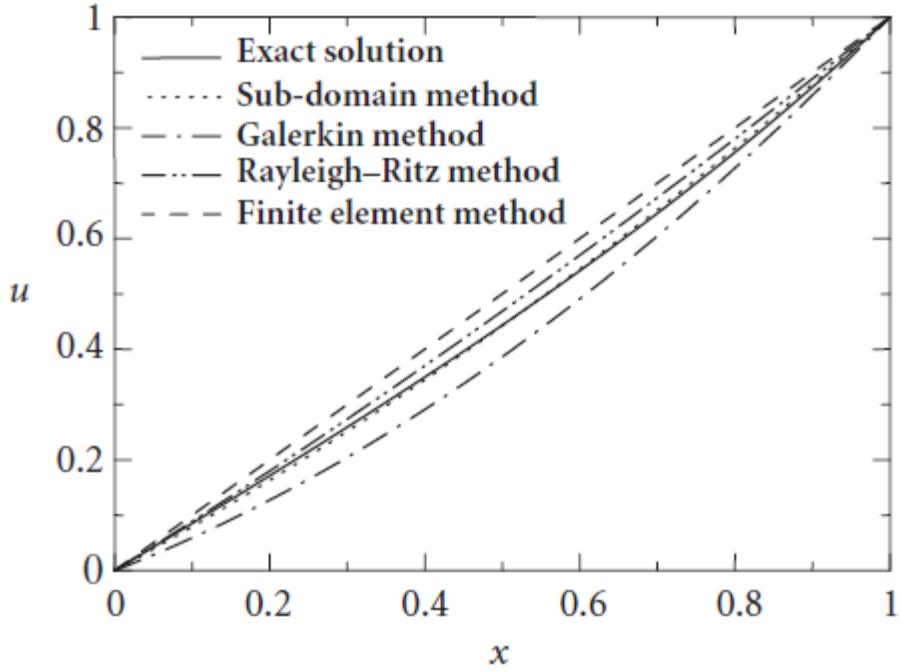

Figure1.2 Comparison of the results obtained by various kinds of discrete analyses.

1.6.2 GALERKIN METHOD

When the weighting function w_i in Equation (1.4) is chosen equal to the trial function$\emptyset_i$, this techniques is named the Galerkin method,i.e.,

$$w_i(x) = \emptyset_i(x) \qquad (i = 1,2, \dots, n) \tag{1.16}$$

And thus Equation (1.4) is changed to

$$\int_D \emptyset_i R dv = 0 \tag{1.17}$$

This technique determines the constants $a_i$by directly using Equation (1.17) or by integrating it by parts.

We must solve the same boundary-value error as described by Equation (1.6) in the preceding Section 1.1 by the Galerkin method.

The trial function $\emptyset_i$ is chosen as the weighting function w_i in order to find the first –order estimate solution:

$$w_1(x) = \emptyset_1(x) = x(x-1) \tag{1.18}$$

Integrating Equation (1.4) by parts, as follow is obtained:

$$\int_0^1 w_i R dx = \int_0^1 w_i \left(\frac{d^2\bar{u}}{dx^2} - \bar{u}\right) dx$$
$$= \left[w_i \frac{d\bar{u}}{dx}\right]^1 - \int_0^1 \frac{dw_i}{dx}\frac{d\bar{u}}{dx} dx - \int_0^1 w_i \bar{u} dx$$
$$= 0 \quad (1.19)$$

Choosing $\bar{u}_1$ in Equation (1.11) as the approximate solution$\bar{u}$, the substitution of Equation (1.18) into (1.19) the results is:

$$\int_0^1 \emptyset_1 R dx = \int_0^1 \frac{d\emptyset_1}{dx}\frac{d\bar{u}}{dx} dx - \int_0^1 (2x-1)[1 + A_1(2x-1)]dx - \int_0^1 (x^2$$
$$- x)[1 + A_1(x^2 - x)]dx = -\frac{A_1}{3} + \frac{1}{12} - \frac{A_1}{30}$$
$$= 0 \quad (1.20)$$

Thus, the following estimate solution is obtained:

$$\bar{u}_1(x) = x + \frac{5}{22}x(x-1) \quad (1.21)$$

Figure 1.1 shows that the estimate solution by the Galerkin method also agrees well with the exact solution and results base on region of interest.

1.7 RAYLEIGH-RITZ METHOD

The Rayleigh- Ritz method can be applied when there exists the functional which is equivalent to a given differential equation.

As an instance the problem explained in Figure 1.3 Where a particle having a mass of M slides from point P_0 to P_1 varies with the shape of the curve defined by y(x) which connects the two points. Hence the time t is a kind of function $t = F[y]$ which is defined by a function y (x) of an independent variable x. The function

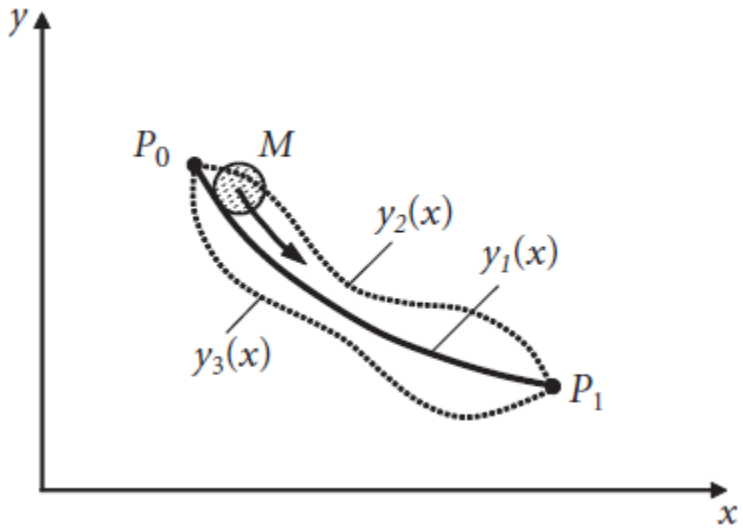

Figure 1.3 Particle M sliding from point P_0 to lower Point P_1 under gravitational force.

Of a function F(y) is called a functional. The method is called the variational method is for defining the minimum or the maximum of a given functional. About Figure 1.3, the method determines the shape of the curve y(x) which provides the possible minimum time t_{min} in which the particle slides from P_0toP_1.

One of the variational principles is the virtual work or the minimum potential energy in the field of the solid mechanics which guarantee the existence of the function which makes the functional maximum or minimum. The variational principle cannot be established in the case of unsteady thermal conductivity and viscous flow problems; in this type of case, the method of weighting residuals can be adopted instead.

Now, let Π [u] be the functional which is equivalent to the differential equation in Equation (1.1). The Rayleigh-Ritz method considers that an approximate solution $\bar{u}(x)$ of u(x) is a linear combination of trial functions $\emptyset_i$ as shown in the following equation:

$$\bar{u}(x) = \sum_{i=1}^{n} a_i \emptyset_i(x) \tag{1.22}$$

Where $a_i (i = 1,2, \dots, n)$ are optional constants$\emptyset_i$ are C^0-class functions which have continuous first-order derivatives for $a \leq x \leq b$ and are chosen in a way that the following boundary conditions are satisfied:

$$\sum_{i=1}^{n} a_i \emptyset_i(a) = u_a \sum_{i=1}^{n} a_i \emptyset_i(b) = u_b \tag{1.23}$$

The approximate solution $\bar{u}(x)$ in Equation (1.22) is the function which provides the functional Π [u] take stationary value and is called the admissible function.

Next, by integrating the functional Π after substituting Equation (1.22) into the functional, the constants a_i are defined by the stationary conditions:

$$\frac{\partial \Pi}{\partial a_i} = 0 \quad (i = 1,2, \dots, n) \tag{1.24}$$

The Rayleigh-Ritz method defines the approximate solution $\bar{u}(x)$ by substituting the constantsa_i into Equation (1.22). It is commonly understood to be a method which defines the coefficients a_i so as to provide the distance between the approximate solution $\bar{u}(x)$ and the exact one u(x) minimum.

Now, let us solve again boundary-value problem considered by Equation (1.6) by the Rayleigh-Ritz method. The functional equivalent to the first equation of Equation (1.6) is written as

$$\Pi[u] = \int_0^1 \left[\frac{1}{2}\left(\frac{du}{dx}\right)^2 + \frac{1}{2}u^2\right] dx \tag{1.25}$$

Equation (1.25) is obtained by intuition, but Equation (1.25) is shown to really give the functional of the first equation of Equation (1.6) as follows: first, let us take the first variation of Equation (1.25) in order to obtain the stationary value of the equation:

$$\delta\Pi[u] = \int_0^1 \left[\frac{du}{dx}\delta + \left(\frac{du}{dx}\right) + u\delta u\right] dx \tag{1.26}$$

Then, integrating the above equation by parts, we have

$$\begin{aligned}\delta\Pi[u] = \int_0^1 \left(\frac{du}{dx}\frac{d\delta u}{dx} + u\delta u\right) dx &= \left[\frac{du}{dx}\delta u\right]_0^1 - \int_0^1 \left[\frac{d}{dx}\left(\frac{du}{dx}\right)\delta u - u\delta u\right] dx \\ &= -\int_0^1 \left(\frac{d^2u}{dx^2} - u\right)\delta u \, dx \end{aligned} \tag{1.27}$$

For satisfying the stationary condition that $\delta\Pi = 0$, the rightmost-hand side of Equation (1.27) should be zero over the interval considered $(a \le x \le b)$, so that

$$\frac{d^2u}{dx^2} - u = 0 \tag{1.28}$$

This is exactly the same as the first equation of Equation (1.6)

Now, let us consider the following first-order approximate solution $\bar{u}_1$ which satisfies the boundary conditions:

$$\bar{u}(x) = x + a_i x(x-1) \tag{1.29}$$

Substitution Equation (1.29) into (1.25) and integration of Equation (1.25) lead to

$$\Pi[\bar{u}_1] = \int_0^1 \left[\frac{1}{2}[1 + a_1(2x-1)]^2 + \frac{1}{2}[x + a_1(x^2 - x)]^2\right] dx$$
$$= \frac{2}{3} - \frac{1}{12}a_1 + \frac{1}{3}a_1^2 \tag{1.30}$$

Since the stationary condition for Equation (1.30) is written by

$$\frac{\partial \Pi}{\partial a_i} = -\frac{1}{12} + \frac{2}{3}a_1 = 0 \tag{1.31}$$

The first-order approximate solution can be obtained as follows:

$$u_1(x) = x\frac{1}{8}x(x-1) \tag{1.32}$$

Figure 1.1 shows that the approximate solution obtained by the Rayleigh-Ritz method agrees well with the exact solution throughout the region considered.

1.8 FINITE-ELEMENT METHOD

There are two ways for the formulation of the FEM: one is based on the direct variational method (such as the Rayleigh-Ritz method) and the on the method of weighted residuals (such as the Galerkin method). In the formulation based on the variational method, the fundamental equations are derived from the stationary conditions of the functional for the boundary-value problems. This formulation conditions of the functional for the boundary-value problems. This formulation has an advantage that the functional for the boundary-value problems. This formulation has an advantage that the process of deriving functional is not necessary, so it is easy to formulate the FEM based on the method of the weighted residuals. In the formulation based on vareational method, however, it is generally difficult to derive the functional except for the case where the variational principles are already established as in the case of the principle of the

virtual work or the principle of the minimum potential energy in the field of the solid mechanics.

This section will explain how to derive the fundamental equations for the FEM based on the Galerkin method.

Let us consider again the boundary-value problem stated by Equation (1.1):

$$\begin{cases} L[u(x)] = f(x)(a \le x \le b) \\ BC(Boundary\ Conditions): u(a) = u_a \ \ u(b) = u_b \end{cases} \tag{1.33}$$

First, divide the region of interest $(a \le x \le b)$ into n sub regions as illustrated in figure 1.4 these sub regions are called "elements" in the FEM.

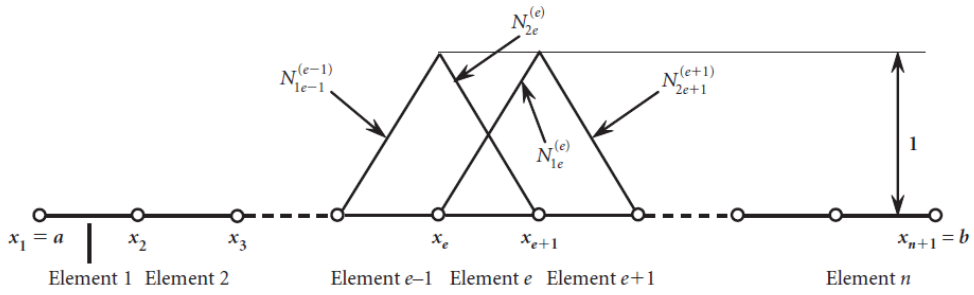

Figure 1.4 Discretization of the domain to analyze by finite elements and their interpolation functions.

Now, let us assume that an approximate solution $\bar{u}$ of u can be expressed by a piecewise linear function which forms a straight line in each sub region,i.e.,

$$\bar{u}(x) = \sum_{i=1}^{n} u_i N_i(x) \tag{1.34}$$

Where u_i represents the value of u in element "e" at a boundary point, or a nodal point 'i' between two one-dimensional elements. Functions $N_i(x)$ are the following piecewise linear functions and are called interpolation or shape function of the nodal point 'i'.

$$\begin{cases} N_{1e}^{(e)} = \dfrac{x_{e+1} - x}{x_{e+1} - x_e} = \dfrac{x_{2e-1} - x}{x_{2e} - x_{1e}} = \dfrac{h^{(e)} - \xi}{h^{(e)}} \\ N_{2e}^{(e)} = \dfrac{x - x_e}{x_{e+1} - x_e} = \dfrac{x - x_{1e}}{x_{2e} - x_{1e}} = \dfrac{\xi}{h^{(e)}} \end{cases} \tag{1.35}$$

Where e (e=1,2,…,n) denotes the element number, x_i the global coordinate of the nodal point i(i=1,…,e-1,e,…n,n+1),$N_{ie}^{(e)}$ the value of the interpolation

function at the nodal point $i_e(i_e = 1_e, 2_e)$which belongs to the eth element, 1_e and 2_e the number of two nodal points of the eth element. Symbolξ is the local coordinate of an arbitrary point the eth element, $\xi = x - x_e = x - x_{1e}(0 \le \xi \le h), h^{(e)}$ is the length of the eth element, and $h^{(e)}$ is expressed as $h^{(e)} = x_{e+1} - x_e = x_{2e} - x_{1e}$.

As the interpolation function, the piecewise linear or quadric function is often used. Generally speaking, the quadric interpolation function gives better solutions than the linear one.

The Galerikin method-based FEM adopts the weighting functions $w_i(x)$ equal to the interpolation functions$N_i(x), i.e.$,

$$w_i(x) = N_i(x)(i = 1,2, \dots, n+1) \tag{1.36}$$

Thus, Equation (1.4) becomes

$$\int_D N_i \, R dv = 0 \tag{1.37}$$

In the FEM, a set of simultaneous algebraic equations for unknown variables of u(x) at the ith nodal point u_i and those of its derivatives du/dx, $(du/dx)_i$are derived by integrating Equation (1.37) by parts and then by taking boundary conditions into consideration. The simultaneous equations can be easily solved by digital computers to determine the unknown variables $u_i$and $(du/dx)_i$at all the nodal points in the region considered.

Let us solve the boundary-value problem stated in Equation (1.6) by FEM. First, the integration of Equation (1.37) by parts gives.

$$\int_0^1 w_i R dx = \int_0^1 w_i \left(\frac{d^2u}{dx^2} - \bar{u} \right) dx = \left[w_i \frac{d\bar{u}}{dx} \right]_0^1 - \int_0^1 \left[\frac{dw_i}{dx} \frac{d\bar{u}}{dx} + w_i \bar{u} \right] dx = 0 \ (i = 1,2, \dots, n+1) \tag{1.38}$$

Then, the substitution of Equations (1.34) and (1.36) into Equation (1.38) gives

$$\sum_{j=1}^{n+1} \int_0^1 \left(\frac{dN_i}{dx} \frac{dN_j}{dx} + N_i N_j \right) u_j dx - \left[N_i \frac{d\bar{u}}{dx} \right]_0^1 = 0 \quad (i = 1,2, \dots, n+1) \tag{1.39}$$

Equation (1.39) is a set of simultaneous liner algebraic equations composed of (n+1) nodal values u_i of the solution u and also (n+1) nodal values $(du/dx)_i$ of its derivativedu/dx. The matrix notation of the simultaneous equations above is written in a simpler from as follows.

$$[K_{ij}]\{u_j\} = \{f_i\} \tag{1.40}$$

Where $[K_{ij}]$ is a square matrix of (n+1) by (n+1),$\{f_i\}$ is a column vector of (n+1) by 1, and the components of the matrix and the vector $[K_{ij}]$ and f_i are expressed as

$$\begin{cases} K_{ij} = \int_0^1 \left(\dfrac{dN_i}{dx}\dfrac{dN_j}{dx} + N_i N_j \right) dx \quad (1 \le i,j \le n+1) \\ f_i = \left[N_i \dfrac{d\bar{u}}{dx} \right]_0^1 \qquad\qquad (1 \le i \le n+1) \end{cases} \tag{1.41}$$

1.8.1 ONE-ELEMENT CASE

As the first example, let us compute Equation (1.37) by regarding the whole region as one finite element as shown in Examples 1.1 through 1.3 From Equations (1.34) and (1.35), since $x_1 = 0$and $x_2 = 1$, the approximate solution $\bar{u}$ and the interpolation function $N_i(i = 1,2)$become

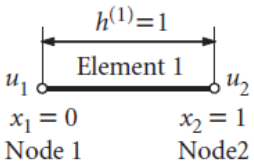

Figure1.5 one-element model of one-dimensional FEM.

$$\bar{u}(x) = u_1 N_1 + u_2 N_2 \tag{1.42}$$

$$\begin{cases} N_1 = N_{11}^{(1)} = \dfrac{x_2 - x}{x_2 - x_1} = 1 \\ N_2 = N_{21}^{(1)} = \dfrac{x - x_1}{x_2 - x_1} = x \end{cases} \tag{1.43}$$

, hus, from Equation (1.41),

$$\begin{cases} K_{ij} \equiv K_{ij}^{(1)} \equiv \int_0^1 \left(\dfrac{dN_i}{dx}\dfrac{dN_j}{dx} + N_i N_j \right) dx = \begin{cases} 4/3 & (i = j) \\ -\dfrac{5}{6} & (i \ne j) \end{cases} \\ f_i = \left[N_i \dfrac{d\bar{u}}{dx} \right]_0^1 = \begin{cases} -\dfrac{d\bar{u}}{dx}\Big|_{x=0} \\ -\dfrac{d\bar{u}}{dx}\Big|_{x=1} \end{cases} \end{cases} \tag{1.44}$$

The global simultaneous equations are obtained as

$$\begin{bmatrix} \dfrac{4}{3} & -\dfrac{5}{6} \\ -\dfrac{5}{6} & \dfrac{4}{3} \end{bmatrix} \begin{Bmatrix} u_1 \\ u_2 \end{Bmatrix} = \begin{Bmatrix} -\dfrac{d\bar{u}}{dx}\Big|_{x=0} \\ -\dfrac{d\bar{u}}{dx}\Big|_{x=1} \end{Bmatrix} \tag{1.45}$$

According to the boundary conditions, $u_1 = 0$ and $u_2 = 1$ in the left-hand side of the above equations are known variables, whereas $(du/dx)_{x=0}$and $(du/dx)_{x=1}$ in the left-hand side are unknown variables. The substitution of the boundary conditions into Equation (1.45) directly gives the nodal values of the approximate solution, i. e.,

$$\begin{cases} \left.\dfrac{d\bar{u}}{dx}\right|_{x=0} = 0.8333 \\ \left.\dfrac{d\bar{u}}{dx}\right|_{x=1} = 1.3333 \end{cases} \tag{1.46}$$

Which agrees well with those of the exact solution?

$$\begin{cases} \left.\dfrac{d\bar{u}}{dx}\right|_{x=0} = \dfrac{2}{e-e^{-1}}0.8333 \\ \left.\dfrac{d\bar{u}}{dx}\right|_{x=1} = \dfrac{e+e^{-1}}{e-e^{-1}}1.3333 \end{cases} \tag{1.47}$$

The approximate solution in this example is determined as

$$\bar{u}(x) = x \tag{1.48}$$

and agrees well with the exact solution throughout the whole region of interest as depicted in Figure 1.2.

1.8.2 THREE- ELEMENT CASE

In this section, let us compute the approximate solution $\bar{u}$ by dividing the whole region considered into three sub regions having the same length as shown in Figure 1.6. From Equations (1.34) and (1.35), the approximate solution $\bar{u}$ and the interpolation functions $N_i(i = 1,2)$are written as

$$\bar{u}(x) = \sum_{i=1}^{4} u_i N_i \tag{1.49}$$

$$\begin{cases} N_{1e} = \dfrac{x_{2e} - x}{x_{2e} - x_{1e}} = \dfrac{h^{(e)} - \xi}{h^{(e)}} \\ N_{2e} = \dfrac{x - x_{1e}}{x_{2e} - x_{1e}} = \dfrac{\xi}{h^{(e)}} \end{cases} \tag{1.50}$$

Where $h^{(e)} = 1/3$ and $0 \leq \xi \leq \frac{1}{3}(e = 1,2,3)$.

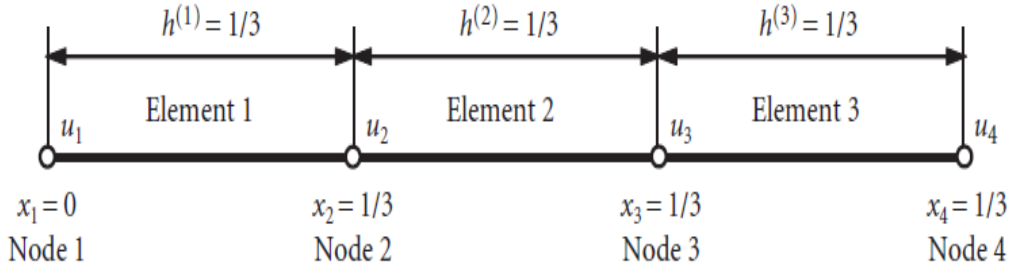

Figure 1.6 Three-element model of a one-dimensional FEM.

The following equation is obtained by calculating all the components of the K-matrix in Equation (1.41):

$$K_{ij}{}^{(e)} = \int_0^1 \left(\frac{dN_i{}^{(e)}}{dx} \frac{dN_j{}^{(e)}}{dx} + N_i{}^{(e)} N_j{}^{(e)} \right) dx$$

$$= \begin{cases} \frac{1}{h^{(e)}} + \frac{h^{(e)}}{3} = \frac{28}{9} (i = j \; and i, j = 1e, 2e) \\ -\frac{1}{h^{(e)}} = \frac{h^{(e)}}{6} = \frac{53}{18} (i \neq j \; and \; i, j = 1e, 2e) \\ 0 \qquad\qquad (i, j \; 1e, 2e) \end{cases} \qquad (1.51a)$$

The related components to the first derivative of the function u in Equation (1.41) are calculated as follows:

$$f_i = \left[N_i \frac{d\bar{u}}{dx} \right]_0^1 = \begin{cases} -\left. \frac{d\bar{u}}{dx} \right|_{x=0} & (i = 1) \\ 0 & (i = 2,3) \\ -\left. \frac{d\bar{u}}{dx} \right|_{x=1} & (i = 4) \end{cases} \qquad (1.51b)$$

The coefficient matrix in Equation (1.51a) that calculated for each element is called "element matrix" and the components of the matrix are obtained as follows:

$$\left[k_{ij}^{(1)}\right]\begin{bmatrix} \frac{1}{h^{(1)}}+\frac{h^{(1)}}{3} & \frac{1}{h^{(1)}}+\frac{h^{(1)}}{6} & 0 & 0 \\ -\frac{1}{h^{(1)}}+\frac{h^{(1)}}{6} & -\frac{1}{h^{(1)}}+\frac{h^{(1)}}{3} & 0 & 0 \\ 0 & 0 & 0 & 0 \\ 0 & 0 & 0 & 0 \end{bmatrix} \qquad (1.52a)$$

$$\left[k_{ij}^{(2)}\right]\begin{bmatrix} 0 & 0 & 0 & 0 \\ 0 & \frac{1}{h^{(2)}}+\frac{h^{(2)}}{3} & -\frac{1}{h^{(2)}}+\frac{h^{(2)}}{6} & 0 \\ 0 & -\frac{1}{h^{(2)}}=\frac{h^{(2)}}{6} & -\frac{1}{h^{(2)}}+\frac{h^{(2)}}{3} & 0 \\ 0 & 0 & 0 & 0 \end{bmatrix} \qquad (1.52b)$$

$$\left[k_{ij}^{(3)}\right]\begin{bmatrix} 0 & 0 & 0 & 0 \\ 0 & 0 & 0 & 0 \\ 0 & 0 & \frac{1}{h^{(3)}}+\frac{h^{(3)}}{3} & -\frac{1}{h^{(3)}}+\frac{h^{(3)}}{6} \\ 0 & 0 & -\frac{1}{h^{(3)}}=\frac{h^{(3)}}{6} & -\frac{1}{h^{(3)}}+\frac{h^{(3)}}{3} \end{bmatrix} \qquad (1.52c)$$

From Equations (1.52a) through (1.52c) above, it is concluded that only components of the element matrix relating to the nodal points which belong to the corresponding element are non-zero and that the other composed of nodal points 2 and 3 and among the components of the element matrix only $k_{22}^{(2)}, k_{23}^{(2)}, k_{32}^{(2)}$ and $k_{33}^{(2)}$ are non-zero and the others are zero. The superscript (2) of the element matrix components above indicates that the components are calculated in element 2, and the subscripts indicate that the components are computed for nodal points 2 and 3 in element 2.

The global matrix is a matrix which relates all the known and the unknown variables for the problem concerned and it can be obtained simply by summing up Equations (1.52c) through (1.52c) as follows:

$$\left[K_{ij}\right] = \left[\sum_{e=1}^{3} k_{ij}^{(e)}\right]$$

$$= \begin{bmatrix} \frac{1}{h^{(1)}} + \frac{h^{(1)}}{3} & -\frac{1}{h^{(1)}} + \frac{h^{(1)}}{6} & 0 & 0 \\ -\frac{1}{h^{(1)}} + \frac{h^{(1)}}{6} & \sum_{e=1}^{2}\left(\frac{1}{h^{(e)}} + \frac{h^{(e)}}{3}\right) & \frac{1}{h^{(2)}} + \frac{h^{(2)}}{6} & 0 \\ 0 & 0 & \sum_{e=2}^{3}\left(\frac{1}{h^{(e)}} + \frac{h^{(e)}}{3}\right) & -\frac{1}{h^{(3)}} + \frac{h^{(3)}}{6} \\ 0 & 0 & -\frac{1}{h^{(3)}} + \frac{h^{(3)}}{6} & \frac{1}{h^{(3)}} + \frac{h^{(3)}}{3} \end{bmatrix} \quad (1.53)$$

Consequently, the global simultaneous equation becomes

$$\begin{bmatrix} \frac{1}{h^{(1)}} + \frac{h^{(1)}}{3} & -\frac{1}{h^{(1)}} + \frac{h^{(1)}}{6} & 0 & 0 \\ -\frac{1}{h^{(1)}} + \frac{h^{(1)}}{6} & \sum_{e=1}^{2}\left(\frac{1}{h^{(e)}} + \frac{h^{(e)}}{3}\right) & \frac{1}{h^{(2)}} + \frac{h^{(2)}}{6} & 0 \\ 0 & -\frac{1}{h^{(2)}} + \frac{h^{(2)}}{6} & \sum_{e=2}^{3}\left(\frac{1}{h^{(e)}} + \frac{h^{(e)}}{3}\right) & -\frac{1}{h^{(3)}} + \frac{h^{(3)}}{6} \\ 0 & 0 & -\frac{1}{h^{(3)}} + \frac{h^{(3)}}{6} & \frac{1}{h^{(3)}} + \frac{h^{(3)}}{3} \end{bmatrix} \begin{Bmatrix} u_1 \\ u_2 \\ u_3 \\ u_4 \end{Bmatrix}$$

$$= \begin{Bmatrix} -\frac{d\bar{u}}{dx}\Big|_{x=0} \\ -\frac{d\bar{u}}{dx}\Big|_{x=1} \end{Bmatrix} \quad (1.54)$$

Note that in the left-hand side of Equation (1.54), the coefficient matrix $[K_{ij}]$ is symmetric with respect to the non-diagonal components $(i \neq j), i.e., K_{ij} = K_{ji.}$ only the components in the band region around the diagonal of the matrix is called the sparse or band matrix.

From the boundary conditions, the values of u_1 and u_4 in the left-hand side of Equation (1.54) are known, i.e., $u_1 = 0$ and $u_4 = 1$ and, from Equation (1.51b), the values of $f_2$and $f_3$in the right-hand side are also known, i.e,$f_2 = 0$ and $f_3 = 0$. On the other hand, u_2 and u_3 in the left-hand side and $\frac{d\bar{u}}{dx}\Big|_{x=0}$ and $-\frac{d\bar{u}}{dx}\Big|_{x=1}$ in the right-hand side are unknown variables.

By changing unknown variables $\frac{d\bar{u}}{dx}\Big|_{x=0}$ and $-\frac{d\bar{u}}{dx}\Big|_{x=1}$ with the first and the fourth components of the vector in the left-hand side of Equation (1.54) and by substituting $h^{(1)} = h^{(2)} = h^{(3)} = 1/3$ into Equation (1.54),

after rearrangement of the equation, the global simultaneous equation is rewritten as follows:

$$\begin{bmatrix} -1 & \frac{53}{18} & 0 & 0 \\ 0 & \frac{56}{9} & -\frac{53}{18} & 0 \\ 0 & -\frac{53}{18} & \frac{56}{9} & 0 \\ 0 & 0 & -\frac{53}{18} & -1 \end{bmatrix} \begin{Bmatrix} \left.\frac{d\bar{u}}{dx}\right|_{x=0} \\ u_2 \\ u_3 \\ \left.\frac{d\bar{u}}{dx}\right|_{x=1} \end{Bmatrix} = \begin{Bmatrix} 0 \\ 0 \\ \frac{53}{18} \\ -\frac{28}{9} \end{Bmatrix} \quad (1.55)$$

Where the new vector in the right-hand side of the equation is a known vector and the one in the left-hand side is an unknown vector.

After solving Equation (1.55), it is understood that $u_2 = 0.2885$, $u_3 = 0.6098$, $\left.\frac{d\bar{u}}{dx}\right|_{x=0} = 0.8496$,and $\left.\frac{d\bar{u}}{dx}\right|_{x=1} = 1.3157$. The exact solutions for u_3 can be computed as $u_2 = 0.2889$ and $u_3 = 0.6102$ from Equation (1.55). For u_2 and u_3 the relative errors are as small as 0.1% and 0.06%, respectively. The calculated values of the derivative $\left.\frac{d\bar{u}}{dx}\right|_{x=0}$,and $\left.\frac{d\bar{u}}{dx}\right|_{x=1}$ are improved when compared to those by the one-element FEM described in Section 1.9.1.

In this section, only one-dimensional finite element method was described. The FEM can be applied two – and three- dimensional continuum problems of various kinds which are described in terms of ordinary and partial differential equations. There is no basic difference between the one-dimensional problems formulations and the formulations for higher dimensions except for the intricacy of formulation.

1.9 FEM IN TWO- DIMENSIONAL ELASTOSTATIC PROBLEMS

Generally, elasticity problems are decreased to solving the partial differential equations known as the equilibrium equations together with the relations of stress-strain or the constitutive equations, the strain-displacement relations, and the compatibility equation under given boundary conditions. The exact solutions can be obtained in quite restricted cases only and in general cannot be solved in closed forms. In order to overcome these difficulties, the FEM has been improved as one of the powerful numerical methods to get approximate solutions for various kinds of elements having arbitrary shapes and finite sizes (called finite

element), by simultaneous algebraic equations approximates partial differential equations, and numerically solves various elasticity problems. Finite elements take the line segment form in one-dimensional problems. Because the process of the FEM is mathematically founded on the variational method, it can be used to structures with elasticity problems and also to the some other different problems related thermodynamics, fluid dynamics, and vibrations which are described by partial differential equations.

1.9.1 ELEMENTS OF FINITE-ELEMENT PROCEDURES IN THE ANALYSIS OF PLANE ELASTOSTATIC PROBLEMS

Limited to static (without time variation) elasticity problems, the process described in the preceding section is essentially the same as that of the stress analyses the FEM. The summarization of the procedure is shown as follows:

- Procedure 1: Discretization; the object of analysis should be divided into a finite number of finite elements.
- Procedure 2: Selection of the interpolation function; the type of element or the interpolation function which approximates displacements and strains in each finite element should be selected.
- Procedure 3: The element stiffness matrices Derivation; the element stiffness matrix which relates forces and displacements in each element should be specified.
- Procedure 4: Assembly of stiffness matrices into the global stiffness matrix; the element stiffness matrices should be assembled into the global stiffness matrix that relates forces and displacements in the whole elastic body to be analyzed.
- Procedure 5: Rearrangement of the global stiffness matrix; the prescribed applied forces (mechanical boundary conditions) and displacements (geometrical boundary conditions) should be substituted into the global stiffness matrix, and the matrix should be rearranged by collecting unknown variables for forces and displacements, in the left-hand by collecting unknown values of the forces and displacements in the right-hand side in order to set up simultaneous equations.
- Procedure6: Unknown forces and displacements derivation; the simultaneous equation set up in Procedure 5 above should be solved in order to solve unknown variables for forces and displacements. For unknown forces the solutions are reaction forces and for unknown displacements the solutions are deformations of the interest elastic body for given geometrical and mechanical boundary conditions, respectively.

- Procedure7: Strains and stresses Computation; the strains and stresses should be computed from the displacements gained in the last Procedure with the strain-displacement relations and the stress-strain relations those are explained later.

1.9.2 FUNDAMENTAL FORMULAE IN PLANE ELASTOSTATIC PROBLEMS

1.9.2.1 EQUATIONS OF EQUILIBRIUM

Consider the static equilibrium status of an infinitesimally small rectangle with the sides parallel to the coordinate axes in a two-dimensional elastic body as shown in Figure 1.7. If the act of body forces F_X and F_y is in the directions of the x- and the y-axes, respectively, the equation of equilibrium in the elastic body can be derived as follows:

$$\begin{cases} \dfrac{\partial \sigma_x}{\partial x} = \dfrac{\partial \tau_{xy}}{\partial y} + Fx = 0 \\ \dfrac{\partial \tau_{yx}}{\partial x} = \dfrac{\partial \sigma_y}{\partial y} + Fy = 0 \end{cases} \tag{1.56}$$

Where σ_x and σ_y are normal stresses in the x-axes and the y-axes, respectively, with τ_{xy} and τ_{yx} shear stresses acting in the x-y plane. The shear stresses τ_{xy} and τ_{yx} are generally equal to each other due to the rotational equilibrium of the two-dimensional elastic body around is center of gravity.

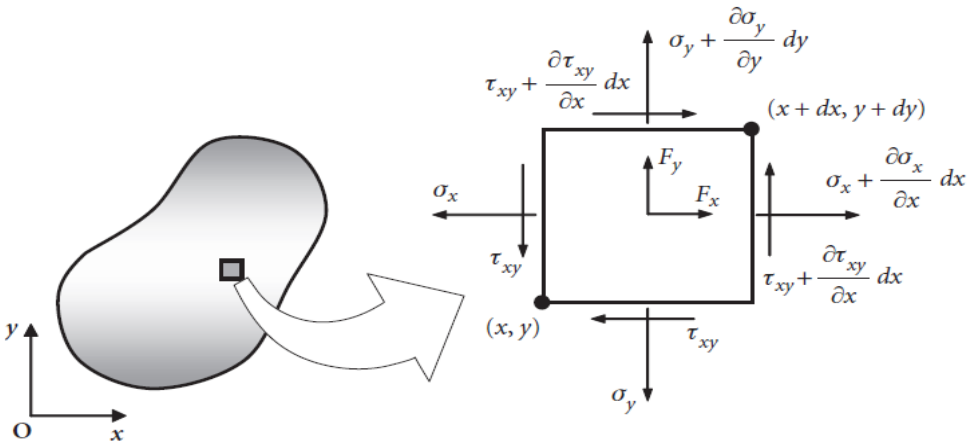

Figure 1.7 Stress states in an infinitesimal element of a two-dimensional elastic body.

1.9.2.2 STAIN-DISPLACEMENT RELATIONS

If the deformation of a two-dimensional elastic body is infinitesimally small under the applied load, the normal strains ε_x and ε_y in the directions of the

x- and y-axes, respectively, and the engineering shearing strain γ_{xy}in the x-y plane are expressed by the following equations:

$$\begin{cases} \varepsilon_x = \dfrac{\partial u}{\partial x} \\ \varepsilon_y = \dfrac{\partial u}{\partial y} \\ \gamma_{xy} = \dfrac{\partial v}{\partial x} + \dfrac{\partial u}{\partial y} \end{cases} \tag{1.57}$$

Where in the directions of the x-axes and y-axes, u and v are infinitesimal displacements, respectively.

1.9.2.3 STRESS-STRAIN RELATIONS (CONSTITUTIVE EQUATIONS)

The states of deformation, strains induced by the internal forces, or stresses resisting against applied loads are described by stress-strain relations. Unlike the other fundamental equations shown in Equations (1.56) and (1.57) which can be determined mechanistically or geometrically, these relations depend on the properties of the material, and they are determined experimentally and often called constitutive relations or constitutive equations. The generalized Hooke's law is one of the most popular relations is which can relates six components of the three-dimensional stress tensor with those of strain tensor through the following simple linear expressions:

$$\begin{cases} \sigma_x = \dfrac{vE}{(1+v)(1-2v)} e_v + 2G\varepsilon_x \\ \sigma_y = \dfrac{vE}{(1+v)(1-2v)} e_v + 2G\varepsilon_y \\ \sigma_z = \dfrac{vE}{(1+v)(1-2v)} e_v + 2G\varepsilon_z \\ \tau_{xy} = G\gamma_{yz} = \dfrac{E}{2(1+v)}\gamma_{xy} \\ \tau_{yz} = G\gamma_{yz} = \dfrac{E}{2(1+v)}\gamma_{yz} \\ \tau_{yz} = G\gamma_{zx} = \dfrac{E}{2(1+v)}\gamma_{zy} \end{cases} \tag{1.58a}$$

Or inversely

$$\begin{cases} \varepsilon_x = \dfrac{1}{E}\left[\sigma_x - v\left(\sigma_y + \sigma_z\right)\right] \\ \varepsilon_y = \dfrac{1}{E}\left[\sigma_y - v(\sigma_z + \sigma_x)\right] \\ \varepsilon_z = \dfrac{1}{E}\left[\sigma_z - v\left(\sigma_x + \sigma_y\right)\right] \\ \gamma_{xy} = \dfrac{\tau_{xy}}{G} \\ \gamma_{yz} = \dfrac{\tau_{yz}}{G} \\ \gamma_{zy} = \dfrac{\tau_{zx}}{G} \end{cases} \qquad (1.58b)$$

Where E is Young's modulus, v poisons ratio, G the shear modulus, and e_v the volumetric strain expressed by the sum of the three normal components of strain, i.e., $e_v = \varepsilon_x + \varepsilon_y + \varepsilon_z$. The volumetric strain e_v can be written in other words as $e_v = \Delta V/V$, where V is the initial volume of the elastic body of interest in an undeformed state and ΔV the change of the volume after deformation.

In the two-dimensional elasticity theory, the three-dimensional Hooke's law is converted into two-dimensional form by using the following two types of approximations:

(1) Approximation of plane stress: For instance, for thin plates, it can be assumed the plane stress approximation that in the direction perpendicular to the plate surface all the stress components vanish, i.e, $\sigma_z = \tau_{zx} = \tau_{yz} = 0$.the stress-strain relations in this approximation are written by the following two-dimensional Hooke's law:

$$\begin{cases} \sigma_x = \dfrac{E}{1-v^2}\left(\varepsilon_x + v\varepsilon_y\right) \\ \sigma_y = \dfrac{E}{1-v^2}\left(\varepsilon_y + v\varepsilon_x\right) \\ \tau_{xy} = G\gamma_{xy} = \dfrac{E}{2(1+v)}\gamma_{xy} \end{cases} \qquad (1.59a)$$

Or

$$\begin{cases} \varepsilon_x = \dfrac{1}{E}\left(\sigma_x - v\sigma_y\right) \\ \varepsilon_y = \dfrac{1}{E}\left(\sigma_y - v\sigma_x\right) \\ \gamma_{xy} = \dfrac{\tau_{xy}}{G} = \dfrac{2(1+v)}{E}\tau_{xy} \end{cases} \qquad (1.59b)$$

The normal strain component ε_z in the thickness direction, however, is not zero, but $\varepsilon_z = -v(\sigma_x + \sigma_y)/E$.

The plane stress approximation satisfies the equations of equilibrium (1.56); nevertheless, the normal strain in the direction of the z-axis $\varepsilon_z$must take a special form, i.e., ε_z must be a liner function of coordinates x and y to satisfy the compatibility conditions which ensures the single-valuedness and continuity conditions of strains. Because this approximation constrains a special need for the strain form ε_z and thus the form of the normal stresses σ_x andσ_y, this approximation cannot be considered as a general rule. Strictly speaking, the plane stress does not exist in reality.

(2) Approximation of plane strain: In situations where plate thickness is large (in the direction of the z-axis), displacement is subjected to large imposes in the direction of the z-axis like that$\varepsilon_z = \gamma_{zx} = \gamma_{yz} = 0$. This case is called the plane stress approximation. The generalized Hooke's law can be written as follows:

$$\begin{cases} \sigma_x = \dfrac{E}{(1+v)(1-2v)}\left[(1-v)\varepsilon_x + v\varepsilon_y\right] \\ \sigma_y = \dfrac{E}{(1+v)(1-2v)}\left[v\varepsilon_y + (1-v)\varepsilon_y\right] \\ \tau_{xy} = G\gamma_{xy} = \dfrac{E}{2(1+v)}\gamma_{xy} \end{cases} \tag{1.60a}$$

Or

$$\begin{cases} \varepsilon_x = \dfrac{1+v}{E}\left[(1-v)\sigma_x - v\sigma_y\right] \\ \varepsilon_y = \dfrac{1+v}{E}\left(-v\sigma_y + (1-v)\sigma_y\right) \\ \gamma_{xy} = \dfrac{\tau_{xy}}{G} = \dfrac{2(1+v)}{E}\tau_{xy} \end{cases} \tag{1.60b}$$

In the thickness direction, the normal stress component σ_z is not zero, but$\sigma_z = vE(\sigma_x + \sigma_y)/[(1+v)(1-2v)]$. These stats can exist in reality because the plane strain state satisfies the equations of equilibrium (1.56) and the compatibility condition.

If we redefine Young's modulus and Poisson's ratio by the following formulae:

$$E' = \begin{cases} E & (plane\ stress) \\ \dfrac{E}{1-v} & (plane\ strain) \end{cases} \tag{1.61a}$$

$$v' = \begin{cases} v & (plane\ stress) \\ \dfrac{v}{1-v} & (plane\ strain) \end{cases} \qquad (1.61b)$$

The two-dimensional Hooke's law can be expressed in a unified form:

$$\begin{cases} \sigma_x = \dfrac{E'}{(1-v'^2)}\left(\varepsilon_x + v'\varepsilon_y\right) \\ \sigma_y = \dfrac{E'}{(1-v'^2)}\left(\varepsilon_x + v'\varepsilon_x\right) \\ \tau_{xy} = G\gamma_{xy} = \dfrac{E'}{2(1+v')}\gamma_{xy} \end{cases} \qquad (1.62a)$$

Or

$$\begin{cases} \varepsilon_x = \dfrac{1}{E'}\left(\sigma_x - v'\sigma_y\right) \\ \varepsilon_y = \dfrac{1}{E'}\left(\sigma_y - v'\sigma_x\right) \\ \gamma_{xy} = \dfrac{\tau_{xy}}{G} = \dfrac{2(1+v')}{E'}\tau_{xy} \end{cases} \qquad (1.62b)$$

The shear modulus G is invariant under the transformations as shown in Equations (1.61a) and (1.61a), i.e.,

$$G = \frac{E}{2(1+v)} = \frac{E'}{2(1+v')} = G'$$

1.9.2.4 BOUNDARY CONDITTONS

When solving the partial differential equation (1.56), there remains indefiniteness in the form of integral constants. To eliminate this indefiniteness, prescribed conditions on stress and/or displacements must be constrained on the bounding surface of the elastic body. These conditions are called boundary conditions. There are two kinds of boundary conditions, i.e. (1) geometrical boundary conditions prescribing displacements and (2) mechanical boundary conditions prescribing stresses or surface tractions.

To denote a portion of the elastic body surface where prescribed stresses by S_σ and the remaining surface where displacements are prescribed byS_u. $S = S_\sigma + S_u$ Denotes the whole surface of the elastic body. Note that it cannot be possible to prescribe stresses and displacements both on a portion of the elastic body surface.

The mechanical boundary conditions on S_σ are given by the following equations:

$$\begin{cases} t_x^* = \bar{t}_x^* \\ t_y^* = \bar{t}_y^* \end{cases} \tag{1.63}$$

Where t_x^* and $t_y^*$are the x-axis and the y-axis components of the traction forcet^*, respectively, while the bar over t_x^* and t_y^* shows that those quantities are prescribed on that surface portion. At a point of a small element of the surface portion S_σ ,taking n= $[\cos\alpha\,, \sin\alpha]$ as the outward unit normal vector, the relations of Cauchy which show the equilibrium condition for forces of surface traction and following equations give the internal stresses:

$$\begin{cases} t_x^* = \sigma_x \cos\alpha + \tau_{xy} \sin\alpha \\ t_y^* = \tau_{xy} \cos\alpha + \sigma_y \sin\alpha \end{cases} \tag{1.64}$$

Where α is the angle between the normal vector n and the x-axis. For free surface where no forces are applied $t_x^* = 0$and$t_y^* = 0$.

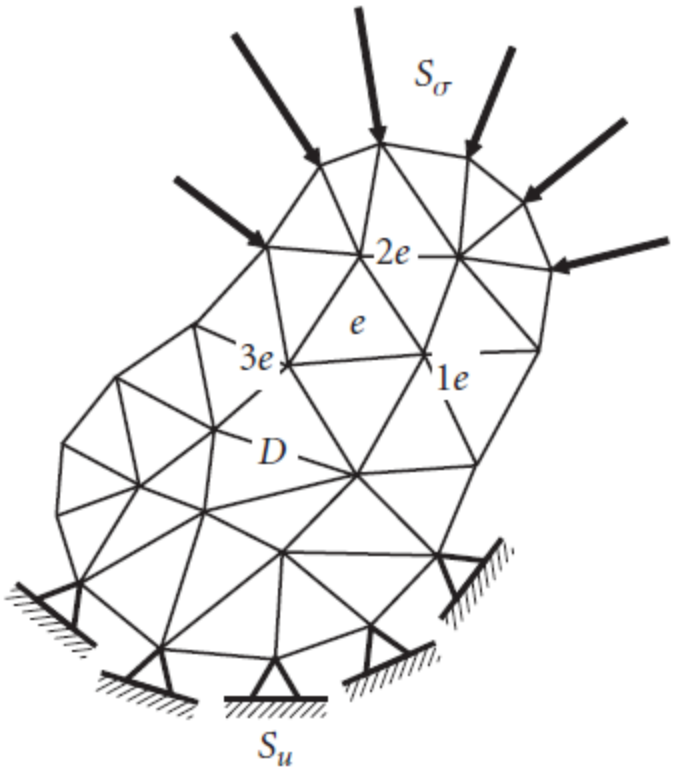

Figure 1.8 Finite-element discretization of a two- dimensional elastic body by triangular elements.

The geometrical boundary conditions on S_u are given by the following equations:

$$\begin{cases} u = \bar{u} \\ v = \bar{v} \end{cases} \tag{1.65}$$

Where $\bar{u}$ and $\bar{v}$ are the x-axis and the y-axis components of prescribed displacements u onS_u. One of the most famous geometrical boundary conditions, i.e., clamped end condition, is defined by u=0 and/or v=0 as it is shown in Figure 1.8.

1.9.3 VARIATIONAL FORMULAE IN ELASTOSTATIC PROBLEMS: THE PRINCIPLE OF VIRTUAL WORK

$$\int_D \int \left(\sigma_x \delta\varepsilon_x + \sigma_y \delta\varepsilon_{y+} \tau_{xy} \delta\gamma_{xy}\right) t \, dx \, dy - \int_D \int \left(F_x \delta u + F_y \delta u\right) t \, dx \, dy - \int_{S_\sigma} \left(\bar{t}_x^* \delta u + \bar{t}_y^* \delta v\right) t \, ds = 0 \tag{1.66}$$

Where D denotes the whole region of a two-dimensional elastic body of interest, S_σ the whole portion of the surface of the elastic body $S(= S_\sigma \cup S_u)$, Where the mechanical boundary conditions are prescribed and t the thickness.

The first term in the left-hand side of Equation (1.66) demonstrates the strain energy increment of the elastic body, the second term the increment of the work done by the body forces, and the third term the increment of the work done by the surface traction forces. Therefore, Equation (1.66) says that the increment of the strain energy of the elastic body is equal to the work done by the forces applied.

The fact that the integrand in each integral in the left-hand side of equilibrium (1.56) and the boundary conditions (1.63) and/or (1.65). Therefore, instead of solving the partial differential equations (1.56), two-dimensional elasticity problems can be solved by using the integral equation (1.66).

1.9.4 FORMULATION OF THE FUNDAMENTAL FINITE- ELEMENT EQUATIONS IN PLANE ELASTOSTATIC PROBLEMS

1.9.4.1 STRAIN-DISPLACEMENT MATRIX OR [B] MATRIX

Let us use the constant-strain triangular element (see Figure1.9 (a)) to derive the fundamental finite-element equations in plane elastostatic problems. The constant-strain triangular element assumes the displacements within the element to be expressed by

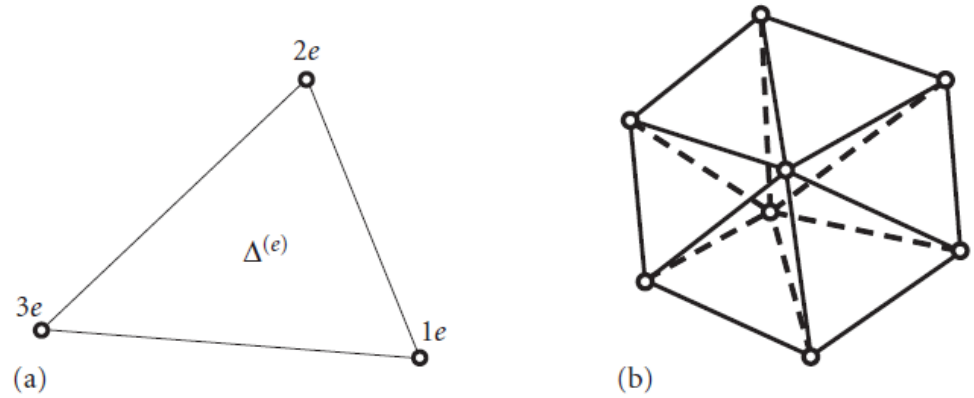

Figure 1.9 (a) Triangular constant strain element and (b) the continuity of displacements.

The following liner functions of the coordinate variables (x,y):

$$\begin{cases} u = \alpha_0 + \alpha_1 x + \alpha_2 y \\ v = \beta_0 + \beta_1 x + \beta_2 y \end{cases} \tag{1.67}$$

The above interpolation functions for displacements, after deformation, convert the two points straight lines joining arbitrarily in the element into straight lines. Since the boundaries between neighboring elements are straight lines to join the apices or nodal points of triangular elements, incompatibility does not happen along the boundaries between adjacent elements and displacements are continuous everywhere in the domain to be analyzed as it is shown in Figure1.9 (b). For the eth triangular element involving of three apices or nodal points $(1_e, 2_e, 3_e)$having the coordinates(x_{1e}, y_{1e}),(x_{2e}, y_{2e}), and (x_{3e}, y_{3e}) and the nodal displacements (u_{1e}, v_{1e}),(u_{2e}, v_{2e}), and (u_{3e}, v_{3e}), the coefficients α_0,α_1, α_2,β_0,β_1, and β_2 in Equations (1.67) are obtained by the following equations:

$$\begin{cases} \begin{Bmatrix} \alpha_0 \\ \alpha_1 \\ \alpha_2 \end{Bmatrix} = \begin{pmatrix} \alpha_{1e} & \alpha_{2e} & \alpha_{3e} \\ b_{1e} & b_{2e} & b_{3e} \\ c_{1e} & c_{2e} & c_{3e} \end{pmatrix} \begin{Bmatrix} u_{1e} \\ u_{2e} \\ u_{3e} \end{Bmatrix} \\ \begin{Bmatrix} \beta_0 \\ \beta_1 \\ \beta_2 \end{Bmatrix} = \begin{pmatrix} \alpha_{1e} & \alpha_{2e} & \alpha_{3e} \\ b_{1e} & b_{2e} & b_{3e} \\ c_{1e} & c_{2e} & c_{3e} \end{pmatrix} \begin{Bmatrix} v_{1e} \\ v_{2e} \\ v_{3e} \end{Bmatrix} \end{cases} \tag{1.68}$$

Where

$$\begin{cases} \alpha_{1e} = \dfrac{1}{2\Delta^{(e)}}(x_{2e}y_{3e} - x_{3e}y_{2e}) \\ b_{1e} = \dfrac{1}{2\Delta^{(e)}}(y_{2e} - y_{3e}) \\ c_{1e} = \dfrac{1}{2\Delta^{(e)}}(x_{3e} - x_{2e}) \end{cases} \quad (1.69a)$$

$$\begin{cases} \alpha_{2e} = \dfrac{1}{2\Delta^{(e)}}(x_{3e}y_{1e} - x_{1e}y_{3e}) \\ b_{2e} = \dfrac{1}{2\Delta^{(e)}}(y_{3e} - y_{1e}) \\ c_{2e} = \dfrac{1}{2\Delta^{(e)}}(x_{1e} - x_{3e}) \end{cases} \quad (1.69b)$$

$$\begin{cases} \alpha_{3e} = \dfrac{1}{2\Delta^{(e)}}(x_{1e}y_{2e} - x_{2e}y_{1e}) \\ b_{3e} = \dfrac{1}{2\Delta^{(e)}}(y_{1e} - y_{2e}) \\ c_{3e} = \dfrac{1}{2\Delta^{(e)}}(x_{2e} - x_{1e}) \end{cases} \quad (1.69c)$$

The numbers that are subscripted with "e", $1_e, 2_e, and\ 3_e$,in the above equations are called element nodal numbers and denote the numbers of three nodal points of the element. Nodal points should be numbered counterclockwise. These three numbers are used only in the eth element. The global nodal numbers that are nodal numbers of the other type are also specified to the three nodal points of the element, being numbered throughout the whole elastic body model. The symbol $\Delta^{(e)}$demonstrates the area of the element and can be only represented by the coordinates of the nodal points of the element, i.e.,

$$\Delta^{(e)} = \frac{1}{2}[(x_{1e} - x_{3e})(y_{2e} - y_{3e}) - (y_{3e} - y_{1e})(x_{3e} - x_{2e})]$$
$$= \frac{1}{2}\begin{vmatrix} 1 & x_{1e} & y_{1e} \\ 1 & x_{2e} & y_{2e} \\ 1 & x_{3e} & y_{3e} \end{vmatrix} \quad (1.69d)$$

Consequently, the components of the displacement vector $[u, v]$can be expressed by the components of the nodal displacement vectors$[u_{1e}, v_{1e}]$, $[u_{2e}, v_{2e}]$, and $[u_{3e}, v_{3e}]$ as follows:

$$\begin{cases} u = (\alpha_{1e} + b_{1e}x + c_{1e}y)u_{1e} + (\alpha_{2e} + b_{2e}x + c_{2e}y)u_{2e} + (\alpha_{3e} + b_{3e}x + c_{3e}y)u_{3e} \\ v = (\alpha_{1e} + b_{1e}x + c_{1e}y)v_{1e} + (\alpha_{2e} + b_{2e}x + c_{2e}y)v_{2e} + (\alpha_{1e} + b_{1e}x + c_{1e}y)v_{1e} \end{cases} \quad (1.70)$$

Matrix notation of Equation (1.70) is

$$\begin{Bmatrix} u \\ v \end{Bmatrix} = \begin{bmatrix} N_{1e}^{(e)} & 0 & N_{2e}^{(e)} & 0 & N_{3e}^{(e)} & 0 \\ 0 & N_{1e}^{(e)} & 0 & N_{2e}^{(e)} & 0 & N_{3e}^{(e)} \end{bmatrix} \begin{Bmatrix} u_{1e} \\ v_{1e} \\ u_{2e} \\ v_{2e} \\ u_{3e} \\ v_{3e} \end{Bmatrix} = [N]\{\delta\}^e \qquad (1.71)$$

$$\begin{cases} N_{1e}^{(e)} = \alpha_{1e} + b_{1e}x + c_{1e}y \\ N_{2e}^{(e)} = \alpha_{2e} + b_{2e}x + c_{2e}y \\ N_{3e}^{(e)} = \alpha_{3e} + b_{3e}x + c_{3e}y \end{cases} \qquad (1.72)$$

And the superscript $\delta^{(e)}$,(e), indicates that $\delta^{(e)}$is the displacement vector determined by the three displacement vectors at the triangular element three nodal points. Equation (1.72) formulates the definitions of the interpolation functions or shape functions $N_{ie}^{(e)}(i = 1,2,3)$for the triangular constant-strain element.

Now, let us consider strains derived from the displacements given by Equation (1.71). Substitution of Equation (1.71) into (1.57) gives.

$$\{\varepsilon\}\begin{Bmatrix} \varepsilon_x \\ \varepsilon_y \\ \gamma_{xy} \end{Bmatrix} = \begin{Bmatrix} \dfrac{\partial u}{\partial x} \\ \dfrac{\partial u}{\partial y} \\ \dfrac{\partial u}{\partial x} + \dfrac{\partial u}{\partial y} \end{Bmatrix}$$

$$= \begin{bmatrix} \dfrac{\partial N_{1e}^{(e)}}{\partial x} & 0 & \dfrac{\partial N_{2e}^{(e)}}{\partial x} & 0 & \dfrac{\partial N_{3e}^{(e)}}{\partial x} & 0 \\ 0 & \dfrac{\partial N_{1e}^{(e)}}{\partial y} & 0 & \dfrac{\partial N_{2e}^{(e)}}{\partial y} & 0 & \dfrac{\partial N_{3e}^{(e)}}{\partial y} \\ \dfrac{\partial N_{1e}^{(e)}}{\partial x} & \dfrac{\partial N_{1e}^{(e)}}{\partial y} & \dfrac{\partial N_{2e}^{(e)}}{\partial x} & \dfrac{\partial N_{2e}^{(e)}}{\partial y} & \dfrac{\partial N_{3e}^{(e)}}{\partial x} & \dfrac{\partial N_{3e}^{(e)}}{\partial y} \end{bmatrix} \begin{Bmatrix} u_{1e} \\ v_{1e} \\ u_{2e} \\ v_{2e} \\ u_{3e} \\ v_{3e} \end{Bmatrix}$$

$$= \begin{bmatrix} b_{1e} & 0 & b_{2e} & 0 & b_{3e} & 0 \\ 0 & c_{1e} & 0 & c_{2e} & 0 & c_{3e} \\ c_{1e} & b_{1e} & c_{2e} & c_{3e} & b_{3e} & \end{bmatrix} \begin{Bmatrix} u_{1e} \\ v_{1e} \\ u_{2e} \\ v_{2e} \\ u_{3e} \\ v_{3e} \end{Bmatrix} = [B]\{\delta\}^e \qquad (1.73)$$

Where [**B**] establishes the relationship between the nodal displacement vector$\{\delta\}^e$ and the element strain vector$\{\varepsilon\}$, and is called the strain-displacement matrix or [**B**] matrix. All the components of the [**B**] matrix are expressed only by the coordinate values of the three nodal points consisting of the element.

According to the above discussion, it can be derived that strains are constant throughout a three-node triangular element, because its interpolation functions are the coordinate variables linear functions within the element. Because of this, a triangular element with three nodal points is named a "constant-strain element". The compatibility condition in the strict sense cannot be satisfied by three-node triangular elements, because strains are discontinuous among elements. It is shown, however, as the size of the elements becomes smaller, the results obtained by elements of this type converge to exact solution.

It is known that elements must fulfill the following three criteria for the finite smaller element is attempted. Namely, the elements must

(1) Represent rigid body displacements,

(2) Represent constant strains, and

(3) Ensure the continuity of displacements among elements.

1.9.4.2 STRESS-STRAIN MATRIX OR [D] MATRIX

Substitution of Equation (1.73) into (1.62a) gives

$$\{\sigma\}\begin{Bmatrix}\sigma_x\\ \sigma_y\\ \tau_{xy}\end{Bmatrix}=\frac{E'}{1-v'^2}\begin{bmatrix}1 & v' & 0\\ v' & 1 & 0\\ 0 & 0 & \dfrac{1-v'}{2}\end{bmatrix}\begin{Bmatrix}\varepsilon_x\\ \varepsilon_y\\ \gamma_{xy}\end{Bmatrix}=[D^e]\{\varepsilon\}$$
$$=[D^e][B]\{\delta\}^e \qquad (1.74)$$

Where $[D^e]$ establishes the relationship between stresses and strains, or the constitutive relations. The matrix $[D^e]$ that is called the elastic stress strain matrix or just $[D]$matrix is for elastic bodies. In situation that initial strains $\{\varepsilon_0\}$ such as thermal strains, plastic strains and residual strains exist, $\{\varepsilon\}-\{\varepsilon_0\}$ is used instead of$\{\varepsilon\}$.

1.9.4.3 ELEMENT STIFFNESS EQUATIONS

Let consider $\{P\}^{(e)}$ defines the equivalent nodal forces that are statically equivalent to the traction forces $t^*=\left[t_x^*,t_y^*\right]$ on the element boundaries and the body forces $\{F\}^{(e)}$ in the element:

$$\{F\}^{(e)T}=\left[F_x,F_y\right] \qquad (1.75)$$

$$\{P\}^{(e)T}=[X_{1e},Y_{1e},X_{2e},Y_{2e},X_{3e},Y_{3e}] \qquad (1.76)$$

In the above equations, $\{F\}$ represents a column vector, [P] a row vector, and superscript T the transpose of a vector or a matrix.

To make differentiations shown in Equation (1.57), displacements considered by Equation (1.71) must be continuous throughout an elastic body of interest. The mechanical boundary conditions (1.63) and the equations of equilibrium (1.56) are the remaining conditions that should be satisfied; nevertheless these equations commonly cannot be satisfied in the strict sense. Therefore, the equivalent nodal forces, for example (X_{1e}, Y_{1e}), (X_2, Y_{2e}), and (X_{3e}, Y_{3e}),are defined on the three nodal points of the element via specifying these forces by the principle of the virtual work in order to satisfy the equilibrium and boundary conditions element by element. Namely, the principle of the virtual work to be satisfied for arbitrary virtual displacements $\{\delta^*\}^{(e)}$of the eth element is derived from Equation (1.66) as

$$\{\delta^*\}^{(e)T}\{P\}^{(e)} = \int_D \int \left(\{\varepsilon^*\}^T\{\sigma\} - \{f^*\}^T\{F\}^{(e)}\right)t\, dx\, dy \tag{1.77}$$

Where

$$\{\varepsilon^*\} = [B]\{\delta^*\}^{(e)} \tag{1.78}$$

$$\{f^*\} = [N]\{\delta^*\}^{(e)} \tag{1.79}$$

Substitution of Equations (1.78) and (1.79) gives

$$\{\delta^*\}^{(e)T}\{P\}^{(e)} = \{\delta^*\}^{(e)T}\left(\int_D \int \left([N]^T\{F\}^{(e)}\right)t\, dx\, dy\right) \tag{1.80}$$

Since Equation (1.80) holds true for any virtual displacements$\{\delta^*\}^{(e)}$, the equivalent nodal forces can be obtained by the following equation:

$$\{P\}^{(e)} = \int_D \int \left([B]^T\{\sigma\}^{(e)}\right)t\, dx\, dy - \int_D \int \left([N]^T\{F\}^{(e)}\right)t\, dx\, dy \tag{1.81}$$

Form Equations (1.73) and (1.74),

$$\{\sigma\} = [D^e](\{\varepsilon\} - \{\varepsilon_0\}) = [D^e][B]\{\delta\}^e - [D^e]\{\varepsilon_0\} \tag{1.82}$$

Substitution of Equation (1.82) into (1.81) gives

$$\{P\}^{(e)} = \left(\int_D \int ([B]^T[D^e][B])t\, dx\, dy\right)\{\delta\}^e - \int_D \int [B]^T[D^e]\{\varepsilon_0\}\, t\, dx\, dy - \int_D \int [N]^T\{F\}^{(e)} t\, dx\, dy \quad (1.83)$$

Equation (1.83) is rewritten in the form

$$\{P\}^{(e)} = \left[K^{(e)}\right]\{\delta\}^e + \left\{F_{\varepsilon_0}\right\}^{(e)} + \{F_F\}^{(e)} \quad (1.84)$$

Where

$$\left[K^{(e)}\right] \equiv \int_D \int [B]^T[D^e][Bt\, dx\, dy = \Delta^{(e)}[B]^T[D^e][B]t \quad (1.85)$$

$$\left\{F_{\varepsilon_0}\right\}^{(e)} \equiv -\int_D \int [B]^T[D^e]\{\varepsilon_0\}t\, dx\, dy \quad (1.86)$$

$$\{F_F\}^{(e)} \equiv -\int_D \int [N]^T\{F\}^{(e)} t\, dx\, dy \quad (1.87)$$

Equation (1.84) is called the element stiffness equation for the eth triangular finite element and $\left[K^{(e)}\right]$ defined by Equation (1.85) the element stiffness matrix. The matrices [B] and $[D^e]$ can be taken out of the integral since they are constant throughout the element and the integral is simply equal to the area of the element $\Delta^{(e)}$ so that the rightmost side of Equation (1.85) is obtained. The forces $\left\{F_{\varepsilon_0}\right\}^{(e)}$ and $\{F_F\}^{(e)}$ are the equivalent nodal forces due to initial strains and body forces, respectively. Except for the case of three-node triangular elements, since the integrand in Equation (1.85) is normally a function of the coordinate variables x and y, the integrals appearing in Equation (1.85) are often three- node triangular elements, the integrals appearing in Equation (1.85) are mostly evaluated by a numerical integration scheme like the Gaussian quadrature.

The element stiffness matrix$\left[K^{(e)}\right]$ in Equation (1.85) is a 6 by 6 square matrix which can be decomposed into nine 2 by sub matrices as shown in the following equation:

$$\left[K^{(e)}_{ieje}\right] = \begin{bmatrix} K^{(e)}_{1e1e} & K^{(e)}_{1e2e} & K^{(e)}_{1e3e} \\ K^{(e)}_{2e1e} & K^{(e)}_{2e2e} & K^{(e)}_{2e3e} \\ K^{(e)}_{3e1e} & K^{(e)}_{3e2e} & K^{(e)}_{3e3e} \end{bmatrix} \quad (1.88)$$

$$K_{ieje}^{(e)} = K_{jeie}^{(e)T} \tag{1.89}$$

$$K_{ieje}^{(e)} = \int_{\Delta(e)} [B_{ie}]^T [D^e][B_{je}]t \ \ dx\, dy \ \begin{cases}(2\times 2) asmmetric\ matrix (i_e \neq j_e)\\ (2\times 2) symmetric\ matrix (i_e = j_e)\end{cases} \tag{1.90}$$

Where

$$[B_{ie}] = \frac{1}{2\Delta^{(e)}}\begin{bmatrix} b_{ie} & 0 \\ 0 & c_{ie} \\ c_{ie} & b_{ie}\end{bmatrix} (i_e = 1,2,3) \tag{1.91}$$

And the subscripts i_e and j_e of $K_{ieje}^{(e)}$ refer to element nodal numbers and

$$K_{ieje}^{(e)} = [B_{ie}]^T [D^e][B_{je}]t\Delta^{(e)} \tag{1.92}$$

In the discussion above, the formulae have been obtained for one triangular element only, but for any elements are available, if necessary, with some modifications.

1.9.4.4 GLOBAL STIFFFNESS EQUATIONS

Element stiffness equations are determined for element by element as shown in Equation (1.84), and then they are assembled into the global stiffness equations for the whole elastic body of interest. It is necessary to mention the following items during the assembly method of the global stiffness equations, because nodal points that belong to different elements but have the same coordinates are the same points:

(1) The displacement components u and v of the same nodal points which belong to different elements are the same; i.e., there exist no incompatibilities such cracks between elements.

(2) The sums of the nodal forces are to be zero for nodal points on the bounding surfaces and for those in the interior of the elastic body to which forces are applied.

(3) Similarly, for nodal points to which forces are applied, the sums of the forces applied to those nodal points are equal to the sums of the nodal forces.

The same global nodal numbers are to be given to the nodal points which have the same coordinates. By considering all above items, let us rewrite the element stiffness matrix $\left[K^{(e)}\right]$ in Equation (1.88) by using the global nodal numbers I,J, and (I,J,K=1,2,…,2n) instead of the element nodal numbers i_e, j_e and $k_e (i_e, j_e, k_e = 1,2,3); i.e.,$

$$\left[K^{(e)}\right] = \begin{bmatrix} K_{II}^{(e)} & K_{IJ}^{(e)} & K_{IK}^{(e)} \\ K_{JI}^{(e)} & K_{JJ}^{(e)} & K_{JK}^{(e)} \\ K_{KI}^{(e)} & K_{KJ}^{(e)} & K_{KK}^{(e)} \end{bmatrix} \tag{1.93}$$

Then, let us embed the element stiffness matrix in a square matrix having the same size as the global stiffness matrix of 2n by 2n as shown in Equation(1.94):

$$\begin{matrix} \\ 1 \\ 2 \\ \vdots \\ 2I-1 \\ 2I \\ \vdots \\ K^{(e)}\{\delta\} = 2J-1 \\ 2J \\ \vdots \\ 2K-1 \\ 2K \\ \vdots \\ 2n-1 \\ 2n \end{matrix} \begin{matrix} 1\ 2\ \cdots\ 2I-1\ 2I\ \cdots\ 2J-1\ 2J\ \cdots\ 2K-1\ 2K\ \cdots\ 2n\ \cdots\ 1\ \ 2n \\ \begin{bmatrix} 0\,0\cdots & 0 & 0\cdots & 0 & 0\cdots & 0 & 0\cdots & 0 & 0 \\ 0\,0\cdots & 0 & 0\cdots & 0 & 0\cdots & 0 & 0\cdots & 0 & 0 \\ \vdots\ \vdots & \vdots & \vdots & \vdots & \vdots & \vdots & \vdots & \vdots & \vdots \\ 0\,0\cdots & K_{II}^{(e)} & \cdots & K_{JI}^{(e)} & \cdots & K_{IK}^{(e)} & \cdots & 0 & 0 \\ 0\,0\cdots & & \cdots & & \cdots & & \cdots & 0 & 0 \\ \vdots\ \vdots & \vdots & \vdots & \vdots & \vdots & \vdots & \vdots & \vdots & \vdots \\ 0\,0\cdots & K_{JI}^{(e)} & \cdots & K_{JJ}^{(e)} & \cdots & K_{JK}^{(e)} & \cdots & 0 & 0 \\ 0\,0\cdots & & \cdots & & \cdots & & \cdots & 0 & 0 \\ \vdots\ \vdots & \vdots & \vdots & \vdots & \vdots & \vdots & \vdots & \vdots & \vdots \\ 0\,0\cdots & K_{KI}^{(e)} & \cdots & K_{KJ}^{(e)} & \cdots & K_{KK}^{(e)} & \cdots & 0 & 0 \\ 0\,0\cdots & & \cdots & & \cdots & & \cdots & 0 & 0 \\ \vdots\ \vdots & \vdots & \vdots & \vdots & \vdots & \vdots & \vdots & \vdots & \vdots \\ 0\,0\cdots & & \cdots & & \cdots & & \cdots & 0 & 0 \\ 0\,0\cdots & & \cdots & & \cdots & & \cdots & 0 & 0 \end{bmatrix} \end{matrix}$$

$$\times \begin{Bmatrix} u_1 \\ u_2 \\ \vdots \\ u_I \\ v_I \\ \vdots \\ u_j \\ v_j \\ \vdots \\ u_k \\ v_k \\ \vdots \\ u_n \\ v_n \end{Bmatrix} \begin{Bmatrix} 0 \\ 0 \\ \vdots \\ X_I^{(e)} \\ Y_I^{(e)} \\ \vdots \\ X_J^{(e)} \\ Y_J^{(e)} \\ \vdots \\ X_k^{(e)} \\ Y_k^{(e)} \\ \vdots \\ 0 \\ 0 \end{Bmatrix} \tag{1.94}$$

Where n denotes the number of nodal points. This process is called the method of extended matrix. Here the number of degrees of freedom indicates the number of unknown variables. In the problems of two-dimensional elasticity, because two of displacements and forces in the x- and y-directions are unknown variable for one nodal point, each nodal point has two degrees of freedom. Therefore, for a finite-element model consisting of n nodal points the number of degrees of freedom is 2n.

By summing up the element stiffness matrices for all the n_e elements in the finite element model, the global stiffness matrix [K] is obtained as shown in the following equation:

$$[K] \equiv [K_{ij}] = \sum_{e=1}^{ne} [K^{(e)}] \quad (i, j = 1,2, \dots ,2n \;\; and \;\; e = 1,2, \dots , n_e) \qquad (1.95)$$

Since the components of the global nodal displacement vector$\{\delta\}$ are common for all the elements, they remain unchanged during the assembly of the global stiffness equations. By rewriting the components of $\{\delta\}, u_1, u_2, \dots , u_n$ as $u_1, u_3, \dots , u_{2i} - 1, \dots , u_{2n-1}$ and $v_1, v_2, \dots , v_n$as $u_2, u_4, \dots , u_{2i}, \dots , u_{2n}$, the following expression for the global nodal displacement vector $\{\delta\}$ is obtained:

$$\{\delta\} = \{u_1, u_2, \dots , u_{2I-1}, u_{2I}, u_{2J}, \dots , u_{2K-1}, \dots , u_{2n-1}, u_{2n}\}^T \qquad (1.96)$$

The global nodal force of a node is the sum of the nodal forces for all the elements to which the node belongs. Hence, the global nodal force vector $\{P\}$ can be written as

$$\{P\} = \{X_1, Y_1, \dots , X_I, Y_I, \dots , X_J, Y_J, \dots , X_K, Y_K, \dots , X_n, Y_n\}^T \qquad (1.97)$$

Where

$$X_I \sum X_I^{(e)} \; Y_1 = \sum Y_I^{(e)} \qquad (I = 1,2, \dots , n) \qquad (1.98)$$

By rewriting the global nodal force vector $\{P\}$in a similar way to $\{\delta\}$ in Equation (1.96) as

$$\{P\} = \{X_1, X_2, \dots , X_{2I-1}, X_{2I}, \dots , X_{2J-1}, X_{2J}, \dots , X_{2K-1}, X_{2K}, \dots , X_{2n-1}, X_{2n}\}^T \quad (1.99)$$

Where

$$X_I \sum X_I^{(e)} \qquad (I = 1,2, \dots ,2n) \qquad (1.100)$$

The symbol Σ in Equations (1.98) and (1.100) represents that the summation is taken over all the elements that possess the node in common. In Equation (1.100) the values of X_I, however, are zero for the nodes of elastic body inside and for the nodes on the bounding surfaces that are subjected to no applied loads.

Consequently, the following formula is obtained as the governing global stiffness equation:

$$[K]\{\delta\} = \{P\} \qquad (1.101)$$

Which is the 2nth degree simultaneous liner equations for 2n unknown variables of nodal displacements and/or forces.

CHAPTER 2

Design of Flexible Link Manipulator

2.1 Introduction

The use of robots has become a necessity in almost all industries. To gain high stiffness and for increasing the accuracy of the motion, industrial robots are usually made very heavy, therefore the robot speed and the manufacturing system performances are limited and also the required energy to move the system increases.

The demand of better performances and higher speed makes in necessary to consider lightweight manipulators because they require less energy to move and have more maneuverability. On the contrary, due to the dynamic effects of structural flexibility, their control is more difficult and accurate dynamic models for design and control such systems are needed.

A flexible multibody system (FMS) is a group of interconnected rigid and deformable components, each of which may undergo large translational and rotational motions. The components may also come into contact with the surrounding environment or with one another. Typical connections between the components include: revolute, spherical, prismatic and planar joints, lead screws, gears, and cams. The components can be connected in closed-loop (or tree) configurations (eg, manipulators).

The term flexible multibody dynamic (FMD) refers to the computational strategies that are used for calculating the dynamic response (which includes time-histories of motion, stress and deformation) of FMS due to external applied forces, constraints, and/or initial conditions. This type of simulation is referred to as forward dynamics. FMD also comprises inverse dynamic, which predicts that the applied forces are really necessary to produce a desired motion response. FMD is important because it can be used in the design, analysis, and control of many practical systems such as: air, ground, and space transportation vehicles (such as airplanes, trains, automobiles, bicycles, and spacecraft); manufacturing machines; manipulators and robots; mechanisms; articulated earthbound structures (such as satellites and space stations); and bio-dynamical systems (human body, animals, and insects). Motivated by these applications, intense research for the last thirty years has been the focus on FMD. To design and control of FMS, FMD is used. In design, FMD can be used to calculate the system parameters (such as dimensions, configuration, and materials) that minimize the system cost while satisfying the design safety constraints (such as static/dynamic stability, strength, and rigidity). FMD is used in control applications for predicting the answer of the multibody system to a given control function and for calculating the changes in control actions essential to direct the system towards the design for optimizing the controller/FMS parameters.

Recently, considerable attempts has been allocated to modeling, design, and control of FMS. In design, FMD can be used to calculate the system parameters (such as dimensions, rigidity, and static/dynamic stability).FMD in used in control applications to predict the answer of the multibody system to a given control function and for calculating the changes in control actions essential to direct the system towards the desired answer (inverse dynamics). FMD can be used also in model-based control as in integral part of the controller like in model-based control as an integral parting the controller/ FMS parameters.

Recently, considerable attempt has been allocated to modeling, design, and control of FMS. The publications number on the subject has been increasing steadily. The Lists of the many contributions on the subject and also the reviews are given in papers of study on FMD [1,2] and on the multibody dynamics general area, that are including rigid and flexible multibody systems both [3-7]. Special study articles have been published on some special aspects of FMD, such as: dynamic analysis of flexible manipulations [8], dynamic analysis of elastic linkages [9-13], and dynamics of satellites with flexible appendages [14]. A number of books on FMD have been published [15-23]. In the last few years, there were some conferences, special sessions, and symposia allocated to FMD [24]. Two archival journals are devoted to the subjects of rigid and flexible multibody dynamics: "Multibody system Dynamics" published by Kluwer Academic Publishers, and "Journal of Multibody Dynamics" published by Ingenta Journal. There are a number of commercial codes for flexible multibody dynamics (eg, ADAMS from Mechanical Dynamics Inc, DADS from CADSI Inc, MECANO from samtech, and SimPack from INTEC GmbH) also many research codes created at research institutions and universities. A study of multibody dynamics software was presented in Schiehlen up to 1990 with benchmarks[25]. There are two compelling motivations for developing FMD modeling techniques. The first motivation is that a number of current problems have not yet been solved to a satisfactory degree. The next motivation is that future multibody systems are maybe need more sophisticated models than has heretofore been presented. This is the reason that the applications of practical FMD are likely to have more stringent requirements of economy, light weight, high performance, high speed/acceleration, and safety.

2.1.1 Deformation reference frames

In multibody dynamics to describing the motion of the multibody system, an inertial frame serves as a global reference frame. Moreover, intermediate reference frames that are attached to each flexible component and follow the average local rigid body motion are often used.

The motion of the component relative to the intermediate frame is, almost, only because of the deformation of the component. This simplifies the calculation of the internal forces because stress and strain measures that are not invariant under rigid body motion, such as the Cauchy stress tensor and the small strain tensor, can be used to calculate these force with respect to the intermediate frame. These tensors result in a linear force displacement relation. Two main types of intermediate frames are used: floating and corotational frames. The floating frame follows an average rigid body motion of the entire flexible component or substructure. The corotational frame conform an average rigid body motion of an individual finite element within the flexible component. In many papers, instead of intermediate frames, for measuring deformations the global inertial frame is directly used. In this method, the motion of an element consists of a combination of rigid body motion and deformation and they are not separated. To calculate the internal forces with respect to the global inertial frame, nonlinear finite strain measures and corresponding energy conjugate stress measures, which are objective and invariant under rigid body motion, are used. In Table 2.1 you can see a comparison between the floating, corotational, and inertial frames as major characteristics of the types of frames.

The floating frame method originated out of research on rigid multibody dynamics in the late 1960s. It was used for extending rigid multibody dynamics codes to FMS. This was done by superimposing small elastic deformations on the large rigid body motion that generated by using the rigid multibody dynamics code. Initial applications of the floating frame approach included: spinning flexible beams (primarily for mechanisms, and flexible manipulators). The floating frame approach was also used to extend model analysis and experimental modal identification techniques to FMS [26-30]. This is performed by identifying the mode shapes and frequencies of each flexible component either numerically or experimentally. The first n modes (where n is determined by the physics of the problem and the by the required accuracy) are superposed on the rigid body motion of the component represented by the motion of the floating frame.

The approach of corotatioanal frame was initially developed as a part of the natural mode method proposed by Argyris et al [31]. In this method, the finite element motion is divided into natural deformation modes and a rigid body motion. The approach was used for static modeling of structures undergoing large displacements and small deformations. Later, Belytschko and Hsiesh [32] introduced element rigid convected frames or corotational frames, for the dynamic modeling of planar continuum and beam type elements, using a total displacement explicit solution procedure.

Table 2.1 Major characteristics of the three types of frames

	Floating frame	Corotational frame	Inertial frame
Frame definition	A floating frame is defined for each flexible component. The floating frame of a component follows a mean rigid body motion of the component (Fig. 2.1)	A corotational frame is defined for each element. The corotational frame of an element follows a mean rigid body motion of the element (Fig. 2.2)	The global inertial reference frame is used as a reference frame for all motions (Fig. 2.3)
Reference frame for:			
a)deformation	**Floating frame (for each flexible component).**	**Corotational frame (for each finite element).**	**Global inertial reference frame.**
b) Internal forces	**Floating frame.** Note: in some implementations, the internal force components are transformed from the floating frame to the global inertial reference frame (eg,[33]).	**Corotational frame/ global inertial reference frame.** Note: the element internal force components are first calculated relative to the corotational frame, then they are transformed from the corotational frame to the global inertial frame using the corotational frame to the global inertial frame using the corotational frame rotation matrix.	**Global inertial reference frame:** Note: the internal forces are calculated using finite stain measures which are invariant under rigid body motion.
c)Inertia forces	**Floating frame.** Note: in some implementations, the flexible motion inertia force components are first evaluated with reference frame and then are transformed to the floating frame (eg,[34,35]).	**Global inertial reference frame.** • In some implementations, the inertia force components are first evaluated relative are transformed to the inertial frame (eg,[36-38]). • In spatial problems, for the rotational part of the equations of motion, the calculated relative to a moving material frame.	**Global inertial reference frame.** Note: in spatial problems, for the rotational part of the equations of motion, the internal and inertia moments are often calculated relative to a moving material frame.
Modeling Considerations			
a)Incorporation of flexibility effects	The floating frame approach is the natural way to extend rigid multibody dynamics to flexible multibody systems.	The corotional frame transformation eliminates the element rigid body motion such that a liner deformation theory can be used for	General finite strain measures that are invariant under superposed rigid body motion are used.

		the element internal forces.
b)Magnitude of angular velocities	No restriction on angular velocities magnitudes. However, when linear model reduction is used, the angular velocity should be low or constant because the stuffiness of the body varies with the angular velocity due to the centrifugal stiffening effect [39].	No restriction on angular velocities magnitudes. In case of very small elastic deformations and large angular velocities, special care must be taken during the solution procedure (time step size, number of equilibrium iterations, etc) to avoid the situation where numerical errors from the rigid body motion are of the order of the elastic part of the response.
c)Large deflections	• Moderate deflections can be modeled by using quadratic strain terms, however, large deflections cannot be modeled unless the body is sub-structured. • Without the assumption that the strains and deflections are small, the high-order terms of the flexible-rigid body inertial coupling terms cannot be neglected and the formulation becomes very complicated.	Can handle large deflections and large strains.
d)Foreshortening	Foreshortening effect can be modeled by adding quadratic axial-bending strain coupling terms.	Naturally included.
e)Centrifugal stiffening	Centrifugal stiffening can be modeled by adding the stress produced by the axial centripetal forces and including axial bending strain coupling terms.	Naturally included.
f)Mixing rigid and flexible bodies	Since the floating frame formulation in based on rigid multibody dynamics analysis methods, both rigid and flexible bodies can be present in the same model in any configuration with no difficulty.	Most implementations place some restrictions on the configuration of the rigid bodies, such as a closed-loop, must contain at least one flexible body.

Table 2.1 (Continued)

	Floating frame	Cototational Frame	Inertial Frame
Characteristics of the semi-discrete equations of motion	• The equations of motion are written such that the flexible body coordinates are referred to a floating frame and the rigid body coordinates are referred to the inertial frame.	• The equations of motion are written with respect to the global inertial frame. • In spatial problems with rotational DOFs, the rotational part of the equations of motion can be written with respect to a body attached nodal frame (material frame) [40-45] or with respect to the global inertial frame (spatial frame) [42,46].	
a) inertia forces	• The inertia forces involve nonlinear centrifugal, Coriolis, and tangential terms because the accelerations are measured with respect to a rotating frame (the floating frame).	• The inertia forces are the product of the mass matrix and the vector of nodal accelerations with respect to the global inertial frame. • In spatial problems with rotational DOFs, the rotational equations (the Euler equations) include quadratic angular velocity terms. (These terms vanish in planar problems).	
	• The mass matrix has nonlinear flexible rigid body motion coupling terms. The coupling terms are necessary for an accurate prediction of the dynamic response, when the magnitude of the flexible inertia forces is not negligible relative to that of the rigid body inertia forces.	• The translational part of the mass matrix is constant. Effect such as coupling between flexible and rigid body motion, centrifugal and coriolis acceleration are not present because the inertia forces are measured with respect to an inertial frame.	
b)Internal (structural) forces	The internal forces are liner for small strains and slow rotational velocities. The liner part of the stiffness matrix is the same as that used in classical liner FEM. The nonlinear part of the stiffness matrix accounts for geometric nonlinearity and coupling between the axial and bending deformations (centrifugal stiffening effect)	For small strains, the internal forces are linear with respect to the corotational frame. The structural forces are transformed to the global frame using the nonlinear corotational transformation.	The internal forces are nonlinear even for small strains because they are axpressed in terms of nonlinear finit strain and stress measures.
Constraints **a)Hinge joints**	Hinge joints require the addition of	Hinge joints (revolute joints in planar problems and spherical joints in spatial problems) do not need an extra algebraic equation and can be	

	algebraic constraint equations in the absolute coordinate formulation.	modeled by letting two bodies share a node.	
b)General constraints	Constraints due to joints prescribed motion and closed-loops are expressed in terms of algebraic equations. These equations must be solved simultaneously with the governing differential equations of motion. The development of general, stable, and efficient solution procedures for this system of differential – algebraic equations is still an active research area [47-49].	Constraints due to joints and prescribed motion are expressed in terms of algebraic equations. If an implicit algorithm is used, then a system of differential- algebraic equations (DAEs) must be solved. If an explicit solution procedure is used, no special algorithm for solving DAEs is needed.	
Applicability of liner model reduction	• can be applied. • can significantly reduce the computational time. • Appropriate selection of the deformation components modes requires experience and judgment on the part of the analyst. • For accuracy, liner modal reduction should be restricted to bodies undergoing slow rotation or uniform angular velocity. • Nonlinear model reduction [50, 51] can be used for bodies undergoing fast non uniform angular velocity in order to include the centrifugal stiffening effect. However, a modal reduction performed at each time step.	Note practical because the element vector of internal forces is nonlinear in nodal coordinates since it involves a rotation matrix.	Not practical because the element vector of internal forces is nonlinear in nodal coordinates since it involves a nonlinear finite strain measure.
Possibility of using model identification experiments	The mode shapes and natural frequencies used in model reduction can be obtained using experimental modal	Experimentally identified modes cannot be directly used in the model. They can, however, be indirectly used to verify the accuracy of the predicted response and to tune the parameters of the model.	

	analysis techniques, Thus, there is a direct way to obtain the body flexibility information from experiments without numerical modeling.		
Most suitable applications	The floating frame formulation along with model reduction and new recursive solution strategies (based on the relative coordinates formulation) offer the most efficient method for the simulation of flexible multibody systems undergoing small elastic deformations and slow rotational speeds(such as satellites and space structures).	The corotational and inertial frame formulations can handle flexible multibody system undergoing large deflections and large high-speed rigid body motion. In addition, if used in conjunction with an explicit solution procedure, then high-speed wave propagation effects (for example, due to contact/ Impact) can be accurately modeled.	
Least suitable applications	Multibody problems, which involve large deflections.	For multibody problems involving small deformations and slow rotational speeds, the solution time is generally an order of magnitude grater that of typical methods based on the floating frame approach with modal coordinates.	
First known application of the approach to FMS.	Adopted in the late 1960s to early 1970s to extend rigid multibody dynamics computer codes to flexible multibody systems.	Developed by Belytscho and Hiseh [32]. It was first applied to beam type FMS in Hosner [52-54].	Used in nonlinear, large deformation FEM since the beginning of the 1970s. It was first applied to modeling beam type FMS in Simo and Vu-Quoc [55,56].

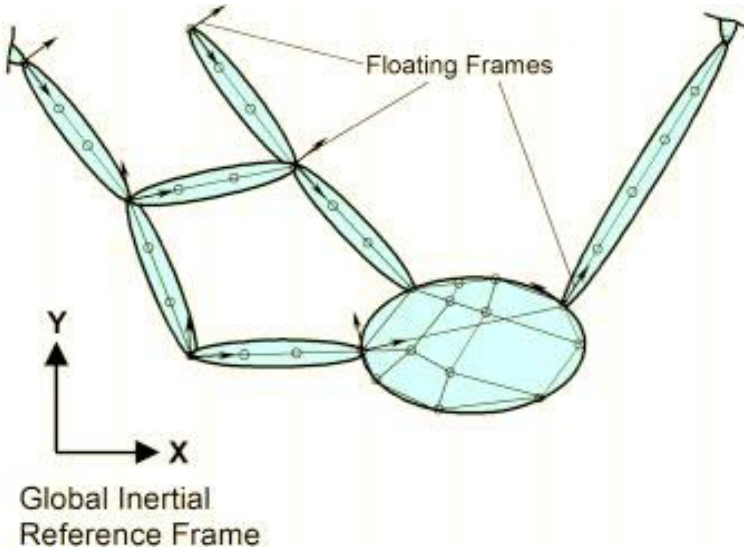

Figure2.1 Floating Frame

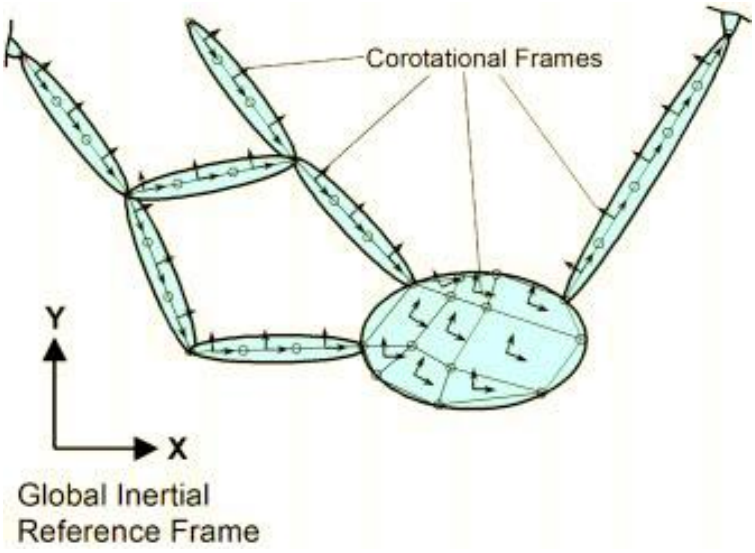

Figure2.2 Corotational Frame

The approach was applied to spatial beams in Belytschko et al [40] and to curved beams in Belytschko and Glaum [57]. In Belytschko et al [58] and Belytschko et al [59], the approach was extended to dynamic modeling of shells using a velocity-based incremental solution procedure.

The inertial frame approach has its origins in the nonlinear finite element method and continuum mechanics principles. These techniques were applied to the dynamic analysis of continuum bodies undergoing large rotations and large deformations (including both large strains and large deflections) since the early 1970s [60, 61].

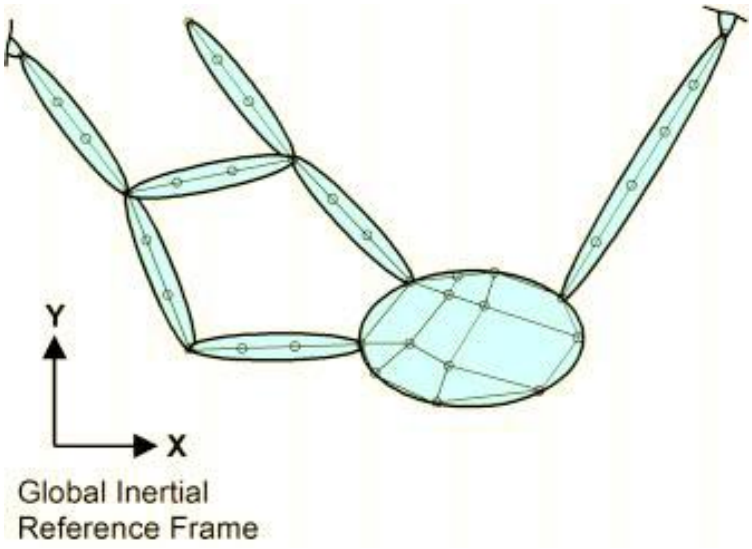

Figure2.3 Inertial Frame

2.1.2 Dynamics of flexible-link manipulators

Dynamics of flexible-link mechanism is a topic that has received wide interests in robotics literature. One of the seminal works on dynamics of this class of mechanisms has been developed by Book, and dates back to 1974 [62]. A brief analysis on the state of the art on modeling of FLM is conducted here, a more complete overview can be found in the review paper [63].

It should be pointed out that robotic systems with flexible link are systems with an infinite number of degrees of freedom, therefore the computation of their dynamics requires to adopt some discretization strategies to bring the dynamic computation to a finite number of DOFs. This is not true if only flexibility at the joints is present, since this kind of effect can be efficiently represented with discrete and concentrated flexible elements, such as springs.

A popular choice is to use the assumed mode formulation, in which the link flexibility is represented by a truncated finite modal series. The main drawback of this method is the difficulty of finding modes for link with non-regular cross section and multi-link manipulators [64].

Another popular approach involves Finite Element Method (FEM), in which the infinite dimension problem is discretized by using some FEM models, the most popular being Euler-Bernoulli beam elements. The use of Timoshenko beams is less frequent, since it allows to perform a better description of the dynamics of FLM only for short links.

In the following some of the most important works reported, making a distinction between single and multi-link manipulators.

Single-link manipulators

The assumed method mode uses a truncated finite model series in terms of spatial mode Eigen functions and time-varying mode amplitudes to represent links deformation. A large number of works on the topics has been done, since there are several ways to choose ling boundary conditions and mode Eigen function. AMM together with Lagrangian dynamics is very popular. Some notable works on the topics are [65], [66], [67], [68], [69], and [70].

AMM has been used together with other formulation, such as Newton-Euler formulation in [71], or Hamilton's principle in [72].

The works reported so far, as well as the vast majority of papers on FLM dynamics, refer only to manipulators with revolute joints. Among the few works including prismatic joints, [73], [74] and [75] should be cited.

The use of FEM discretization has gained popularity in the 90s, as testified by the notable works by Nagarayan and Turcic [76, 77] and Bricout [78]. An Equivalent Rigid Links System (ERLS) has been developed by Chang and Gannon [79]. ERLS formulation has been used also in [80, 81], i.e. the formulation used for the simulation and control design in this dissertation. The formulation by Giovagnoni is based on the virtual work principle. Lagrangian dynamics with FEM discretization is a quite popular approach, as testified by some works such as [82], [83], [84], and [85]. All the papers cited so far deals with planar mechanisms. Analysis of 3D mechanisms appears to be less popular: among the few works available on the subject, [86] deals with a single-link mechanism. While [87] deals with a spatial robot with a flexible prismatic link.

Another frequently adopted strategy for the modeling of FLM is the lumped parameter model. This approach tries to describe the dynamics of FLM using concentrated elements of mass and elasticity, often substituting a continuous flexible elements with a set of rigid elements kept together by flexible elements. Some notable works in this field are [88], [89], [90].

Multi-link maniplutors

Describing the dynamics of a flexible two-link manipulator is not a simple task, since basic models usually not sufficiently accurate. This happens because, as shown by Milford and Ashokanathan [91], the eigenfrequencies of a two-link FLM can vary up to 30% as the manipulators sweeps across its range of motion. Thus a large number of different

approaches have been proposed. Among them, [92] and [93] uses a Lagrangian based finite dimension model with assumed mode method. Morris and Madani in [94], [95] and [96] develop the equation of motion for a two-link manipulator using the Lagrange-Euler formulation and assumed method mode. On the other hand Lee showed in [97] that conventional Lagrangian modeling of FLM is not very accurate for links with rotation, and therefore he proposed a new approach to solve this problem. Newton-Euler formulation together with finite element method has been investigated by Rosado in [98] and [99].

cannot and Schimtz also showed in [65] that multi-link manipulators cannot be described by a linearized model when dealing with large displacement, since the influence of nonlinearities change significantly with the robot configuration. For this class of mechanism a popular approach is based on Lagrangian dynamics, as testified, among others, by the works [100, 62] by Book, [101] by Siciliano, [102] by Chadmil et. al., [103] by Arteage. Moreover, Asada et. al. proposed in [104] an approach based on assumed mode model for a n-link robot using a special moving coordinate systems called virtual rigid link coordinates. Special moving coordinate systems called virtual rigid link coordinates.

FEM is used by Bayo in [66] considering Timoshenko beams including nonlinear Coriolis and Gentrifugal effects for the elastic behavior. The same nonlinear terms are also included in the model by Giovagnoni [81], which has the benefit of considering the fully coupled dynamics of both rigid and flexible motion of a planer FLM with an arbitrary number of revolute joints. The same model can also include rigid elements. Such modeling is based on virtual work principle, FEM with Euler-Bernoulli beams, and ERLS principle. This model has been recently extended to 3D mechanisms in the work by Vidoniet. al. [105]. Such investigation deals with a 3 links flexible robot, and the proposed model is compared with the results from ADAMS software. Other works on mechanisms moving in a 3D environment are [106] by Beres and Sasiadek and [107] by Beres et al. Here Lagreangian finite elements approach and Denavit-Hartemberg method is used. Among the others, [108] should be cited as one of the few (if not only) paper focusing on modeling of five-bar linkages.

2.2 Kinematics of the system

In the formulation here adopted Equivalent Rigid Link Mechanism (ERLS), with respect to which the elastic displacements are defined, is considered. Each link is subdivided into finite elements; in this work, the Euler-Bernoulli model for a spatial beam has been considered for the definition of each finite element. The vector of the nodal elastic displacements of the k-th finite element belonging to the l-th link is called u_k while the vector of the

nodal position and orientation for the k-th finite element of the l-th link of the ERLS is called r_k (Fig.2.4.) The vector b_k, which represents the absolute nodal position and orientation of k-th finite element with respect to the global reference frame, expresses the sum of the nodal elastic displacements and of the ERLS position:

$$b_k = r_k + u_k \tag{2.1}$$

By considering a generic point inside the l-th link, w_x be the positions vector of the generic point of the ERLS and v_x its elastic displacement. Hence, the absolute position p_x of a generic point is given by:

$$P_x = w_x + v_x \tag{2.2}$$

The vectors in eq.2.2.are with respect to a fixed global reference frame {X,Y,Z}: moreover, for each finite element, a local coordinate system $\{x_k, y_k, z_k\}$, which follows the ERLS motion, is defined. The position and orientation of a local reference frame with respect to the global one is given by the position and orientation of the ERLS, which in turn can be expressed by means of a set of generalized coordinate's q. The number of the generalized coordinates of the ERLS is the number of the rigid degrees of mobility of the mechanism (m).

2.2.1 Kinematics of the ERLS

The ERLS kinematics can be described by means of a finite number of degrees of freedom, expressed by a set of generalized coordinate's q. The Denavit-Hartenberg (DH) notation [109] is adopted in this work to describe the translational and rotational motion between different links of a rigid multibody system. Thus, four kinematic entities are sufficient to build a transformation (also called roto-translation) matrix A_i^j between the frames of two links along the kinematic chain of the mechanism:

$$A_i^j = \begin{bmatrix} R_i^j & O_i^j \\ 000 & 1 \end{bmatrix} \tag{2.3}$$

Where R_i^j is the rotation matrix between the j-th and i-th frames and O_i^j the position of the origin of the i-th frame with respect the j-th frame. The nodal position and orientation vector r_k for the k-th element can then be expressed with respect to a suitable local frame. All the r_k s can then be gathered into a unique vector r,

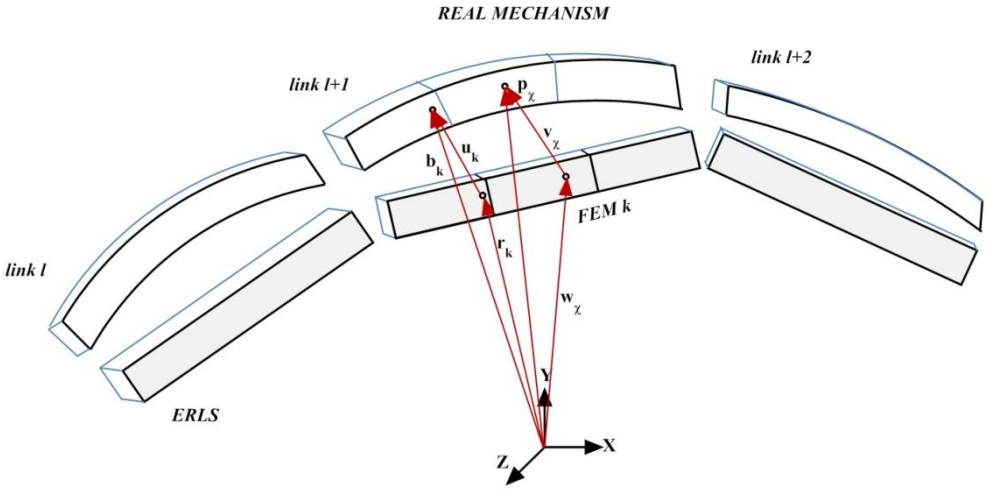

Figure2.4 Model of the mechanism and kinematic definitions; as an example, the l+1-link is discretized with finite elements.

Representing position and orientation of the whole ERLS. The variation dr of the vector r can be expressed as a function of the variation of the vector of the generalized coordinates by means of the Jacobian matrix:

$$dr = j(q)dq \tag{2.4}$$

Where the Jacobian matrix is a function of the generalized coordinates q of the ERLS. The relation which holds between the velocities is:

$$\dot{r}j(q)\dot{q} \tag{2.5}$$

By differentiation eq.2.5. The second order differential kinematics (i.e. the expression for the acceleration) can be obtained:

$$\ddot{r} = j(q)\ddot{q} + \dot{j}(q,\dot{q})\dot{q} = j(q)\ddot{q} + \left(\sum_j \frac{\partial j}{\partial q_j}\dot{q}_j\right)\dot{q} \tag{2.6}$$

Where $\dot{j}(q,\dot{q})$ is the time derivative of the Jacobianmatrix.

2.2.2 Kinematics of the elastic multibody system

Inside the finite elements a rotation matrix $R_l(q)$ frame, and a block-diagonal rotation matrix $T_i^l(q)$, that expresses the transformation from a frame I, in which are expressed the nodal elastic displacements of the considered k-th finite element u_i^j to the reference frame of the l-th link, must be defined. Being two nodes per beam element (six elastic dofs per node) in the Euler-Bernoulli beam formulation, the T-matrix dimension is [12×12]:

$$T_i^l(\mathrm{q}) = \begin{bmatrix} R_i^l & 0 & 0 & 0 \\ 0 & R_i^l & 0 & 0 \\ 0 & 0 & R_i^l & 0 \\ 0 & 0 & 0 & R_i^l \end{bmatrix} \tag{2.7}$$

By introducing the shape function matrix for the interpolation of the k-th finite element defined in the local frame $N_l(x_x, y_x, z_x)$, eq.2.2. Can be rewritten as:

$$P_x = w_x + R_l(q)N_l(x_x, y_x, z_x)T_i^l(q)u_k^i \tag{2.8}$$

In the ERLS, the rotation matrix from the reference frame of each finite element of l-th link to the fixed global reference frame is equal to the rotation matrix from the reference frame of l-th link to the fixed global reference frame.

In order to apply the virtual work principle, the virtual displacements should be used:

$$\delta p_x = \delta w_x + \delta v_x \tag{2.9}$$

Where the first term on the right hand side, i.e. the virtual displacement of point p_x according to the rigid-body kinematics, is given by:

$$\delta w_x = R_l(q)N_l(x_x, y_x, z_x)T_i^l(q)\delta r_k^i \tag{2.10}$$

And the second virtual term of the right hand side δv_xin equation 9 is obtained by considering both virtual nodal displacements δu_k^i and virtual displacementsδqofthe generalized coordinates. This leads to the expression the virtual displacements in the reference frame:

$$\begin{aligned} \delta p_x = {} & R_l(q)N_l(x_x, y_x, z_x)T_i^l(q)\delta r_k^i + \delta R_l(q)N_l(x_x, y_x, z_x)T_i^l(q)u_k^i \\ & + R_l(q)N_l(x_x, y_x, z_x)\delta T_i^l(q)u_k^i \\ & + R_l(q)N_l(x_x, y_x, z_x)T_i^l(q)\delta u_k^i \end{aligned} \tag{2.11}$$

The nodal displacement (the elastic displacement of the node) are small with respect to the rigid body displacement of the ERLS due to the small deformations and large rotations assumption.

The second and third term of eq.2.11 contain the virtual rigid body rotation δR_l or δT_i^l , that can be expressed as:

$$\delta R_l(q)\left(\sum_j \frac{\partial R_l}{\partial q_j}\right)\delta q = R_l'\delta q, \delta T_i^l(q) = \left(\sum_j \frac{\partial T_i^l}{\partial q_j}\right)\delta q = T_i^{l'}\delta q \tag{2.12}$$

Now, the expression of the acceleration of a generic point inside the i-th finite element can be computed by differentiating twice equation 2.8:

$$\begin{aligned}\ddot{p}_x = {} & R_l(q)N_l(x_x, y_x, z_x)T_i^l(q)\ddot{r}_k^i + R_l(q)N_l(x_x, y_x, z_x)T_i^l(q)\ddot{u}_k^i \\ & + 2(\dot{R}_l(q)N_l(x_x, y_x, z_x)T_i^l(q) + R_l(q)N_l(x_x, y_x, z_x)\dot{T}_i^l(q)u_k^i \\ & + (\ddot{R}_l(q)N_l(x_x, y_x, z_x)T_i^l(q) + 2\dot{R}_l(q)N_l(x_x, y_x, z_x)\dot{T}_i^l(q) \\ & + R_l(q)N_l(x_x, y_x, z_x)\ddot{T}_i^l(q))u_k^i \end{aligned} \quad (2.13)$$

The term $\ddot{r}_k^i$ is the linear and angular acceleration of the k-th element of the ERLS expressed in the i-th reference frame. By grouping the kinematic entities of all the finite elements into a unique vector and taking into account equation 2.1, after differentiation:

$$db = dr + du \quad (2.14)$$

If equation 2.4 is substituted into equation 2.14, and the expression set in matrix form, it holds:

$$db = [I \quad J]\begin{bmatrix} du \\ dq \end{bmatrix} \quad (2.15)$$

Where, if the mechanism is discretized into N beam elements, i.e. 2N nodes, and with m the number of ridigdofs of the ERLS mechanism, dim $(db) = [6 \times 2N, 1]$,dim (du) =$[6 \times 2N, 1]$, dim(dq)=[m,1] and dim(j)= $[6 \times 2N, m]$.

The coefficient matrix of equation 2.15 is not square and, thus, more sets of increments $[du^T \quad dq^T]$ of the generalized coordinates of the system are possible for a given contigurationdb of infitesimal nodal displacements. To eliminate this redundancy, the easiest way to force to zero a number of elements of du equal to the number of generalized coordinates of the ERLS. Then, by partitioning du into its independent part (du_{in}) and into its zeroed part (du_0), the elements forced to zero can be eliminated from equation 2.15:

$$db = \begin{bmatrix} I & J_{in} \\ 0 & J_0 \end{bmatrix}\begin{bmatrix} du_{in} \\ dq \end{bmatrix} \quad (2.16)$$

The square matrix of coefficient of equation 2.16 must be non-singular, i.e. the determinant of j_0 must be different from zero, and the generalized coordinates of the ERLS have to be chosen in such a way that no singular configuration is encountered during the motion.

The use of the ERLS allows to exploit a solution for direct kinematics based on consolidated robotic methodologies, i.e. the Denavit-Hartenberg notation, to compute all the $R_l, \dot{R}_l, T_i^l, \dot{T}_i^l, J, j$ matrices in a symbolic form

and, hence, virtual displacements, velocities and accelerations of r without including a specific kinematic solution into the dynamic formulation.

2.3 Dynamic modeling

By applying the principle of virtual work, the dynamic equations of motion for the flexible links mechanism can be obtained:

$$\delta W^{inertia} + \delta W^{ejastic} + \delta W^{external} = 0 \tag{2.17}$$

Where gravity effects are included among external force effects. Equation 2.17 can be rewritten as:

$$\Sigma k \int_{vk} \delta P_k^T \ddot{P}_k \rho_k d_v + \Sigma k \int_{vk} \delta \epsilon_k^T D_k \epsilon_k d_V = \Sigma k \int_{vk} \delta P_k^T g \rho_k dv + (\delta u^T + \delta r^T) \tag{2.18}$$

Where D_k , ϵ_k and ρ_k are respective the stress-strain matrix, the strain vector and the mass density for the k-th volume (finite) element, g is the gravity acceleration vector, and f is the vector of the concentrated external forces and torques. By considering equations 2.8, 2.13, 2.18, the following holds:

$$\begin{aligned}
\Sigma k \int_{v_{k(l)}} & \left[R_l N_l T_i^l \delta r_k^i + \delta R_l N_l T_i^l u_k^i + R_l N_l \delta T_i^l u_k^i + R_l N_l T_i^l \delta u_k^i\right]^T \left[R_l N_l T_i^l \ddot{r}_k^i \right. \\
& + R_l N_l T_i^l \ddot{u}_k^i + 2\left(\dot{R}_l N_l T_i^l + R_l N_l \dot{T}_i^l\right)\dot{u}_k^i \\
& \left. + \left(\ddot{R}_l N_l T_i^l + 2\dot{R}_l N_l \dot{T}_i^l + R_l N_l \ddot{T}_i^l\right) u_k^i \right] \rho_k d_v \\
& + \Sigma k \int_{v_{k(l)}} \left(\delta u_k^i T_i^l B_k^T\right) D_k B_k T_i^l u_k^i d_V \\
& + \Sigma k \int_{v_{k(l)}} \left(u_k^{i\,T} \delta T_i^{l\,T} B_k^T\right) D_k B_k T_i^l u_k^i d_V \\
& = \Sigma k \int_{v_{k(l)}} \left(\delta u_k^{iT} T_i^l N_l^T R_l^T\right) g \rho_k d_v + (\delta u^T + \delta r^T) f
\end{aligned} \tag{2.19}$$

Where $v_{k(l)}$ represents the volume of the k-th finite element of the system, each one blonging to its own l-th link; T_i^l is the block-diagonal matrix of the k-th element belonging to the l-th link that expresses the rotation between the appropriate l-th frame and the local i-th frame, and B_k is the strain-displacement matrix.

The equilibrium equations can be computed by exploiting the complete independence of the nodal elastic virtual displacements δu_k^i and the virtual

displacements of the ERLS δr_k^i that depend on the virtual displacements of the generalized coordinates δ_q .

2.3.1 Local nodal equilibrium

The local nodal equilibrium equations can be obtained from eq. 2.19 by considering:

$$\begin{aligned} &\delta u \neq 0; \\ &\delta r = 0 \Rightarrow \delta R = 0; \delta T = 0; \end{aligned} \tag{2.20}$$

So, eq (2-11) becomes:

$$\delta P_x = R_l(q) N_l(x_x, y_x, z_x) T_i^l(q) \delta u_k^i \tag{2.21}$$

By considering equations 2.13, 2.18, 2.21, the following holds:

$$\begin{aligned} +\Sigma k \int_{v_{k(l)}} \Big[\delta u_k^{i\,T} T_i^{l\,T} N_e^T R_e^T\Big] \big[&R_l N_l T_i^l \ddot{r}_k^i + R_l N_l T_i^l \ddot{u}_k^i \\ &+ 2\big(\dot{R}_l N_l T_i^l + R_l N_l \dot{T}_i^l\big)\dot{u}_k^i \big(\ddot{R}_l N_l T_i^l + 2\dot{R}_l N_l \ddot{T}_i^l\big) u_k^i\big] + \rho_k d_v \\ &+ \Sigma k \int_{v_{k(l)}} \Big(\delta u_k^{i\,T} T_i^{l\,T} B_k^T\Big) D_k B_k T_i^l u_k^i d_V \\ &= \Sigma k \int_{v_{k(l)}} \big(\delta u_k^{iT} T_i^{lT} N_l^T R_l^T\big) g \rho_k d_v \\ &+ (\delta u^T + \delta r^T) f \end{aligned} \tag{2.22}$$

The elements of the mass, Coriolis, gyroscopic damping, centrifugal stiffness and stiffness contributions can be obtained from the integrals appearing in equation 2.22.

$$\int_{v_{k(l)}} T_i^{lT} N_l^T R_l^T \, R_l N_l T_i^l \rho_k d_v = \int_{v_{k(l)}} T_i^{lT} N_l^T R_l^T \, R_l T_i^l \rho_k d_v = M_k \tag{2.23}$$

The stiffness matrix of the k-th element is:

$$\int_{v_{k(l)}} T_i^{lT} B_k^T D_k \, B_k T_i^l d_v = K_k \tag{2.24}$$

The vector of the equivalent nodal loads due to gravity is:

$$\int_{v_{k(l)}} T_i^{lT} N_l^T R_l^T \, g \rho_k d_v = f_{gk} \tag{2.25}$$

The Coriolis terms are related to the terms:

$$\int_{v_{k(l)}} T_i^{lT} N_l^T \dot{R}_l^T R_l N_l T_i^l \rho_k d_v = f_{gk} \tag{2.26}$$

$$\int_{v_{k(l)}} T_i^{lT} N_l^T R_l^T R_l N_l \dot{T}_i^l \rho_k d_v = \int_{v_{k(l)}} T_i^{lT} N_l^T R_l^T R_l \dot{T}_i^l \rho_k d_v = M_{G2k} \tag{2.27}$$

The centidifugal stiffness terms are:

$$\int_{v_{k(l)}} T_i^{lT} N_l^T R_l^T \ddot{R}_l N_l T_i^l \rho_k d_v = M_{C1k} \tag{2.28}$$

$$\int_{v_{k(l)}} T_i^{lT} N_l^T R_l^T 2\dot{R}_l N_l \dot{T}_i^l \rho_k d_v = 2M_{C2k} \tag{2.29}$$

$$\int_{v_{k(l)}} T_i^{lT} N_l^T R_l^T R_l N_l \ddot{T}_i^l \rho_k d_v = \int_{v_{k(l)}} T_i^{lT} N_l^T N_l \ddot{T}_i^l \rho_k d_v = M_{C3k} \tag{2.30}$$

Some equations contain the first andsecond order derivatives of the rotation metrices$R_l$and T_i^l . The $\dot{R}_l$ term can be written as:

$$\dot{R}_l = S(\omega_l) R_l \tag{2.31}$$

Where $S(\omega_l)$ is the skew matrix, function of the $\omega_l = [\omega_{l,x}, \omega_{l,y}, \omega_{l,z}]$ angular velocity:

$$S(\omega_l) = \begin{bmatrix} 0 & -\omega_{lz} & \omega_{ly} \\ \omega_{lz} & 0 & -\omega_{lx} \\ -\omega_{ly} & \omega_{lx} & 0 \end{bmatrix} \tag{2.32}$$

The $\dot{R}_l^T R_l$ term inner M_{G1k} can be expressed as:

$$\dot{R}_l^T R_l = -R_l^T S(\omega_l) R_l = -s(R_l^T \omega_l) = -s\left(\omega_l^l\right) \tag{2.33}$$

The second order derivatives and, thus, the centrifugal stiffness terms, can be expressed in a simple formulation:

$$\ddot{R}_l = \dot{S}(\omega_l) R_l + s(\omega_l) \dot{R}_l = s(\dot{\omega}_l) R_l + S^2(\omega_l) R_l \tag{2.34}$$

Then, also the Coriolis terms can be computed as functions of the generalized coordinates and their derivatives since the angular veloctity and accelerations depend only on them.

Equation 2.22 can be rearranged in a more compact from:

$$\Sigma k\delta u_k^{iT} M_k(\ddot{r}_k + \ddot{u}_k) + 2\Sigma k\delta u_k^{iT}(M_{G1k} + M_{G2k})\dot{u}_k^i + \Sigma k\delta u_k^{iT}(M_{C1k} + M_{C2k} + M_{C3k})u_k^i + \Sigma k\delta u_k^{iT} K_k u_k^i = \Sigma k\delta u_k^T f_{gk} + \delta u^T f \quad (2.35)$$

2.3.2 Global equilibrium

A second set of equilibrium equations, i.e. global equilibrium, can be obtained by considering alternatively:

$$\delta q_j \neq 0, j = 1, \dots, m \Rightarrow \delta r_l \neq 0 \Rightarrow \delta R_l \neq 0; \delta T_e \neq 0; \quad \delta u = 0; \quad (2.36)$$

With m number of the generalized coordinates of the ERLS. So, eq2.11 results:

$$\delta p_x = R_l(q)N_l(x_x, y_x, z_x)T_i^l(q)\delta r_k^i + \delta R_l(q)N_l(x_x, y_x, z_x)T_i^l(q)u_k^i + R_l(q)N_l(x_x, y_x, z_x)\delta T_i^l(q)u_k^i \quad (2.37)$$

And the $\delta R_i, \delta T_i^l$ andδr_k^iterms, taking into account that $\delta q_j \neq 0$, can be viewed as:

$$\delta R_l = \left(\partial R_l/\partial q_j\right) = \delta q_j = R_{l.j}\delta q_j; \quad \delta T_i^l = \left(\partial T_i^l/\partial q_j\right) = \delta q_j = T_{i.j}^l \delta q_j; \quad \delta r_k^i = \left(\partial r_k^i/\partial q_j\right) = \delta q_j = j_{k.j}^i \delta q_j; \quad (2.38)$$

Thus, 2.37 results:

$$\delta p_x = R_l(q)N_l(x_x, y_x, z_x)T_i^l(q)\left(j_{k.j}^i \delta q_j\right) + \left(T_{i.j}^l \delta q_j\right)N_l(x_x, y_x, z_x)T_i^l(q)u_k^i + R_l(q)N_l(x_x, y_x, z_x)\left(T_{i.j}^l\right)u_k^i \delta q_j \quad (2.39)$$

If equations 2.13, 2.18, 2.39, are considered, the following expression can be obtained for each j-th generalized coordinate:

$$\sum_k \int_{v_{k(l)}} \left[R_l N_l T_i^l\left(j_{k.j}^i \delta q_j\right) + \left(R_{l.j}\delta q_j\right)N_l T_i^l u_k^i + R_l N_l\left(T_{i.j}^l \delta q_j\right)u_k^i\right]^T \left[R_l N_l T_i^l \ddot{r}_k^i + R_l N_l T_i^l \ddot{u}_k^i + 2\left(\ddot{R}_l N_l T_i^l + 2\dot{R}_l N_l \dot{T}_i^l + R_l N_l \ddot{T}_i^l\right)\dot{u}_k^i + \left(\ddot{R}_l N_l T_i^l + 2\dot{R}_l N_l \dot{T}_i^l + R_l N_l \ddot{T}_i^l\right)u_k^i\right]\rho_k d_v + \sum_k \int_{v_{k(l)}} \left(u_k^{i\,T} \delta T_i^{lT} B_k^T D_k B_k T_i^l u_k^i\right) dv = \sum_k \int_{v_{k(l)}} \left(\delta q^T j_k^{iT} T_i^{lT} N_l^T R_l^T\right) g\rho_k d_v + \delta r^T f \quad (2.40)$$

The integrals that rise from the inertia virtual work term and, in particular, due to the first term on the right side of eq.2.39, are the same previously computed (eq.2.23, 2.26, 2.27, 2.28, 2.29, and 2.30). As regards as the other terms, the following integrals arise:

$$\int_{v_{k(l)}} T_i^{lT} N_l^T R_{l.j}^T R_l N_l T_i^l \rho_k d_v = M_{1kj} \tag{2.41}$$

$$\int_{v_{k(l)}} T_i^{lT} N_l^T R_{l.j}^T 2\left(\dot{R}_l N_l T_i^l + R_l N_l \dot{T}_i^l\right)\rho_k d_v = 2\left(M_{G11kj} + M_{G12kj}\right) \tag{2.42}$$

$$\int_{v_{k(l)}} T_i^{lT} N_l^T R_{l.j}^T \left(\ddot{R}_l N_l T_i^l + 2\dot{R}_l N_l \dot{T}_i^l + R_l N_l \ddot{T}_i^l\right)\rho_k d_v = M_{C11kj} + 2M_{C12kj} + M_{C13kj} \tag{2.43}$$

$$\int_{v_{k(l)}} T_{i.j}^{lT} N_l^T R_l^T N_l T_i^l \rho_k d_v = M_{2kj} \tag{2.44}$$

$$\int_{v_{k(l)}} T_{i.j}^{lT} N_l^T R_l^T 2\left(\dot{R}_l N_l T_i^l + R_l N_l \dot{T}_i^l\right)\rho_k d_v = 2\left(M_{G12kj} + 2M_{G22kj}\right) \tag{2.45}$$

$$\int_{v_{k(l)}} T_{i.j}^{lT} N_l^T R_l^T \left(\ddot{R}_l N_l T_i^l + 2\dot{R}_l N_l \dot{T}_i^l + R_l N_l \ddot{T}_i^l\right)\rho_k d_v = M_{C12kj} + 2M_{C22kj} + M_{C32kj} \tag{2.46}$$

The $\delta T_{k,i}^{iT}$ elastic virtual work term in equation 2.40 can be transformed into an equivalent from by taking into account the eq2.38:

$$\Sigma k \int_{v_{k(l)}} u_k^{iT} \delta T_i^{lT} B_k^T D_k B_k T_i^l u_k^i \, dv = \sum_j \delta q_j \sum_k \int_{v_{k(l)}} u_k^{iT} T_{i.j}^{lT} B_k^T D_k B_k T_i^l u_k^i \, dv$$

$$= \sum_j \delta q_j \sum_k u_k^{iT} K_{1,k,j} u_k^i$$

$$= \sum_j \delta q_j \, \delta q_j u^T K_{1.j} u \tag{2.47}$$

Now, equation 2.40, for each q_j , can be rearranged in the form:

$$\sum_j \delta q_j \sum_k j_{k,j}^T \big[M_k(\ddot{r}_k + \ddot{u}_k) + 2(M_{G1k} + 2M_{G2k})\dot{u}_k + \big(M_{C1kj} + 2M_{C2kj} + M_{C3kj}\big)u_k\big] + \delta q_j \sum_k u_k^T \big[\big(M_{1kj} + 2M_{2kj}\big)(\ddot{r}_k + \ddot{u}_k) + 2\big(M_{G11kj} + M_{G21kj} + M_{G12kj} + M_{G22kj}\big)\dot{u}_k + \big(M_{1kj} + 2M_{2kj}\big)(\ddot{r}_k + \ddot{u}_k) + 2\big(M_{C11kj} + M_{C21kj} + M_{C31kj} + M_{C22kj} + M_{C12kj} + M_{C32kj}\big)u_k\big] + \delta q_j u^T K_{1.j} u = \delta q_j r_j^T \big(f_g + f\big) \quad (2.48)$$

2.3.3 Constraints

In multi-link robotic system, the system coordinates are not independent because of the specified motion trajectories as well as mechanical joints. These kinematic constraints have to be imposed to the elastic displacements at the joints and introduced into the dynamic formulation. If Fig 2.5. Is considered, it can be seen how two consecutive links have different local frames, fixed according to the DH notation. If the nodal displacements are expressed with respect to the frame of the link to which they belong, the compatibility equations cannot be written without considering both rigid and elastic terms. Indeed, each joint imposes relations between the elastic displacements of the second node of the finite element of the l-th link and the first node of the first finite element of the (l+1)-th link.

If the elastic deformations of the second node of the last finite element of the l-th link and those of the first node of the first finite element of the (l+1)-th link are expressed in the frame of the latter, the compatibility equations can be written in a trivial manner avoiding the necessity to have mixed rigid and elastic terms, and allowing to write only identity equalities case of elementary joints.

According to this idea, the bolck-diangonal rotation matrix T_i^l becomes:

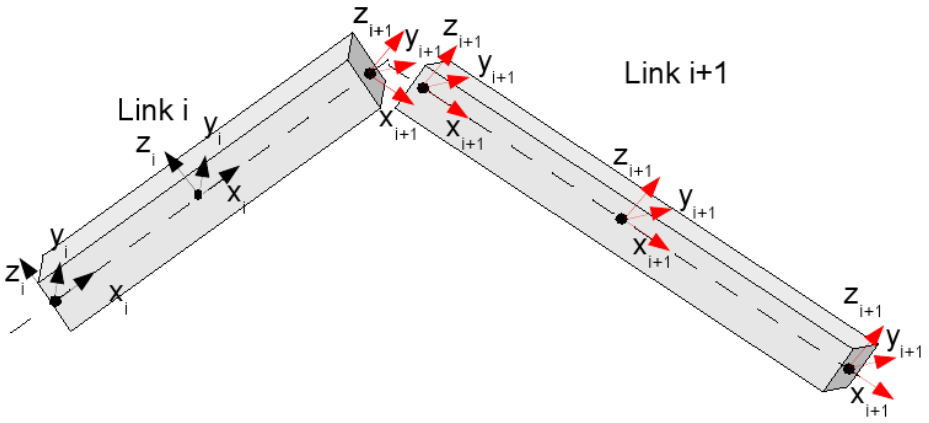

Figure2.5 Considered local frame between two consecutive links

- In case of all the finite elements except the last of a l-th link, a block-diagonal identity matrix:

$$T_i^l = T_l^l \begin{bmatrix} R_l^l & 0 & 0 & 0 \\ 0 & R_l^l & 0 & 0 \\ 0 & 0 & R_l^l & 0 \\ 0 & 0 & 0 & R_l^l \end{bmatrix} = \begin{bmatrix} I & 0 & 0 & 0 \\ 0 & I & 0 & 0 \\ 0 & 0 & I & 0 \\ 0 & 0 & 0 & I \end{bmatrix} \tag{2.49}$$

- In case of the last beam element of a l-th link:

$$T_i^l = T_l^l \begin{bmatrix} R_l^l & 0 & 0 & 0 \\ 0 & R_l^l & 0 & 0 \\ 0 & 0 & R_{l+1}^l & 0 \\ 0 & 0 & 0 & R_{l+1}^l \end{bmatrix} = \begin{bmatrix} I & 0 & 0 & 0 \\ 0 & I & 0 & 0 \\ 0 & 0 & R_{l+1}^l & 0 \\ 0 & 0 & 0 & R_{l+1}^l \end{bmatrix} \tag{2.50}$$

As an example, considering a spherical joint, the rotations about the three axes of the joint are free while the other three elastic dofs are constrained. Thus, if the elastic displacements of the two nodes are expressed in the same frame, the positional elastic dofs have to be set equal. In many other flexible-link multibody models (e.g.FFR), the constraint equations depend on the elastic deformations as well as the reference motion of the deformable system consisting of interconnected links are usually

formulated by mean of a set of nonlinear algebraic constraint equations containing both flexible and rigid terms.

In the FFR formulation, if independent coordinates are considered (i.e. embedding techniques [110]), the constraint forces can be eliminated from the formulation. Even if there is no need to use Lagrange multipliers for dynamic formulation, the mixed constraint equations have to be written and the terms related to the independent and dependent coordinates into the constraint jacobian matrix (i.e. mixed rigid and elastic coordinates) have to be found to reach the final embedded formulation. Thus, one of the main advantages of the proposed formulation with respect to the FFR formulation is that it allows to decouple the kinematic equations of the Equivalent Rigid Link System from the compatibility equations of the displacements at the joints.

2.3.4 Equations of motion and final dynamic formulation

By computing the sums for all the elements of the mechanism, a system of differential equations, that contains local nodal and global equilibrium equations, can be written:

$$\delta u^T[M(\ddot{r}+\ddot{u})+2(M_{G1}+M_{G2})\dot{u}+(M_{C1}+2M_{C2}+M_{C3})u]+\delta u^T K u = \delta u^T(f_g+f) \tag{2.51}$$

$$\begin{aligned}\delta q_j j_j^T[&M(\ddot{r}+\ddot{u})+2(M_{G1}+M_{G2})\dot{u}+(M_{C1}+2M_{C2}+M_{C3})u]\\ &+\delta q_j u^T\big[(M_{1j}+M_{2j})(\ddot{r}+\ddot{u})\\ &+2\big(M_{G11j}+M_{G21j}+M_{G12j}+M_{G22j}\big)\dot{u}\\ &+\big(M_{C11j}+M_{C21j}+M_{C31j}+M_{C22j}+M_{C12j}\\ &+M_{C32j}\big)u\ \big]\delta q_j u^T K_{1.j} u\\ &=\delta q_j j_j^T\big(f_g+f\big)\end{aligned} \tag{2.52}$$

The $\delta u's$ and the $\delta q's$ can be eliminated from equation 2.51 and equation 2.52. Hence, it results a coupled approach for the analysis of a chain of flexible bodies. Local nodal equilibrium:

$$[M(\ddot{r}+\ddot{u})+2(M_{G1}+M_{G2})\dot{u}+(M_{C1}+2M_{C2}+M_{C3})u]+Ku = f_g+f \tag{2.53}$$

Global equilibrium for each $q_j \neq 0, j=1,\dots,m$:

$$
\begin{aligned}
j_j^T[M(\ddot{r}+\ddot{u})+2(M_{G1}+M_{G2})\dot{u}+(M_{C1}+2M_{C2}+M_{C3})u] \\
&+u^T\big[\big(M_{1j}+M_{2j}\big)(\ddot{r}+\ddot{u}) \\
&+2\big(M_{G11j}+M_{G21j}+M_{G12j}+M_{G22j}\big)\dot{u} \\
&+\big(M_{C11j}+2M_{C21j}+M_{C12j}+2M_{C22j}+M_{C31j} \\
&+M_{C32j}\big)u\ \big]u^TK_{1.j}u \\
&=j_j^T\big(f_g+f\big) \qquad (2.54)
\end{aligned}
$$

Where equation 2.53 is a statement of nodal equilibrium, i.e. equivalent loads applied to each node must be in equilibrium, and equation 2.54 is a statement of overall equilibrium, i.e. all equivalent nodal loads applied to the linkage produce no work for a virtual displacement of the ERLS. Some damping has to be introduced to simulate practical applications. If simple Rayleigh damping is introduced and the ERLS nodes accelerations are rewritten by means of the second order differential kinematics equation, equations 2.53 and 2.54, for each $q_j \neq 0, j = 1, \dots, m$, become:

$$M(j\ddot{q}+\ddot{u})+(2M_G+\alpha M+\beta k)\dot{u}+(M_C+K)u=f_g+f \qquad (2.55)$$

$$
\begin{aligned}
j_j^T\big[M\big(J\ddot{q}+\dot{J}\dot{q}+\ddot{u}\big)+2M_G\dot{u}+M_Cu\big] \\
&+u^T\big[M^*j\big(J\ddot{q}+\dot{J}\dot{q}+\ddot{u}\big)+2M^*Gj\dot{u}+M^*cju\big]+\alpha J_j^TM\dot{u} \\
&+u^TK_{1j}u=J_j^T\big(f_g+f\big) \qquad (2.56)
\end{aligned}
$$

$$
\begin{aligned}
where\ {M^*}_j &= M_{1j}+M_{2j}, {M^*}_{G\,j} \\
&= M_{G11j}+M_{G21j}+M_{G12j}+M_{G22j} and {M^*}_{Cj} \\
&= M_{C11j}+2M_{C21j}+M_{C12j}+2M_{C22j}+M_{C31j}+M_{C32j}.
\end{aligned}
$$

Equations 2.55 and 2.56 can be grouped together and rearranged matrix form after discarding the equations for the elastic degrees of freedom that have been zeroed:

$$
\begin{bmatrix} M & MJ \\ J_1^TM+u^T{M^*}_1 & (J_1^TM+u^T{M^*}_1)J \\ \dots & \dots \\ J_m^TM+u^T{M^*}_m & \big(J_m^TM+u^T{M^*}_m\big)J \end{bmatrix} = \begin{bmatrix}\ddot{u}\\ \ddot{q}\end{bmatrix} = -
$$

$$
\begin{bmatrix} 2M_G+\alpha M+\beta k & Mj & M_C+K \\ J_1^T(2M_G+\alpha M)+u^T2M_{G1}^* & J_1^TMj+u^TM^*1^j & J_1^TMj+u^T\big({M^*}_{C1}+K_{11}\big) \\ \dots & \dots & \dots \\ J_m^T(2M_G+\alpha M)+u^T2M_{Gm}^* & J_m^TMj+u^TM^*m^j & J_m^TMj+u^T\big({M^*}_{Cm}+K_{1m}\big) \end{bmatrix}. \qquad (2.57)
$$

$$
\cdot\begin{bmatrix}\dot{u}\\ \dot{q}\\ \dot{q}\end{bmatrix}+\begin{bmatrix} I & I \\ J_1^T & J_1^T \\ \dots & \dots \\ J_m^T & J_m^T \end{bmatrix}\begin{bmatrix} f_g \\ f \end{bmatrix}
$$

In this way, the values of the accelerations can be computed at each step by solving the system 2.57, while the values of velocities of displacements can be obtained by an appropriate integration scheme (e.g. the Runge-

Kutta algorithm) and, hence, the dynamic behavior of the system can be simulated.

2.3.5 Remarks

In order to state the advantages and the differences of the proposed ERLS formulation with respect to others techniques, in particular whit respect to the FFR formulation, some remarks have to made.

If flexible multibody systems are considered, in the FFR formulation, a system of coupled differential equations is obtained being no separation between the rigid body motion and the elastic deformation of the flexible body. Indeed:

- The constraint equations depend on the elastic deformations as well as the reference motion of the deformable bodies;
- The kinematic constraints that describe the joints in the multibody system consisting of interconnected links are usually formulated by means of a set of nonlinear algebraic constraint equations containing both flexible and rigid terms.

If embedding techniques are used:

- From the general formulation it is necessary to find the independent coordinates that, in a large-scale flexible- multibody-system, may be a difficult task (numerical techniques can be adopted);
- The constraint jacobian (equations) can be eliminated from the dynamic formulation, i.e. there is no need to use Lagrange multiopliers for the dynamic formulation, but, to do so, the constraint equations have to be written and the terms related to the independent and dependent coordinates into the constraint jacobian matrix (i.e. terms with mixed rigid and elastic coordinates) have to be found and exploited to reach the final embedded formulation.

In the formulation here proposed, the adoption of an ERLS allows to maintain the kinematice of the rigid system decoupled with respect to the compatibility equations. Hence:

- To set up dynamic equations, the ERLS formulation needs the knowledge of only the rigid dofs;
- The remaining independent dofs (elastic) are automatically chosen when choosing the ERLS, i.e. by forcing to zero a number of elements of DU equal to the number of generalized coordinates fo the ERLS.

- The compatibility equations at the joints are written and included considering only the elastic displacements. Hence, the compatibility equations work only on the elastic displacements;
- The compatibility equations are never used explicitly since they are automatically taken into account when assembling the system matrices. The need to write a set of nonlinear algebraic constraints equations is avoided.

2.4 A (novel) Matlab implementation for the ERLS 3D model

In the previous part a mathematical structure based on the ERLS 3D model was presented. Now, a software implementation of this model has to be stated in order to use it. In the previous works on this model, the Matlab™ computing and the Matlab™ files set was arranged in a serial way, i.e. the mechanism was assembled adding sequentially the links starting from the base one and arriving to end-effector one. For general parallel manipulators is not further possible to use this system, since more than one closed loop-chains can be stated in the kinematic model.

Moreover in the previous simulator a fully symbolic approach was used in order to automate and speed the simulation. For general parallel manipulators is not any more possible to use this approach, since there isn't any way to automate the kinematics analysis.

In this section a new Matlab™ implementation is proposed. The old fully serial structure will be rearranged and a new-tradeoff between symbolic and numeric approach will be taken in order to allow the numeric kinematic analysis and, in the meanwhile, get the faster simulation with the higher versatility.

In the following the structure of the Matlab™ files set will be presented in a top-down way, starting from the integration scheme found out in the last chapter, and going deeper to the basic functions of the systems.

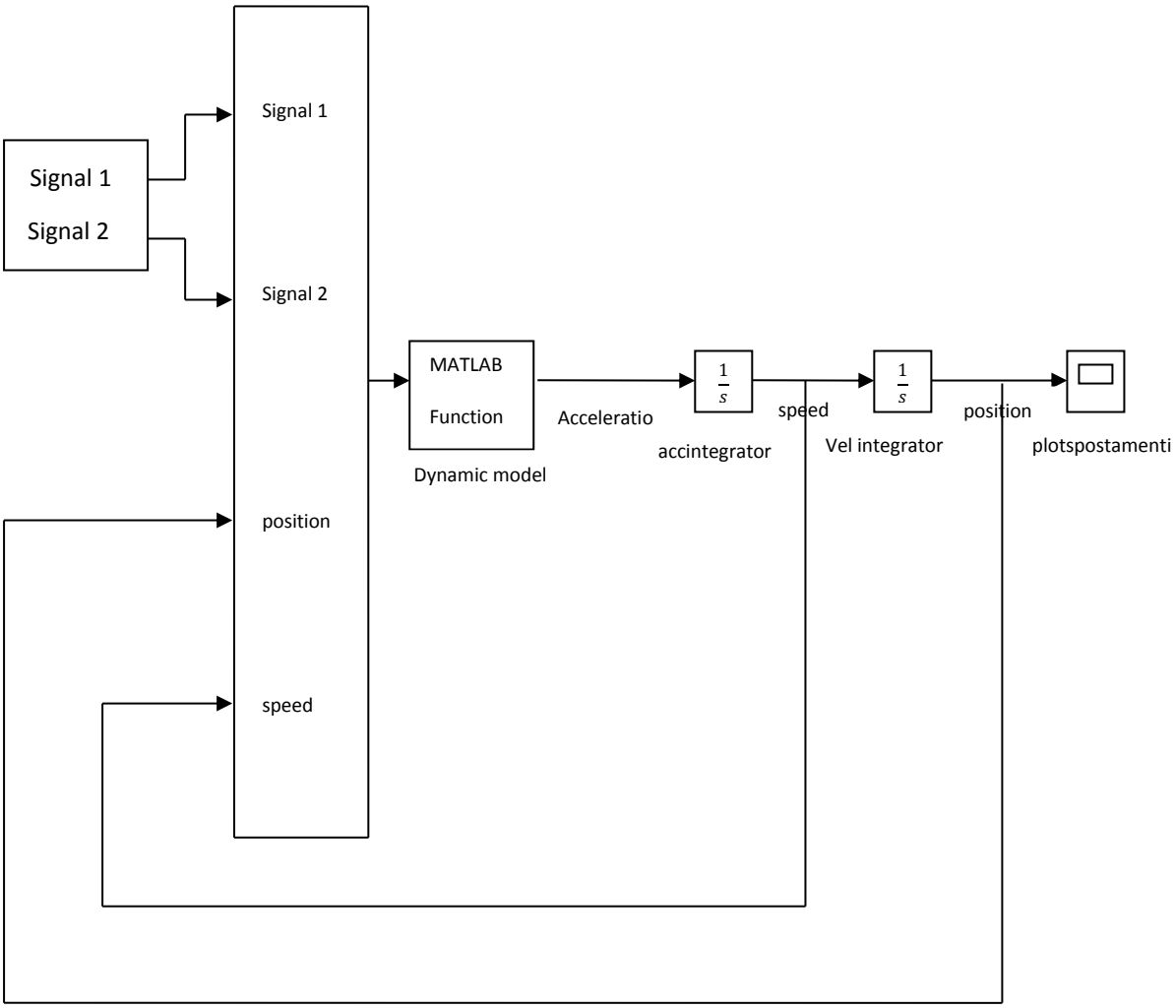

Figure 2.6 Screenshot of the Simulink integration scheme

2.4.1 The Simulink integration scheme

The integration scheme implemented in Simulink is shown in fig (2.6). The Matlab function dynamic. M has the front-end showed fig.(2.7): it takes as input a torque vector, that, for instance, can be a column vector with the torques that can be applied to generalized coordinate of the system (but, in a more complex system, they can be also the external forces on the end effector). The other two inputs are the position X, and the elastic speed vectors$\dot{X}$. They both are a column vector whose length is the number of degrees of freedom of the system (translational and rotational) plus the free coordinates status. While the torque vector is stated external by the user, the position and speed vectors are computed by Simulink at each

time step though integrations from the unique output of the under analysis Matlab function, that is the acceleration vector$\ddot{X}$.

More detailed information about the setup of the simulation (solver, time step,…) will be given further on in the case analysis studies, since they are dependent on the mechanism under analysis and, in particular, on its flexibility factor.

2.4.1.1 The Matlab function core

The core of the simulation is the previously cited Matlab function dynamic. M that has to be evaluated for each time step. Its structure is showed in fig (2.7):

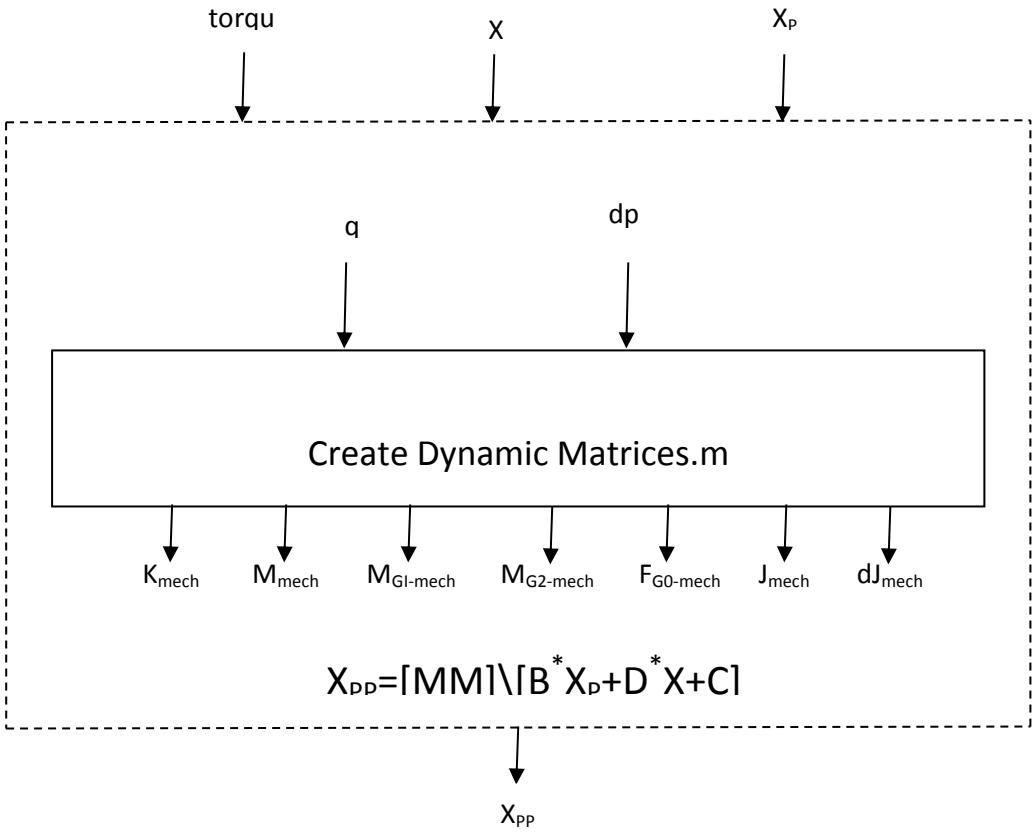

Figure 2.7 Flow-chart to the dynamic. M Matlab function that is the core of the integration scheme for the Simulink model.

The position q and speed $\dot{q}$ of the free coordinates are extracted from the position x and speed $\dot{x}$ vectors and used as a unique input for the create Dynamic Matrices. M function that will compute the basic dynamic matrices$M_{mech}, K_{mech}, M_g1 - mech, M_g2 - mech, F_{mech}$and the kinematic jacobian matrices j_{mech} and its time derivative that whole highlighted in the previous chapter. They are the matrices representing the whole

assembled/ constrained mechanism. The input and output of this function is fully numeric.

These kinematics and dynamic matrices are put together in order to write the integration scheme and highlight the matrix MM that multiplies the column acceleration vector $\ddot{x}$, matrix B that multiplies the column speed vector $\dot{x}$, the D matrix that multiplies the x vector and the known vector C. After that, the system has to be solved for $\ddot{x}$ and, in order to do that, the coefficient matrix has to be squared, neglecting a number of elastic degress of freedom equals to the number of generalizedcoordinantes added to find an ERLS as much as possible close to the real flexible manipulator in order to fit better the small displacement assumption. With the chosen ERLS, the matrices are squared and the $\ddot{x}$ solution/output can be found.

2.4.2 Creation of the dynamic mechanisms matrices

In the previous section, the create Dynamic Matrices. M function was used. In this section a description of it will be given. The internal algorithm and the front-end of this function is shown in fig.(2.9). This function takes as input the vector of position q and speed $\dot{q}$ of the free coordinates. As output, the mass, damping, Coriolis, gravity matrices $M_{mech}, K_{mech}, M_g 1 - mech, M_g 2 - mech, F_{mech}$ will be given.

In the serial simulator of the past works, this function was just a substitution: the matrices were offline computed in a symbolic way as a function of the free coordinates of the system. This approach is not more possible, since the direct kinematics of parallel manipulators has not an analytical description. This means that a numerical approach has to be taken. As it will be showed in the following, a trade-off between numerical and symbolic approach will be taken, otherwise a fully numeric approach will result too much time-consuming. For these issues, the function under consideration has been completely rearranged. Inside it, four parts can be highlighted, and they will be discussed with more detail in the following subsections

- Kinematics analysis
- Compute useful rotation matrices and speed vectors
- Compute dynamic link matrices
- Assembly dynamic mechanism matrices

2.4.2.1 Kinematics analysis

The analysis computed by the Matlab software was about direct kinematics, speed and acceleration analysis. For the ERLS model not the whole stuff in needed, and some of it can be avoided, granted a boost in

time-consuming. In particular from the direct kinematics, just only the angle described by each link is needed (in order to compute the rotation matrices useful to compute the links dynamic matrices). From the speed and acceleration analysis only the jacobian matrix and its time derivative have to be given. Since the time derivative jacobian matrices has to be found out, the jacobian matrix has to be written in an analytical way in order to make possible its analytical differentiation. So, it is not possible to use the previously used.

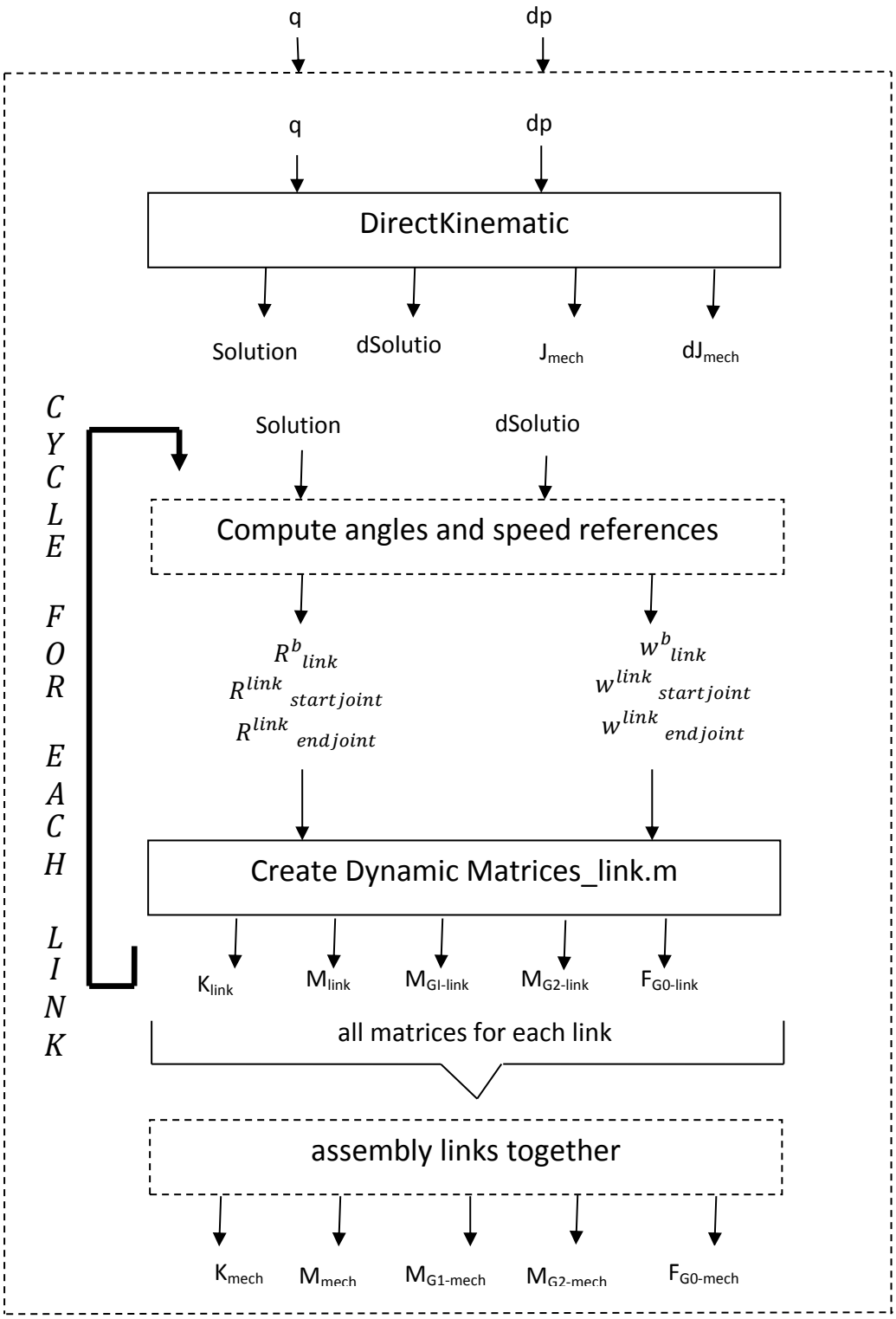

Figure2.8 Flow-chart of the create Dynamic Matrices. M function that is used online in order to create the needed dynamic matrices for the ERLS model

Numerical way to get the jacobian, since there isn't an easy numerical way to get the time derivative jacobian.

Moreover the jacobian matrices have to encompass the speed relations not only among the free coordinates and the reference frames spread for each joint, but also for each node inside each link. This stuff has to be computed in a different way for each mechanism we would like to deal with, since there is no way to automate the direct kinematic analysis for parallel manipulator.

Once the jacobian matrix and its time derivative have been computed, the task is to assembly these informations with the constraint mechanism, i.e. according to the degrees of freedom constranints stated in the ERLS model chapter. For serial manipulators, this was an easy task: just overwrite the jacobian of the last node of a link, with the jacobian of the first node of the following link. This was done by means of a connectivity vector as shown below

$$C = [19{:}30 \quad 36{:}41]$$

Where the size of C (18 in this example) is the number of degrees of freedom of the under analysis link. For the above connectivity vector the index number is the jacobian row number of the link, while the actual number written on the vector C is the number of the row of the mechanisms jacobian in which that links jacobian row has to be placed. Applying this procedure sequentially from the link connected with the base frame to the end effector, the jacobian of the first node of the following link overwrites the jacobian of the last node of the previous link.

However, for parallel manipulators a new strategy has been used, since the fully sequentially approaches are not more possible, since it is not move well defined what next link means. For this issue, according with the rule for the order of the degrees of freedom stated in the ERLS model chapter, a double connectivity vector can be written as follow

$$C = [19{:}30 \quad 36$$
$$1{:}12 \quad 18] ;$$

Where the second row indicates the jacobian rows of the link under analysis while the first row represents the mechanism jacobian rows. This means, for the above example, that the 1 to 12 rows of the links jacobian has to be placed into the 19 to 30 mechanisms jacobian rows and, finally, the 18^{th} row of the links jacobian has to be placed into the 36^{th} row of the mechanisms jacobian. So, for each mechanism, the kinematic part has to compute:

- Angular position of each link
- Angular speed of each link
- Full mechanisms jacobian matrix
- Full mechanisms time derivative jacobian matrix

This is done by means of the direct Kinematic. M and differential Direct Kinematic with Node jacobian. M Functions that have to be written ad hoc for each mechanism since, so far, hasn't been found a way to automatic compute the kinematics analysis of general parallel manipulators.

2.4.2.2 Compute useful rotation matrices and speed vectors

In order to compute the dynamic links matrices (in the following part), there will be needed some relative rotation matrices, and some relative angular speeds of the links with respect to the base reference frame and with respect to the joint reference frame. In particular, for each joint, there will be needed:

- The links rotation matrix of the link with respect to the base reference frame, i.e. $R^{b}_{i-th-link}$
- The links start joint rotation matrix with respect to the links reference frame, i.e.$R^{i-th-link}_{i-th-link-startjoint}$
- The links end joint rotation matrix with respect to the links reference frame, i.e$R^{i-th-link}_{i-th-link-endjoint}$
- The links angular speed of the link with respect to the base reference frame, i.e$\omega^{b}_{i-th-link}$
- The links start joint angular speed with respect to the links reference frame, i.e$\omega^{i-th-link}_{i-th-link-startjoint}$
- The links end joint angular speed with respect to the links reference frame, i.e$\omega^{i-th-link}_{i-th-link-endjoint}$

For the first three matrices, its not necessary to compute and fed the following part with the whole nine elements of the 3x3 rotation matrices, but if the mechanism is planer, just one rotation angle will be enough to represent one rotation matrix; on the other hand, for spatial manipulators, three angles will be enough to reconstruct the whole nine elements (the three Euler angles). Summarizing,

- For planer manipulators it will be enough to compute three revolute angles (one for each rotation matrix), and three angular speeds (just the orthogonal one to the plane)
- For spatial manipulators it will be enough to compute the three Euler angles for each rotation matrix, and the whole three elements for each angular speed.

For further information's have a look at the Matlab code and its comments in Create Dynamic Matrices.

2.4.2.3 Compute dynamic link matrices

In the previous simulator for spatial robot described with ERLS 3D-model, the whole dynamic mechanisms matrices were symbolic computed off-line, as a function of the generalized coordinates q and their speeds $\dot{q}$. In the on-line there was just a substitution of their values, and the job was done. As discussed previously, for a parallel manipulator is not more possible this approach, since the direct kinematics is pretty complicate and it is not more feasible to manage such a complicate symbolic structure. It has been decided to stop the symbolic offline compute the previously discussed angle position and speed, and substitute them into the just offline computed dynamic link matrices. Of course, the user that is simulating the model can choose to use on or more beams for modeling each link: for this reason, in the create Dynamic Link Matrices. M there are just offline computed the symbolic dynamic link matricesexpression for links modeled with one or more beams, and the right matrix will be chosen just for the set of precomputed matrices.

In has been chosen to stop the symbolic computing at the links dynamic matrices creation as an optimal tread-off between flexibility and good time consuming. Indeed, more stuff is computed offline, speeder will be the simulation: however, if weve decided to get an upper level symbolic description, we should have just fixed the number of beams for model each link, reducing the flexibility for the user that want to simulate different number of beams combination for each link. Moreover, the number of Euler angles and speed rotations of each link and joint were going to exponentially increase, leading to an unmanageable model due to the big amount of data to be substituted. So this is the reason for not choose a lower level symbolic offline description. The reason for not choose a lower level symbolic description is straightforward: it will get a more time-consuming task.

A deeper description of how to precompute offline this matrices will be given in a following section.

2.4.2.4 Assembly dynamic mechanism matrices

As a last task for the create Dynamic Matrices. M function, the previously computed dynamic link matrices have to been assembled in order to satisfy the various links constraints.

The first step is to write an empty matrix with the total dimension of the mechanism dynamic matrices size. These matrices will be filled up with the

dynamic matrices of each link, conveniently constrained following the rules previously stated. Hence, for each link, it is possible to define a connectivity vector for each link, for instance,

$C = [19{:}30 \quad 36{:}41]$

With the meaning that the first 12 row/ column of the dynamic matrices under analysis have to been added to the 19 to 30 row/ column of the mechanism matrices, and the last 6 row/ column of the link dynamic matrices have to been added to the 36 to 41 row/ column of the mechanism matrices. In parallel manipulator it is possible that more than two links add some constraint information to the same row/ column, since more than two links can converge to the same joint, whilst in serial manipulator this was not possible. In this case, differently from the creation the jacobianJ_{mech} and its time derivative matrices, it is not necessary to define a double connectivity vector C since addition is obviously commutative, while overwriting is not.

2.4.3 Creation of the dynamic links matrices

As described before, these matrices are computed offline in order to save time during the online computation. Hence, the create Dynamic Matrices Link. M function computes the symbolic expressions of $M_{mech}, K_{mech}, M_g1 - mech, M_g2 - mech, F_{mech}$ of a generic link, given the rotation matrices and the angular speeds with respect to the base frame, start-joint and end-joint references that describe it.

The job of this function is carried out in the way showed in fig (2.9).

1. Firstly the functions that create the single beam dynamic matrices are computed, just making use of the mechanical information stored in a mechstruct (mass, density, flexibility…), the $R^b_{i-th-link}$ rotation matrix that is needed for the gravity vector F_{link} and the $\omega^b_{i-th-link}$ angular speed that is needed for the First Coriolis Matrix $M_g1 - link$. All these matrices will be used as a starting points for the whole others beam into the same link.

2. The previous computed matrices for each beam are stached up creating square matrix of size 12, 18, 24… the means links built respectively with

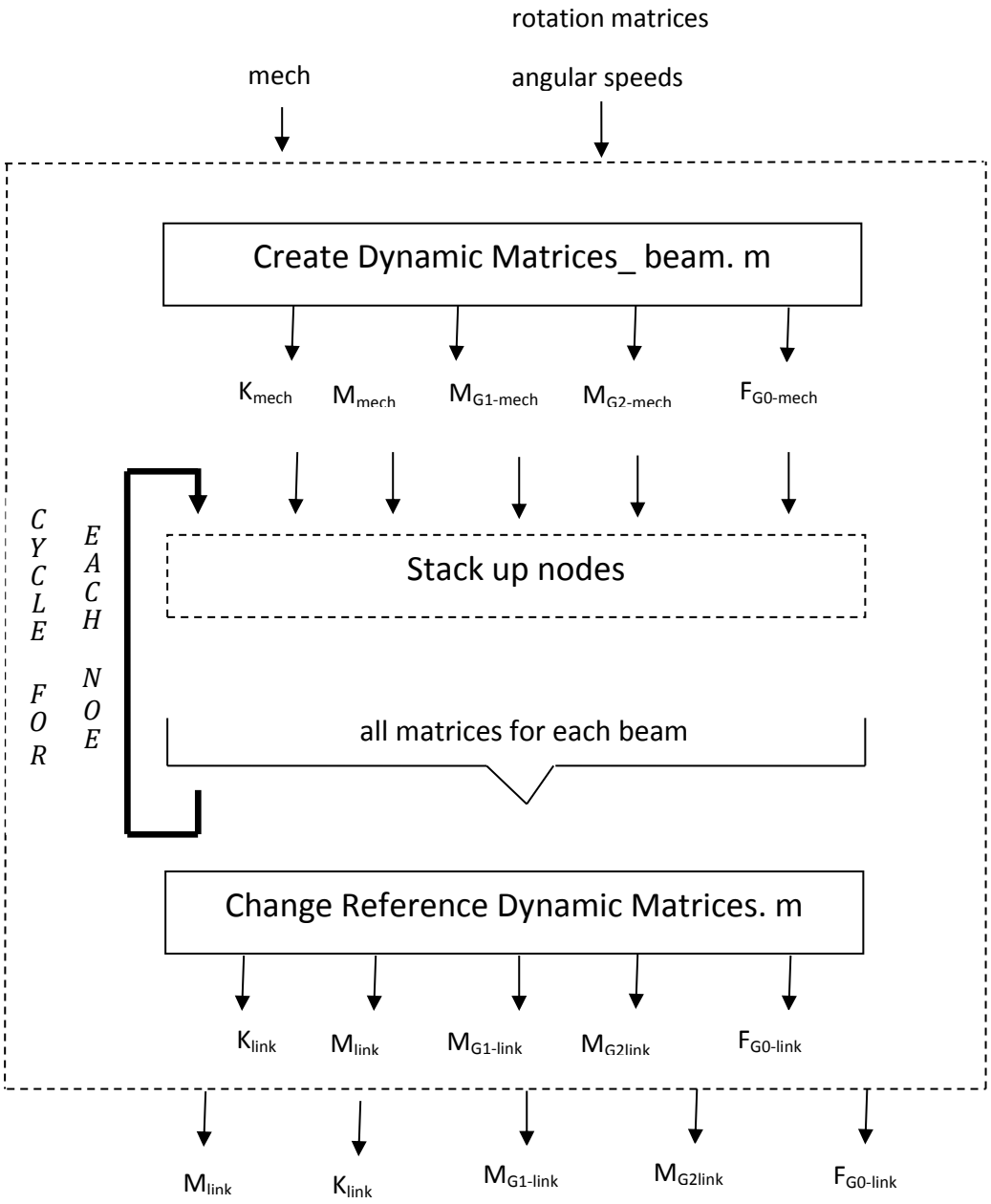

Figure2.9 Flow-chart of the create Dynamic Matrices Link. M function that is used offline in order to create a library for the dynamic links matrices.

1, 2, 3… beams each. Indeed the internal degrees of freedom inside each link are always independent among themselves so they can be easily stacked up. This piling up has to be done for each beam inside the link.

3.As a last job, the first and last node information's have to be rotated into the reference frame chosen for the joint they will be placed. For this task the change Dynamic Reference Matrix. M taken the link matrices as a input

an, given the Euler angle of the rotation matrix that describe the first and last joint for each link, the first and the last 6 degrees of freedom for each link are multiplied for the right rotation matrix, hence put in the correct reference frame.

It is easy to understand that this function will take quite a lot time to be computed: the internal integral that has to been computed for the beams are quite time-consuming. Anyway this is not a problem, since this function is run just one in the life of the simulator, since its results are generally valid for each link of whatever mechanism, so these results are just memorized and simply replaced on line with the actual parameters of the robot under analysis.

2.4.4 Graphic view of Matlab software simulator

The Matlab^{TM} simulator is structured in three main parts:

a) The first is related to the DH, geometrical and mechanical parameters definition.

In this part, the main concepts of robotics kinematics, e.g. Denavit-Hartenberg notation, have been exploited in order to give to the user the possibility to create a generic serial robot.

The starting page of the simulator user interface is presented as a list of pre-analyzed robots which have been previously evaluated from the symbolic point of view. In this case, the user can decide which configuration of the robots wants to load. Robots provided by default have been chosen considering the benchmarks proposed by the literature of multibody dynamics and the most common serial spatial robots They are as follows:

- Simple pendulum;
- Planar double pendulum;
- Spatial double pendulum;
- Anthropomorphic manipulator;
- Anthropomorphic robot with spherical wrist;
- Manipulator DLR with spherical wrist.

Alternatively, the user can place any other mechanisms to analyze with pressing the New Configuration button. The first menu of the simulator is shown in Figure 2.10.

Once one of the options is chosen by the user, a second interface is loaded; in this page the kinematic, geometrical and mechanical data essential for the definition of the robot are required.

To descried unambiguously the type of manipulator is to be analyzed from the kinematic point of view, the simulator asks DH parameters in this page.

The additional parameters that have to be entered by the user are related to characteristics of each link of the robot. In particular, the length L [m], the width in y direction [m], the depth in the z direction [m], the density $[kg/m^3]$, the module of elasticity E $[N/m^2]$, the coefficient to poisson v and, finally, the number of elements for each link have to be defined.

Also, the user must enter other effective parameters on the mechanism performance, like the direction the force of gravity which can be in the direction of y axis or z axis, and the damping coefficients.

The final set of data, that covers a very important aspect of the entire analysis, is the inhibited degrees of freedom, i.e. degrees of freedom that are set to zero.

b) The second is related to the symbolic matrix calculus of the dynamic model and to the visualization of the mechanism;

After loading and defining the data to the simulator, by pressing the Robot Looks button the simulation begins. The purpose of this phase is to create and build all the necessary data to perform the dynamic analysis of the chosen spatial robot.

First of all the parameters are checked in order to evaluate their feasibility; after that the first and second order kinematics are computed; then, an iterative symbolic algorithm, based on he previously described ERLS formulation, allows to build the main matrices of the dynamic formulation; finally all the symbolic variables and created symbolic matrices such as jacobian matrix, mass matrix, stiffness matrix, Coriolis and external forces matrices are saved.

The procedure is completely iterative and the constraint equations are automatically taken into account when constructing the matrices allowing to avoid the need of a new set of equations. Matrices are computed along the links chain starting from the chassis.

After the initial calculation of the characteristic matrices of the robot, the simulator plots the position of the entire mechanism as shown in Figure 2.11. The upper figure shown the robot with the main frames according to DH parameters while the bottom figure shows the robot where the local reference coordinate frames are highlighted.

c) The third part is related to the dynamic simulation and results evaluation.

The dynamics of the system are implemented and simulated thanks to the Simulink toolbox of Matlab™.

The time of simulation and the solver to use in Simulink are the two parameters that are introduced directly while external input forces or torques have to loaded and defined in the Simulink environment. After that, the system in a static condition is evaluated in order to obtain the initial conditions of the system. Then, the real values are substituted into the symbolic part. Finally, by using and linking the suitable Matlab™ functions in Simulink, the dynamic behavior of the robot is simulated and the results visualized and saved.

The simulator, as output, plots the displacement of the nodes of the system according to the time and also the trajectory followed both by the flexible-link robot and by the chosen ERLS.

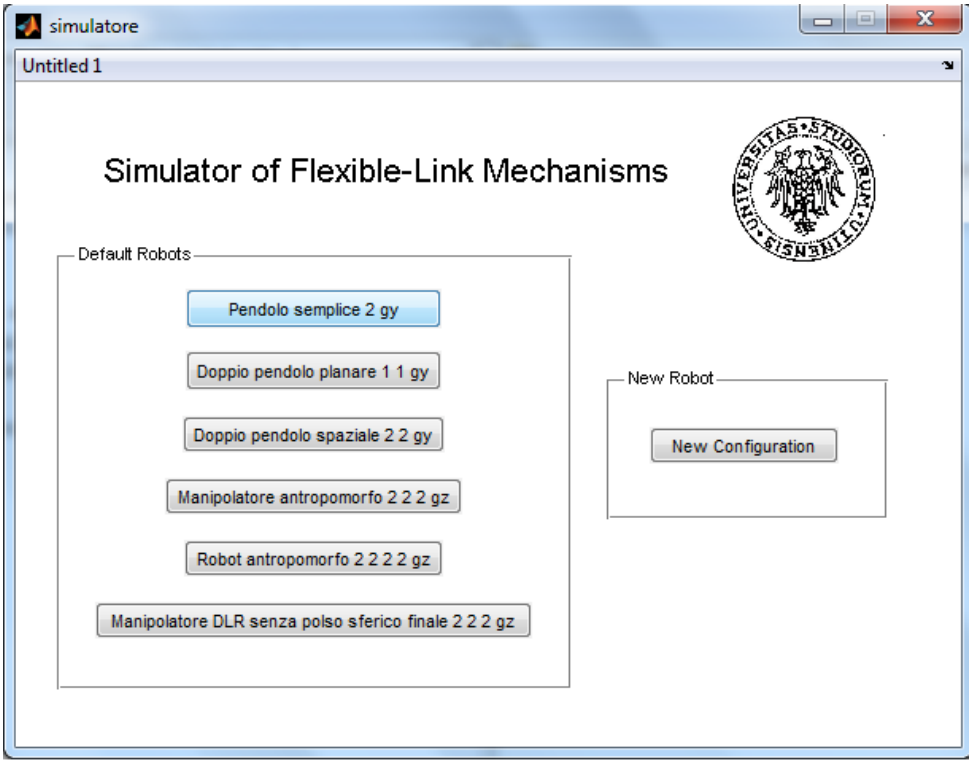

Figure2.10 The first menu of the simulator

2.5 SIMULATION RESULTS

In order to show the capabilities of the simulator and to validate if, the ERLS simulation results are compared with those obtained by means of the Adams-FlexTM software that exploits the FFR approach and models the flexible mechanisms by means of a component mode synthesis (CMS) technique based on the Craig-Bampton method [111].

In this paper, two different mechanisms have been considered as benchmarks:

a) The first mechanism considered as a benchmark is a three degrees of freedom anthropomorphic robot (Figure 2.12).

Which main kinematic, geometrical and mechanical parameters are shown in Table2.2. It has three links end three revolute joints.

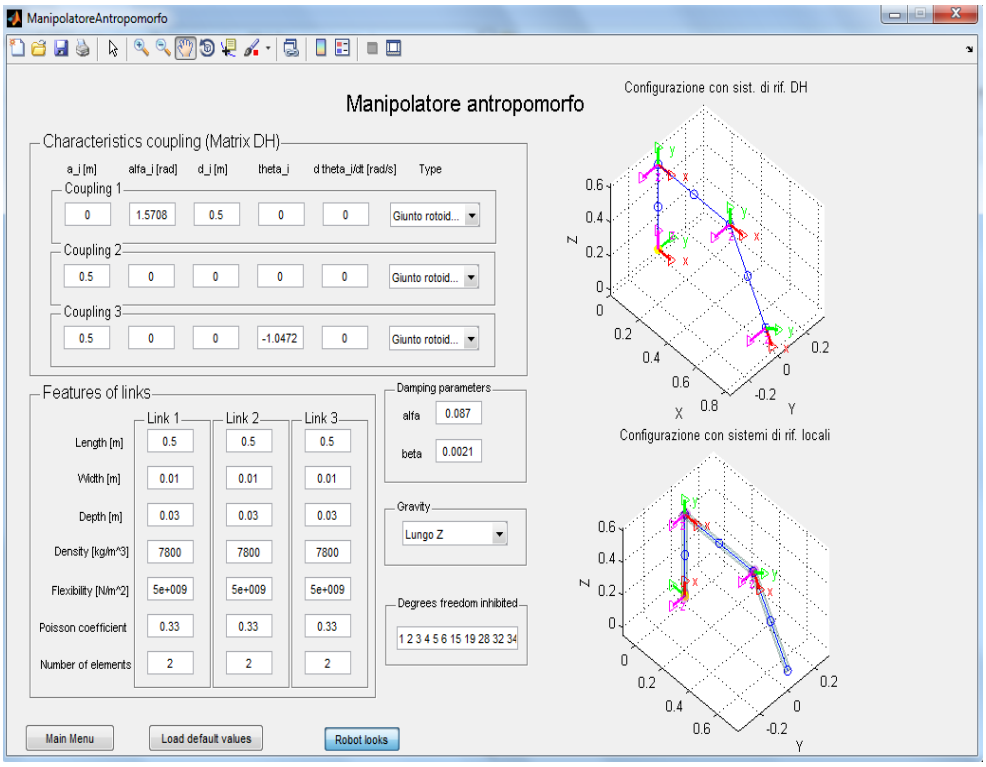

Figure2.11 Starting position of the entire mechanism for anthropomorphic robot

The beam section is rectangular and external forces and torques are present as gravity effect and torque applied on the first joint. For each link of the mechanism, only two beam elements (thus three nodes) has been considered, so nine nodes and three rigid degrees of freedom (represented in Figure 2.12. as q1,q2 and q3) are present.

In order to fulfill the data requested, the fake degrees of freedom have to be considered and the related equations imposed. Let $s_x(i), s_y(i), s_z(i)$ be the X and Y rotations, respectively, the compatibility equations impose:

$$
\begin{aligned}
&s_x(1) = s_y(1) = s_z(1) = 0; s_{rx}(1) = s_{ry}(1) = 0 \\
&s_x^k(3) = s_{rx}^k(4); s_y^k(3) = s_y^k(4); s_z^k(3) = s_z^k(4) \\
&s_{rx}^k(3) = s_{rx}^k(4); s_{ry}^k(3); s_{rx}^k(6) = s_{ry}^k(4) \\
&s_x^k(6) = s_x^k(7); s_y^k(7); s_z^k(6) = s_z^k(7) \\
&s_{rx}^k(6) = s_{rx}^k(7); s_{ry}^k(6) = s_{ry}^k(7)
\end{aligned} \tag{2.58}
$$

Where k superscript refers to a generic common local frame. Now to be able to correctly define the ERLS, values of the elastic displacements of the three among the remaining degrees of freedom must be zero. In this case, three sets of degrees of freedom have been chosen:

$$s_{rz}^k(3) = 0; s_{rz}^k(4) = 0; s_{rz}^k(7) = 0 \quad (A)$$
$$s_{rz}^k(3) = 0; s_{rz}^k(4) = 0; s_{rz}^k(9) = 0 \quad (B)$$
$$s_{rz}^k(3) = 0; s_{rz}^k(6) = 0; s_{rz}^k(9) = 0 \quad (C)$$

In order to simulate the flexible-link mechanism with different equivalent rigid-link systems and show the effectiveness of a correct choice.

In the first simulation, Rayleigh damping coefficients are introduced as $\alpha = 0.087$and $= 0.0021$, the Yongs module is $9^*10^9(N/m^2)$ and the input torque is applied on the first joint. In this case, for zeroed degrees of freedom in Matlab™ software simulator, set of A has been chosen.

The Y coordinates of the tip of the second and third links of the anthropomorphic robot for the three selected sets of degrees of freedom have been plotted in Figures 2.13 and 2.14 where the simulation result of the three sets can be seen.

Table 2.2 Mechanism parameters

Link	ai	oi	di	Θi	Length (m)	Width (m)	Depth (m)	Density (kg/m^3)	Poissons Ratio
1	0	π/2	L_1	q_1	0.5	0.03	0.01	7800	0.33
2	L_2	0	0	q_2	0.5	0.01	0.03	7800	0.33
3	L_3	0	0	q_3	0.5	0.01	0.03	7800	0.33

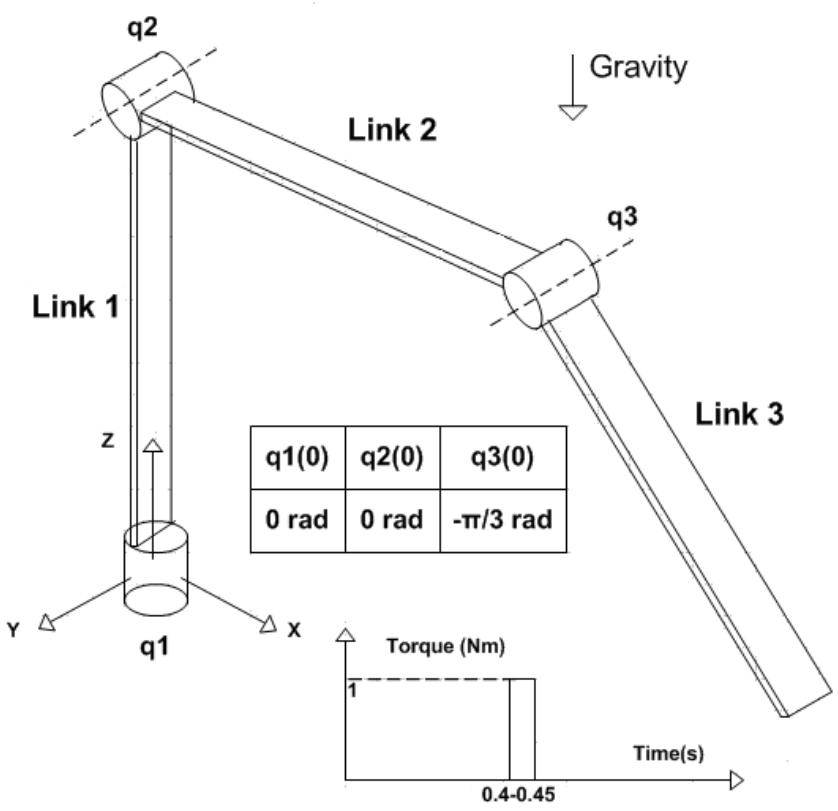

Figure2.12 Anthropomorphic robot

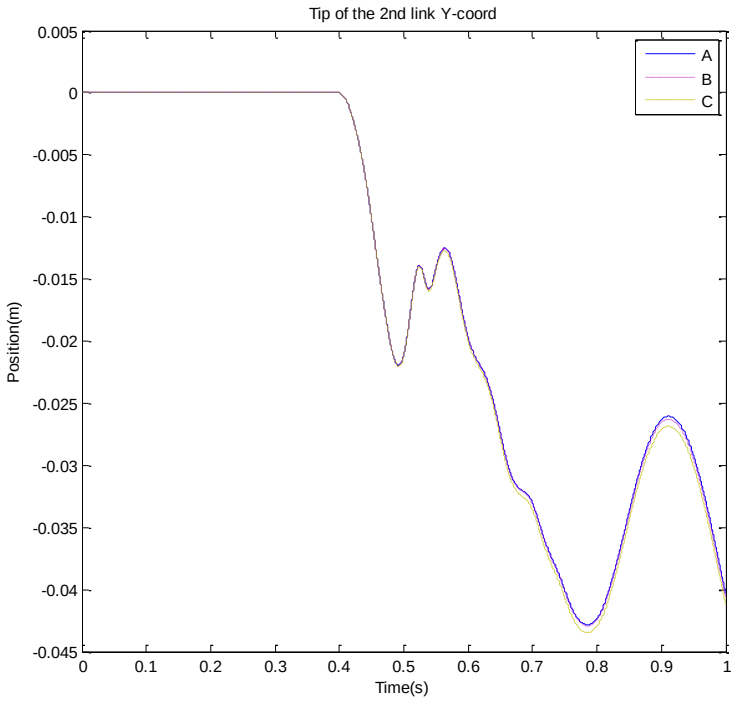

Figure2.13 Tip of the 2nd link Y-coord

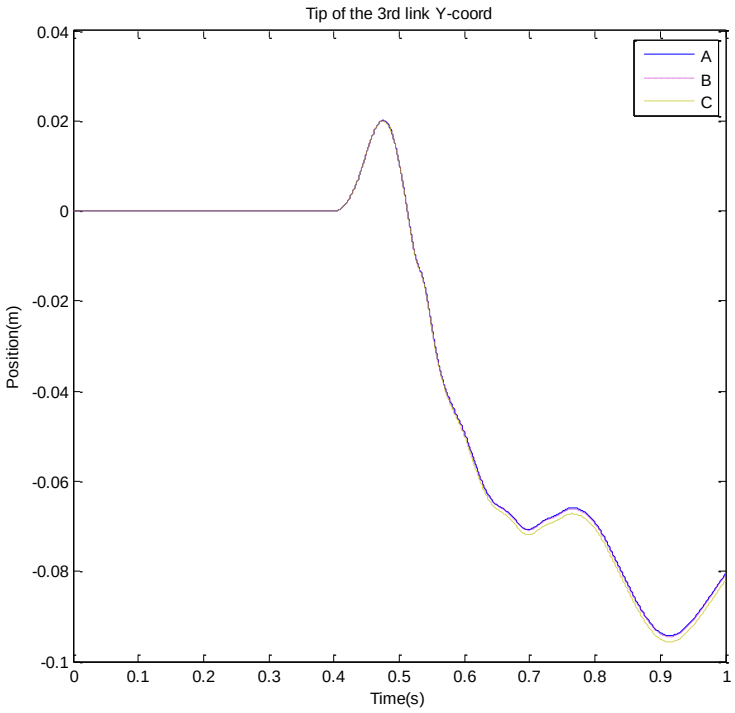

Figure2.14 Tip of the 3rd link Y-coord

A second simulation has been carried out by changing some parameters: the Rayleigh damping coefficients are set to $\alpha = 0.087$and $\beta = 0.00.21$ and the Yongs module to $5^{*}10^{9}(N/m^{2})$. The input torque is applied on the first joint and its trend is the one shown in Fig2.12. The zeroed degrees of freedom in Matlab™ software simulator have been chosen as the A set previously defined.

The positions of the links of anthropomorphic robot are plotted (Figures 2.15-2.20.) and compared with the results provided by the Adams™ software (Figures2.21-2.24.) Showing a very good agreement both in amplitude and frequency.

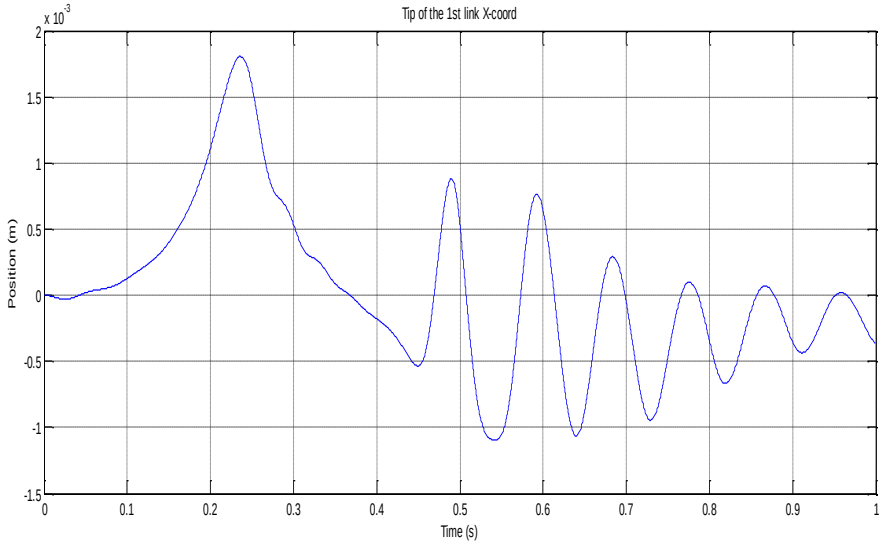

Figure2.15 Tip of the 1st link X-coord

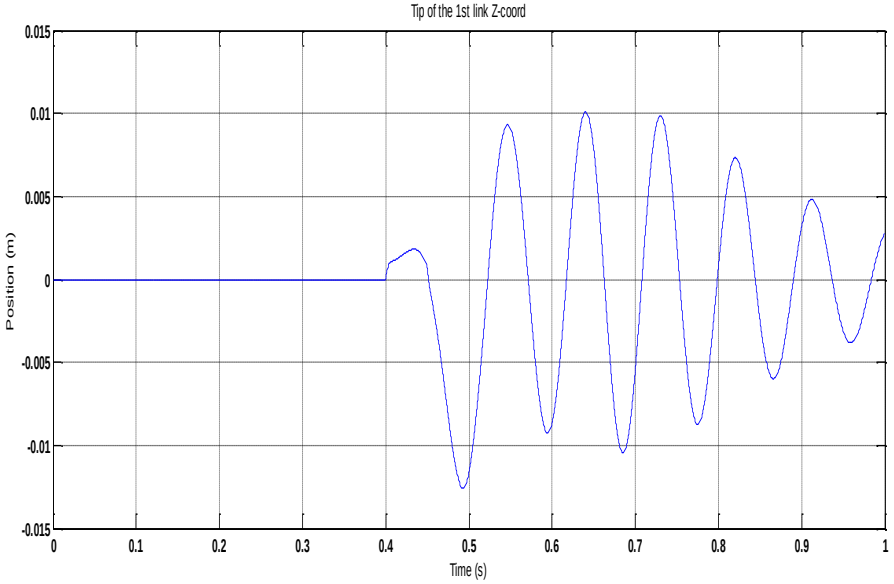

Figure2.16 Tip of the 1st link Z-coord

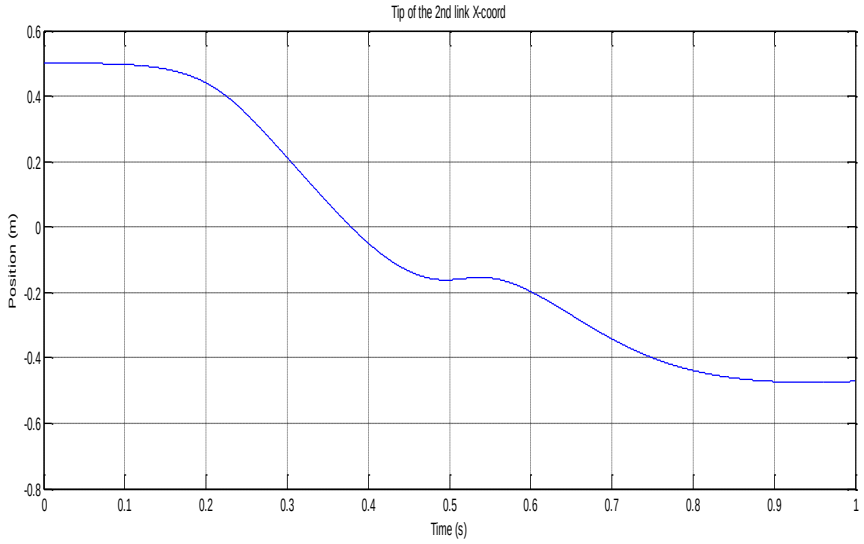

Figure2.17 Tip of the 2nd link X-coord

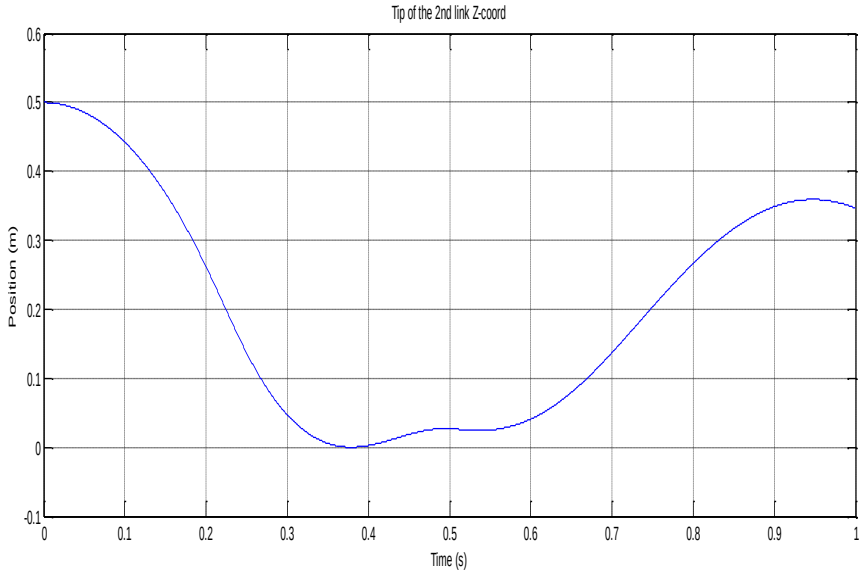

Figure2.18 Tip of the 2nd link Z-coord

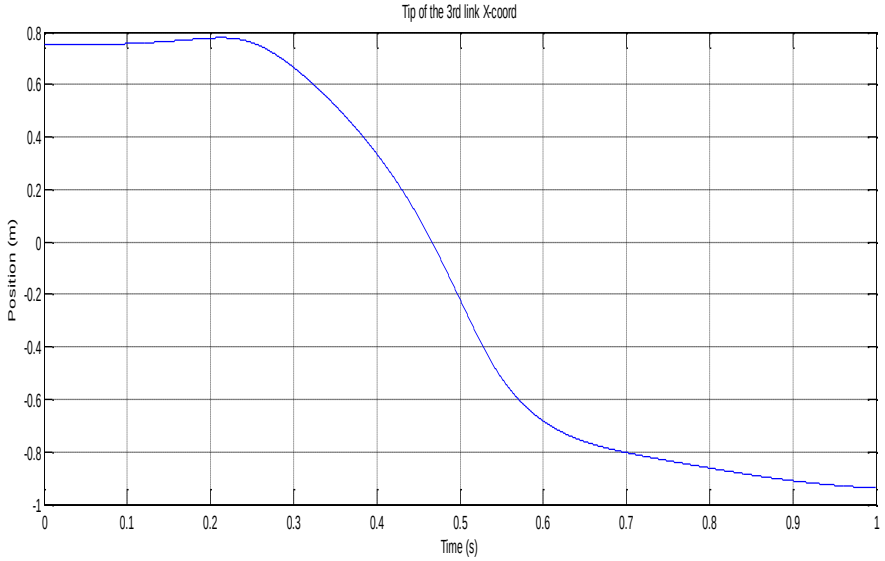

Figure2.19 Tip of the 3rd link X-coord

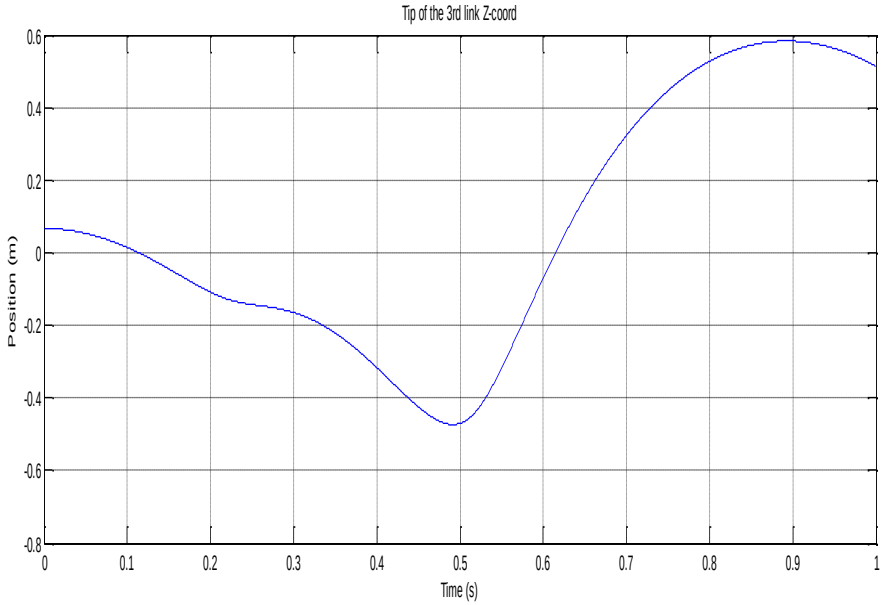

Figure2.20 Tip of the 3rd link Z-coord

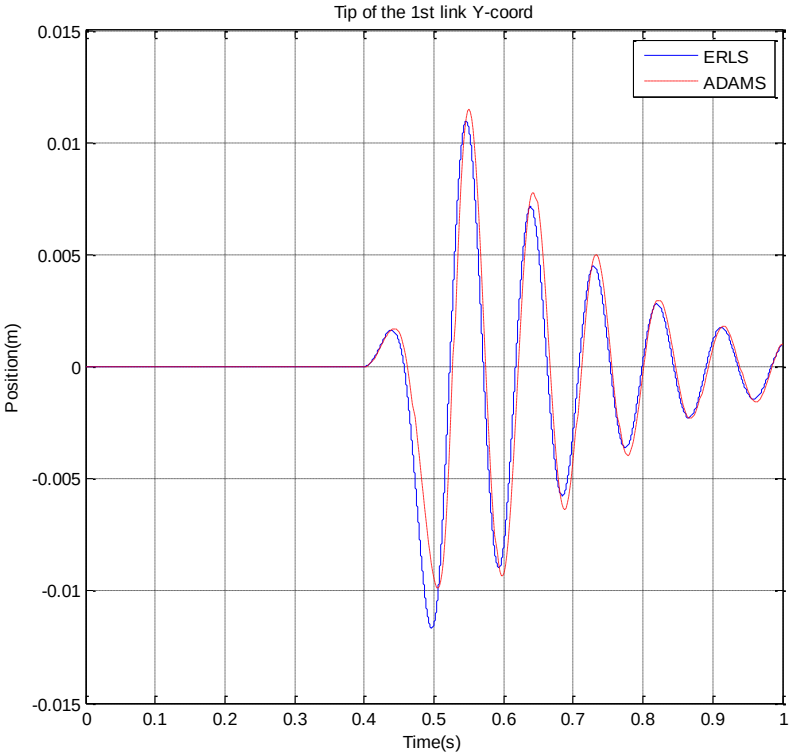

Figure2.21 Tip of the 1st link Y-coord

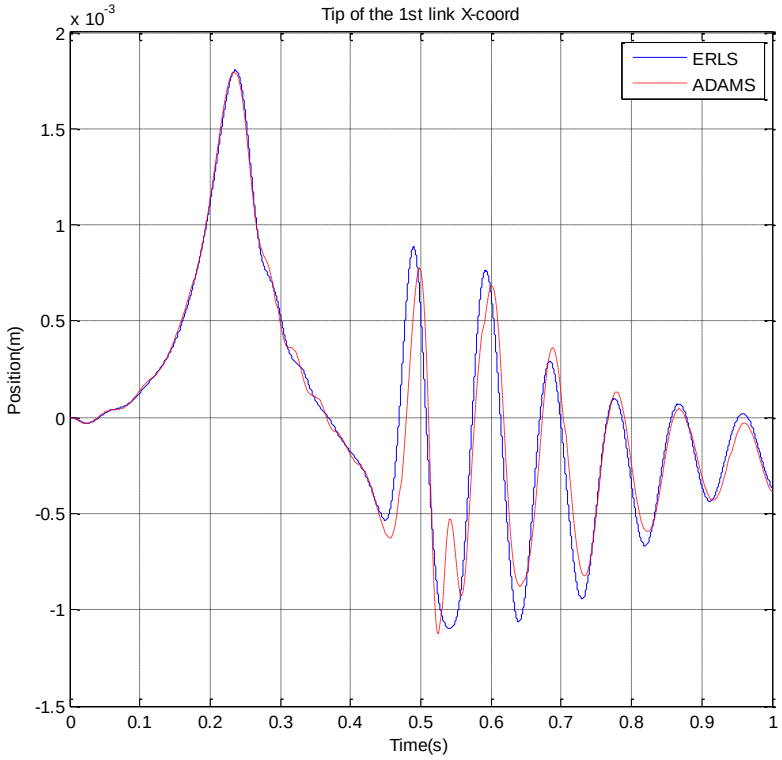

Figure2.22 Tip of the 1st link X-coord

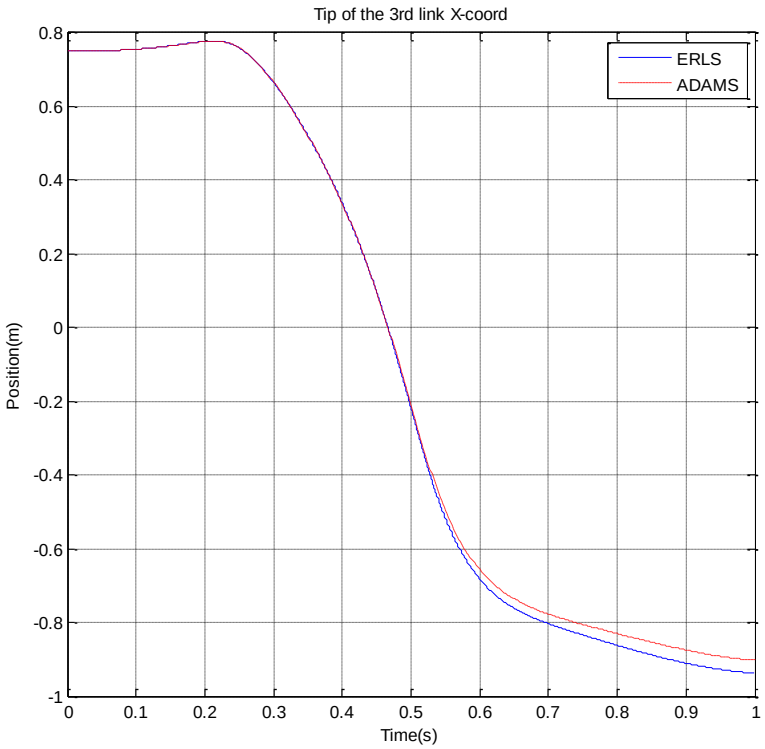

Figure2.23 Tip of the 3rd link X-coord

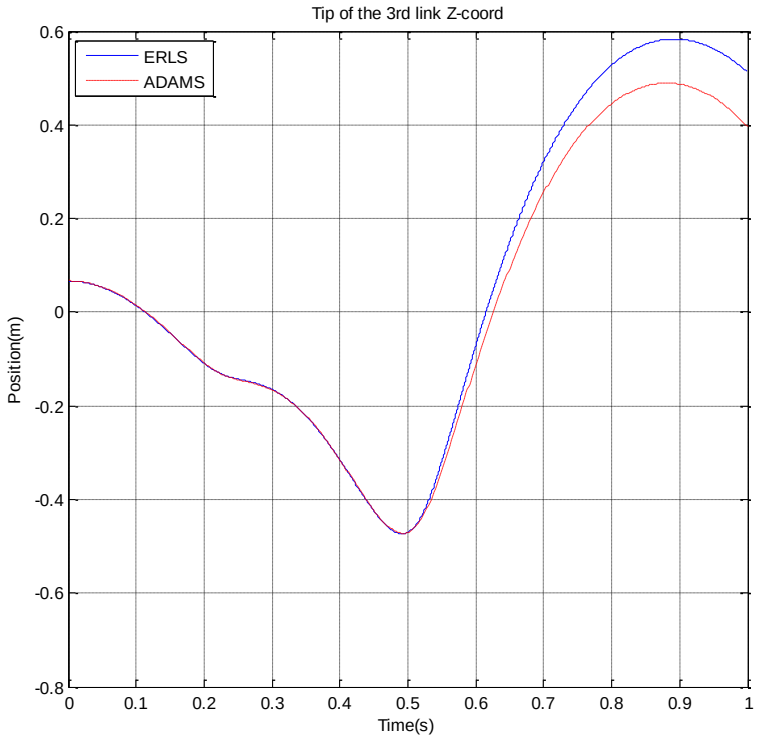

Figure2.24 Tip of the 3rd link Z-coord

b) The second considered robot as a benchmark is a double planer robot (Figure 2.25). Its main kinematic, geometrical and mechanical parameters are shown in Table 2.3. For each link of the mechanism, one beam element (thus two nodes) has been considered, so four nodes and two rigid degrees of freedom (represented in Figure 2.25. as q1 and q2) are present. As can be seen, even if the system is planar, it is under spatial external forces and torques. Thus, the overall motion and vibrational effect is in 3D.

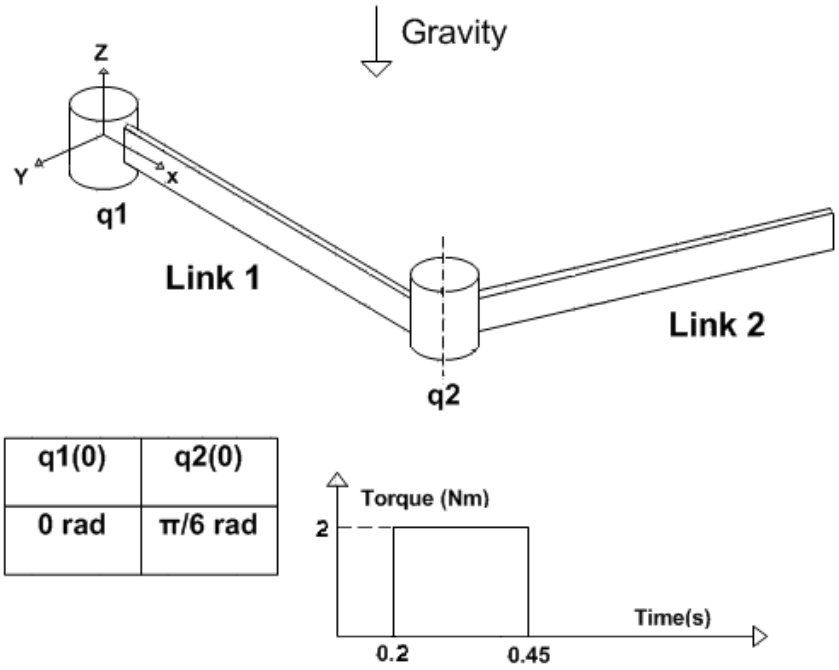

Figure2.25 Double planar pendulum

Table 2.3 DH and mechanical parameters

Link	ai	oi	di	Θi	Length (m)	Width (m)	Depth (m)	Density (kg/m^3)	Poissons Ratio
1	L_1	0	0	q_1	0.5	0.03	0.01	7840	0.3
2	L_2	0	0	q_2	0.5	0.01	0.03	7840	0.3

And the compatibility equations impose:

$$\begin{aligned} &s_x(1) = s_y(1) = s_z(1) = 0; s_{rx}(1) = s_{ry}(1) = 0 \\ &s_x^k(2) = s_x^k(3); s_y^k(2) = s_y^k(3); s_z^k(2) = s_z^k(3) \\ &s_{rx}^k(2) = s_{rx}^k(3); s_{ry}^k(2); s_{rx}^k(3) \end{aligned} \quad (2.59)$$

In this case, it was chosen to set to zero the Y translation of node 2 and the z rotation of node3.

$$s_y^k(2) = 0; s_{rz}^k(3) = 0 \qquad (2.60)$$

Rayleigh damping coefficients are $\alpha = 2$ and $\beta = 0.0005$Young's module is $2^*10^{11}(N/m^2)$. The input torque is applied on the first joint and its trend is shown in Fig2.25.

For double planer pendulum robot, the mechanism modeled by considering two beam elements for each link. Figures 2.26 and 2.27 show the positions of the first and second links of the double planar pendulum modeled by Matlab™ software simulator in case of one element and two elements for each link of the mechanism (from top to down X,Y and z coordinates).

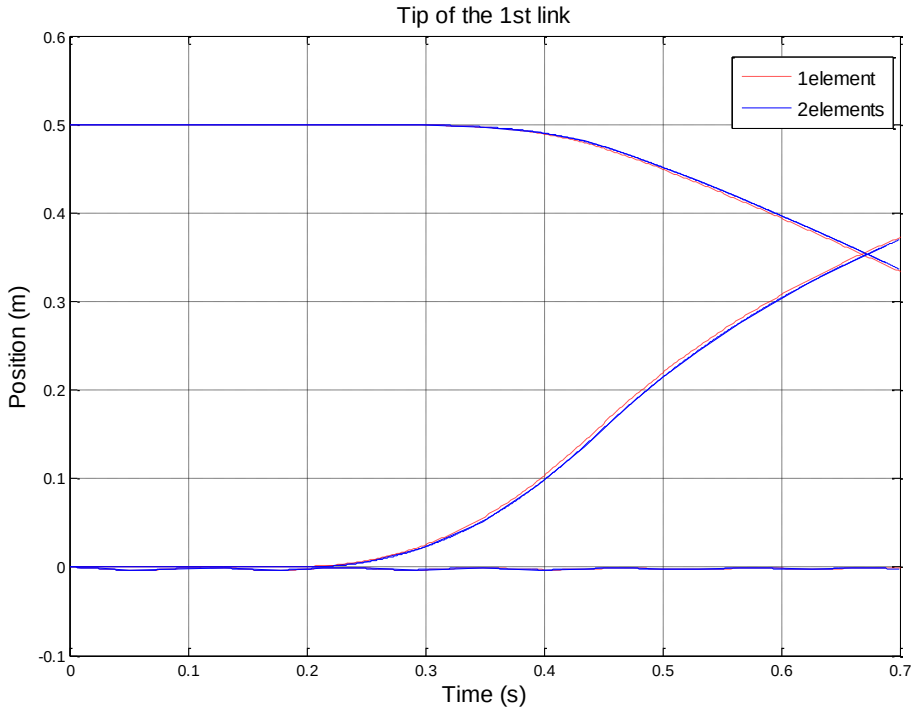

Figure2.26 Tip of the 1st link with one and two elements for each link

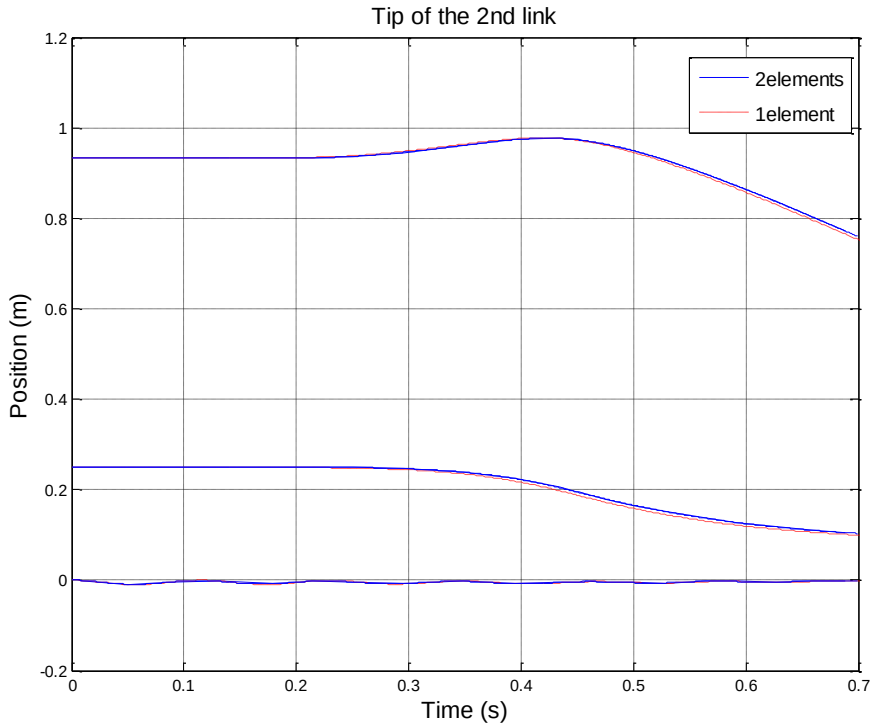

Figure2.27 Tip of the 2nd link for one and two elements for each link

Also Figures 2.28 and 2.29 show the extreme positions of the first and second links of the double planar pendulum obtained by Matlab™ software simulator in Comparison with results provided by the Adams™software and the results show very good agreement.

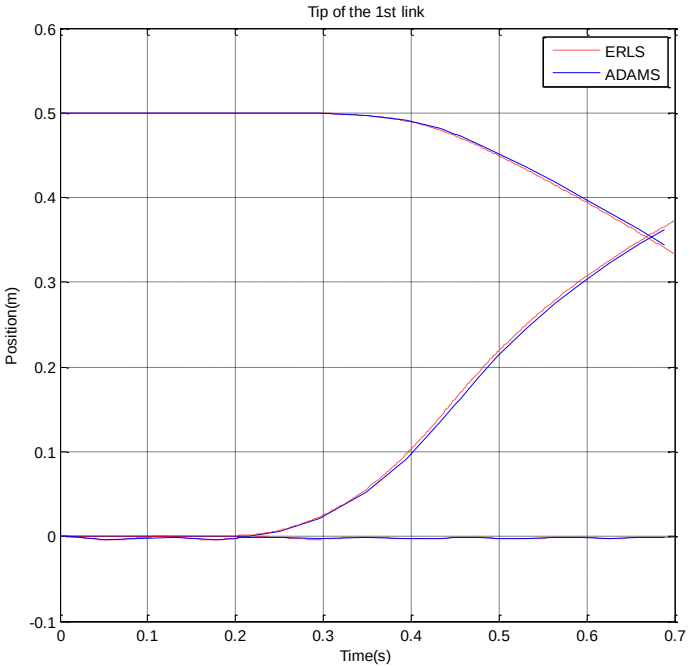

Figure2.28 Tip of the 1st link

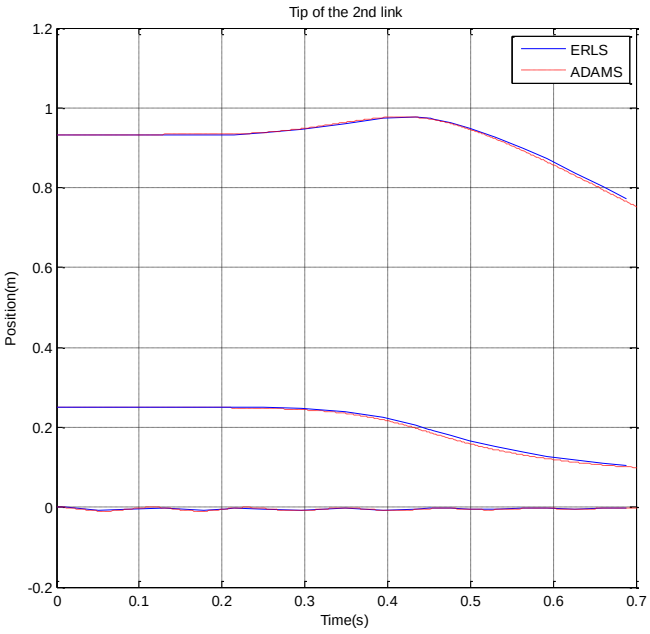

Figure2.29 Tip of the 2nd link

2.6 Conclusion

In this chapter, the dynamic formulation for flexible-link mechanisms based on an ERLS approach, where the basic idea is to decompose the overall motion of the mechanism into the rigid motion of a suitably defined ERLS and an overlapped elastic motion, has been evaluated.

A generic Matlab™ software simulator that allows to simulate rigid-flexible link systems, based on ERLS approach, has been implemented. Thanks to the ERLS based formulation, since it exploits the DH notation and the main concepts of the robotics kinematics, the approach to the flexible-link robots remains the same of the rigid ones allowing an easy approach. Then, in order to show the effectiveness of the method and of the simulator, different behaviors of specific robots with respect to different working conditions and mechanical parameters have been investigated. The results have been compared with respect to Adams™ showing a very good agreement.

CHAPTER 3

Design of Innovative Fire Door for Use in Naval Environment

In this chapter a thermo-mechanical analysis of fire door subjected to a fire was carried out using finite element method. First, a fire door was subjected to standard fire tests to evaluate fire resistance. The thermal and structural response of the three-layer fire door exposed to high temperature was modelled using finite element software and the accuracy of the model was evaluated by a comparison between the response of the software simulator and the experimental data.

3.1 Introduction

Fire doors are important elements in the fire safety de-sign of buildings and ships in general. They are complex structures made of materials with different thermal and mechanical properties and designed to have complimentary performances in order to comply fire safety requirements. In the design of fire doors the dominant practice involves the selection of the doors with individual fire resistance ratings based on standard fire tests [112]. In these tests the door is placed within a specially constructed furnace, which provides a heat flux according to a prescribed time-temperature curve [113].

Many experimental and numerical investigations have been carried out studying various aspects of the standard fire resistance test. Thomson and Preston examined the variations in heating rates of furnaces considering different construction schemes, fuels and types of operation [114]. Also two fire tests were carried out with two almost identical butted steel frames with steel door leaves subjected to the standard fire [113].

Sultan compared the measurements on specimens undergoing fire test in a furnace performed with two different measurement devices: shielded thermocouples and plate thermometers [115]. Results of finite element (FE) thermal analysis of a fire resistance test were reported by Chow and Chan [116]. They made a comparison between finite elements results with data from test specimens constructed from different materials. Wang and Quintiere [117] also investigated on compartment fire doors.

Hugi, Wakili and Wullschleger [118] evaluated the thermal response of a steel door frame subjected to a fire test. Tabaddor and Gandhi and Jones [119] studied the thermo-mechanical behavior of a fire door under endurance test. Some papers present the fire resistance of various building components covering a range of materials by means of physical testing and numerical modelling [120], [121], [122] and [123].

As many standard tests on fire resistance are carried out regularly, it could be useful to develop a mathematical model which could give a realistic prevision of the physical behavior of the component [124].

A realistic simulation of the heating process is needed during the design phase in order to reduce as much as possible the number of fire tests. Moreover, large size doors, for which an experimental trial is not feasible with standard equipment, must be tested only through computer aided simulations. The problem of defining a suitable mathematical model is then dealt with in this chapter. By a comparison with the experimental data, the accuracy of the model is evaluated.

3.2 Component Description and Fire Test

Fire doors are one of the key elements in the fire safety design of buildings in general. They have to fulfill two functionalities at the same time: usability under normal conditions and safety and security in fire conditions. This leads to a complex structure made of different materials. Figure 3.1 shows the standard fire door under investigation, whose structure is depicted in Figure 3.2: the outer part is constituted by steel sheets, while the inner portion is filled with an insulation material that acts as a thermal barrier to heat flux through the door.

Figure 3.1 Example of fire door under investigation

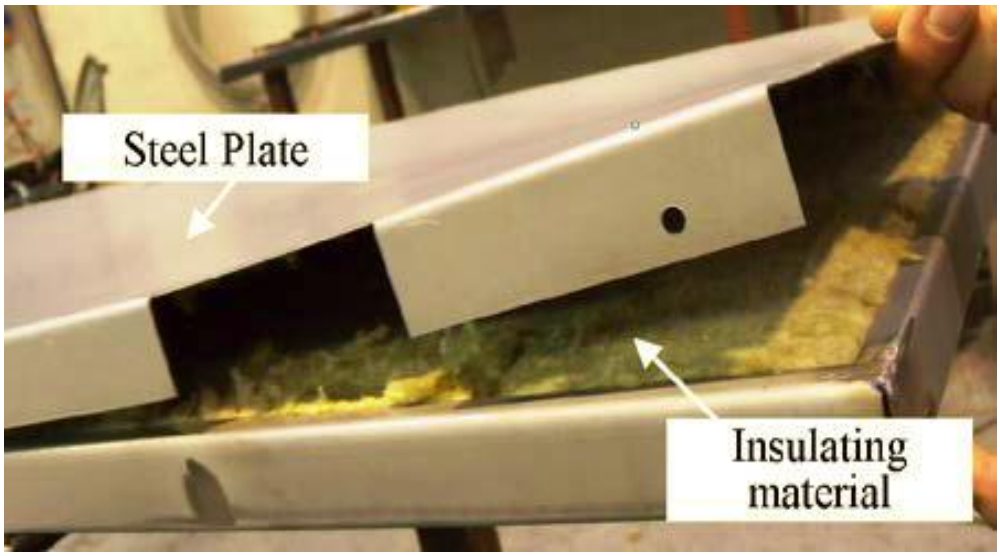

Figure 3.2 Close view of door's structure

Fires doors are subjected to a standard fire test in order to evaluate their fire resistance. The test needs to be performed by means of an appropriate furnace.

According to FTP code of the International Maritime Organization [113], the door should satisfy some requirements; the main relevant, with respect to this work are the following. The mean temperature on the unexposed surface should not exceed a defined value. Only small gaps between the door and the frame are tolerated, since no flame or smoke must pass through the door.

Although the standard fire resistance test is a convenient way for quality control and grading the relative fire performance of different types of structural members, it could be not sufficient to completely understand the realistic structural behavior in fire. In Purkiss [125] the drawbacks of the standard fire resistance test method are pointed out. The main concerns the fact that the standard fire exposure is only one of various types of realistic fire conditions. The thermal action from the convention-al fire can be considered representative or over-designed compared to the natural fire in many situations. Some conditions, however, lead to more severe thermal actions compared to conventional fire. Some works in literature, such as [126], attempt to correlate real-world fires with standard fire tests, while in [127] an experimental investigation of fire doors during a natural fire is performed.

Another limitation is related to furnace dimensions: as test furnaces are restricted in size, it is generally impossible to test large elements of construction and thus only representative specimens are considered.

A well calibrated predictive model can be useful to overcome some of these drawbacks: if the model response under a simulated standard fire fits well with experimental measurements, different loading conditions, such as longer or real fire exposure, can be simulated. Furthermore, the behavior of doors with different sizes can be obtained (in general it is difficult to apply scaling to fire test results due to the nonlinear behavior of materials) by reducing the number of tests needed.

During the test, temperature rose to 945^{o}C in 60 minutes following the curve shown in Figure 3.3.

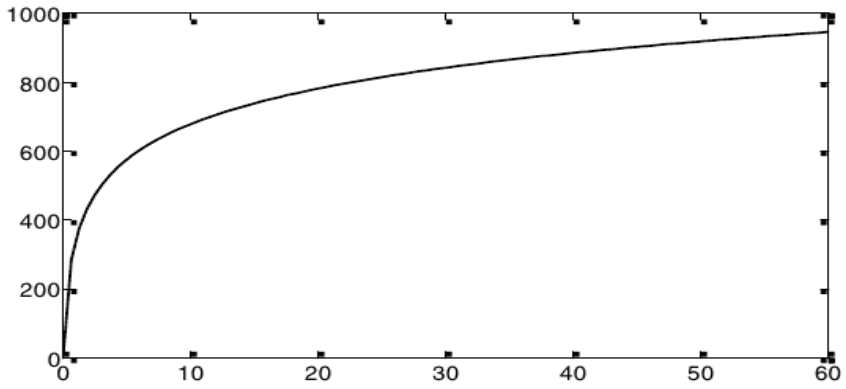

Figure 3.3 Temperature during standard fire test

3.3 Experimental Measurements

In order to gain insights into the thermal behavior of the component, the temperature distribution on both ex-posed and unexposed side of fire door were monitored during a standard fire test. The adopted furnace is a vertical one (4 m horizontally and 3 m vertically) with four burners (two per side) that guarantee a quite uniform temperature during the heating phase. The experimental set-up includes:

- A set of 12 magnetic TC Direct thermocouples, type K to monitor the temperature variation on different points of unexposed side assembly.
- 4 rigid thermocouples TC Direct with mineral insulation, located inside the furnace.

- A 16 channel isothermal thermocouple input module NI9214, embedded in a real time controller NIcRIO-9014, used to log all the output signals from the thermocouples.

- An infrared camera Optris PI 400, adopted to gain insights into the heat transfer mechanisms on the unexposed side.

In Figure 3.4 the average temperature variation inside the furnace is plotted against the theoretical distribution, showing a good calibration of the burners, also Figure 3.5 includes some details of the adopted experimental apparatus.

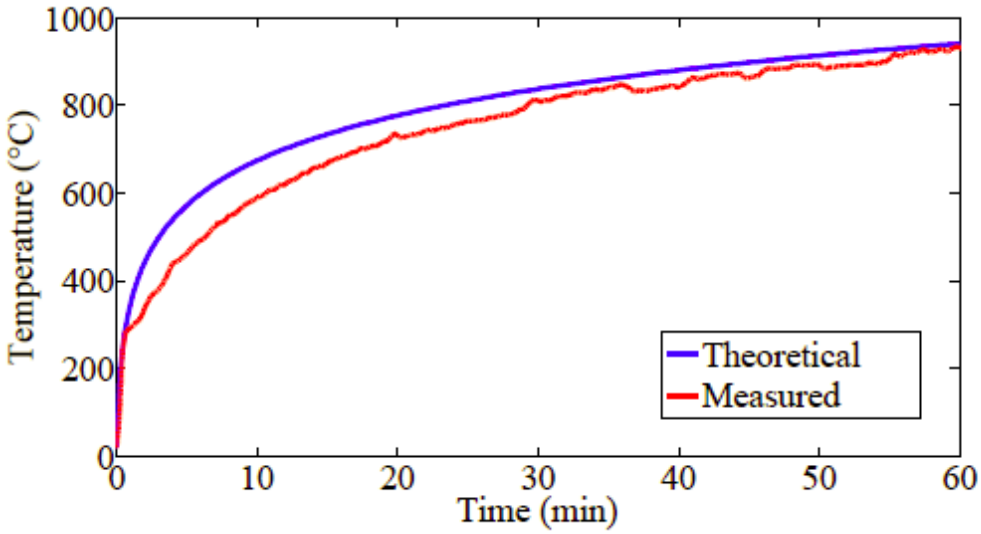

Figure 3.4 Average temperature inside the furnace

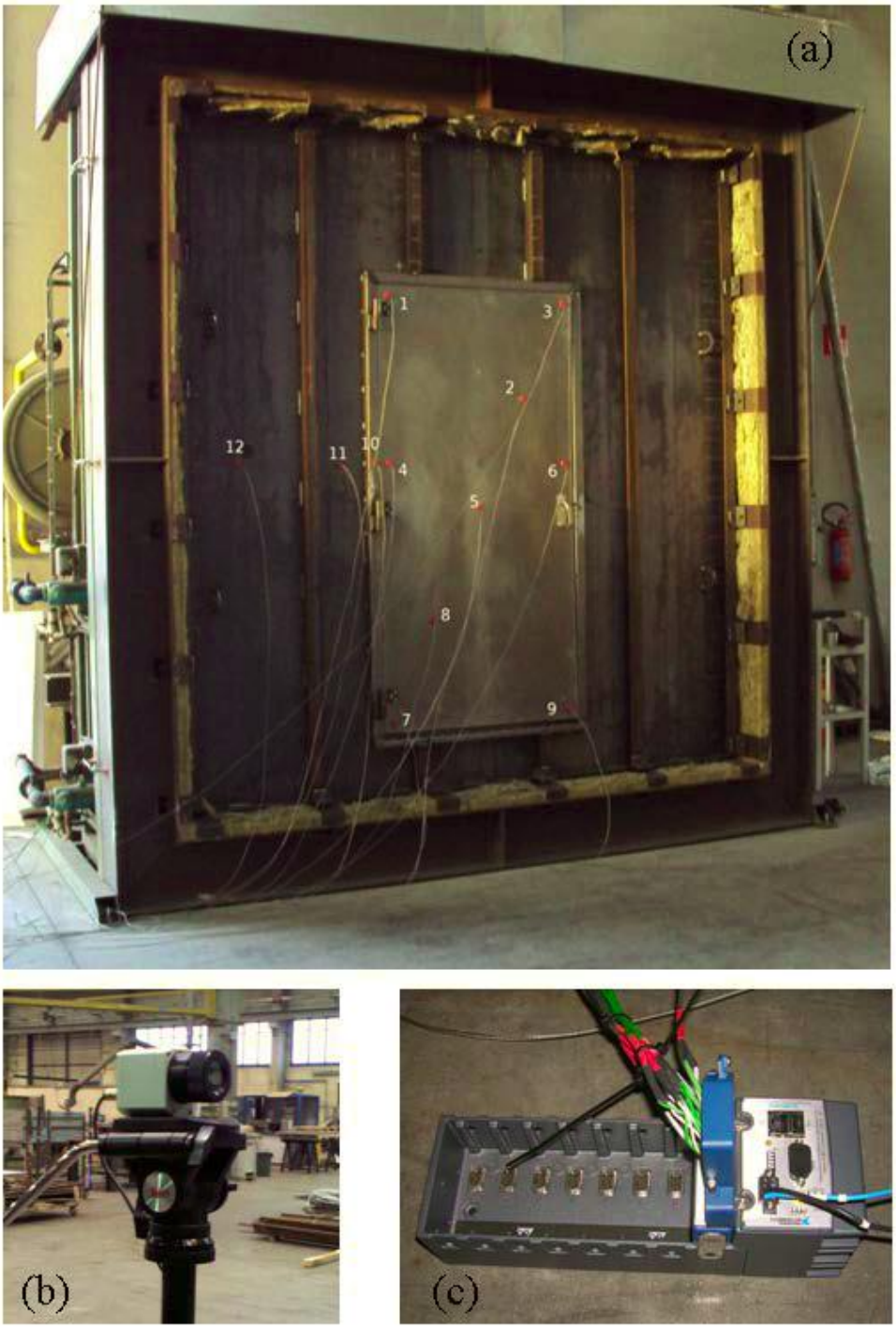

Figure 3.5 Experimental apparatus: (a) thermocouples on the unexposed side, (b) infrared camera and (c) data acquisition system

A sample of images recorded from thermo graphic camera is shown in Figure 3.6.

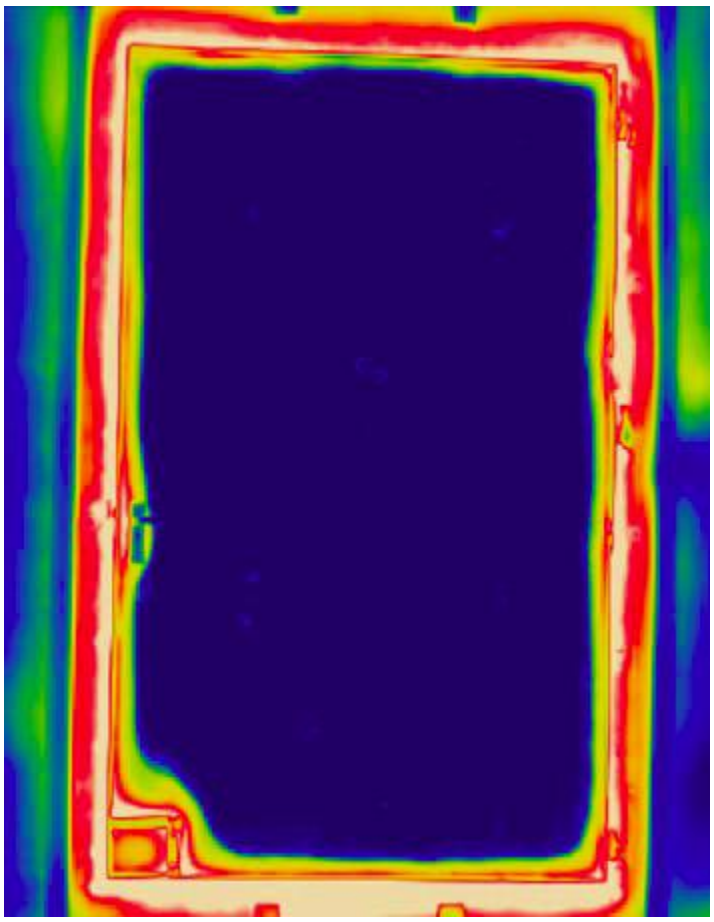

Figure 3.6 Image from thermographic camera during the test

Also, measurements obtained from thermocouples on the unexposed side of the door plotted in the figures 3.7-3.18.

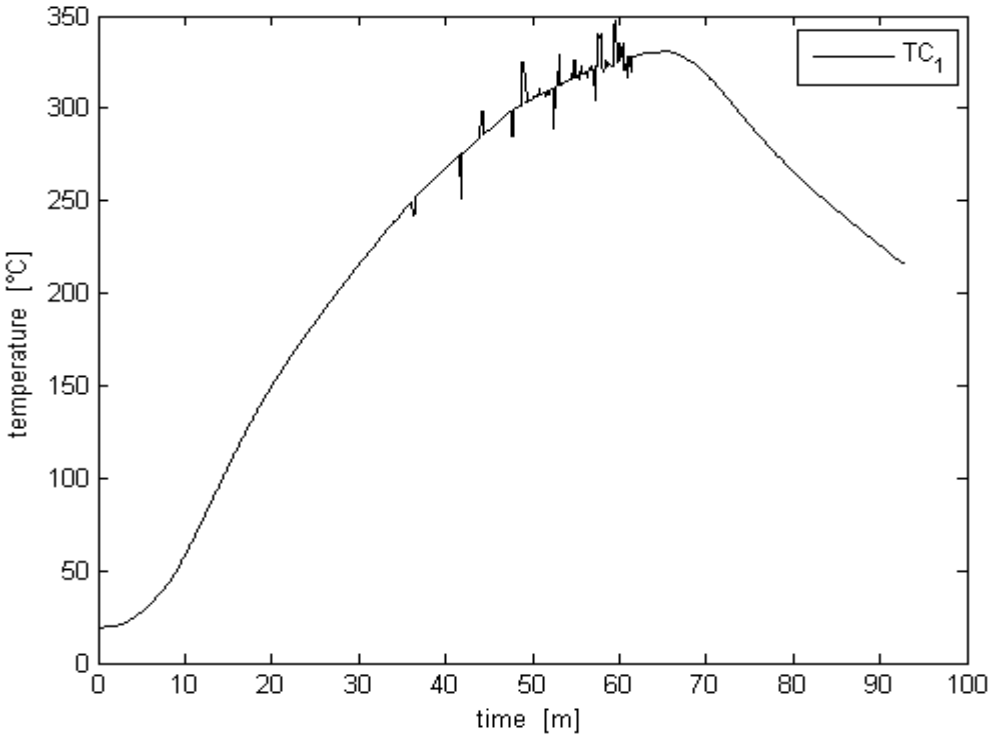

Figure 3.7 Temperature measured by thermocouple No. 1

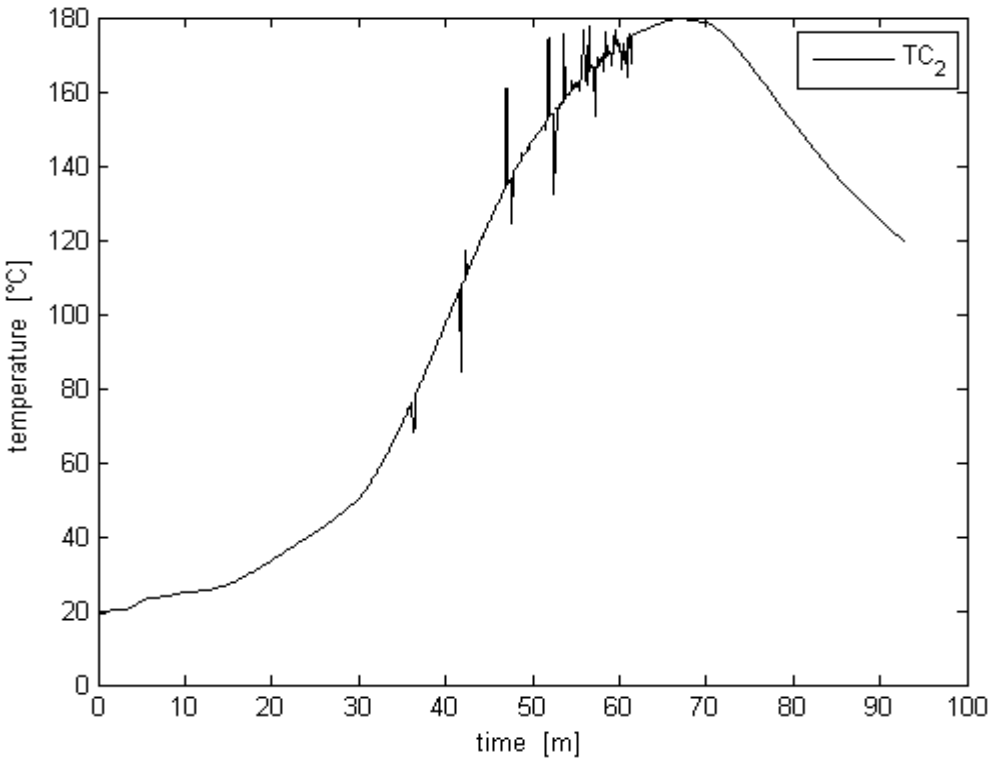

Figure 3.8 Temperature measured by thermocouple No. 2

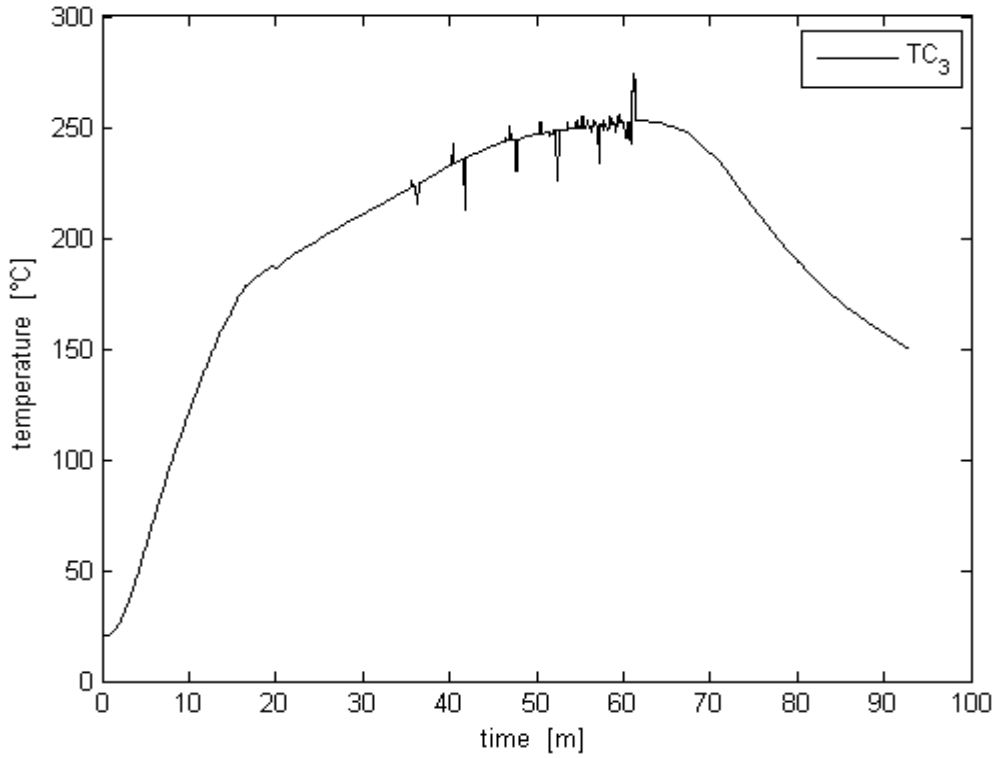

Figure 3.9 Temperature measured by thermocouple No. 3

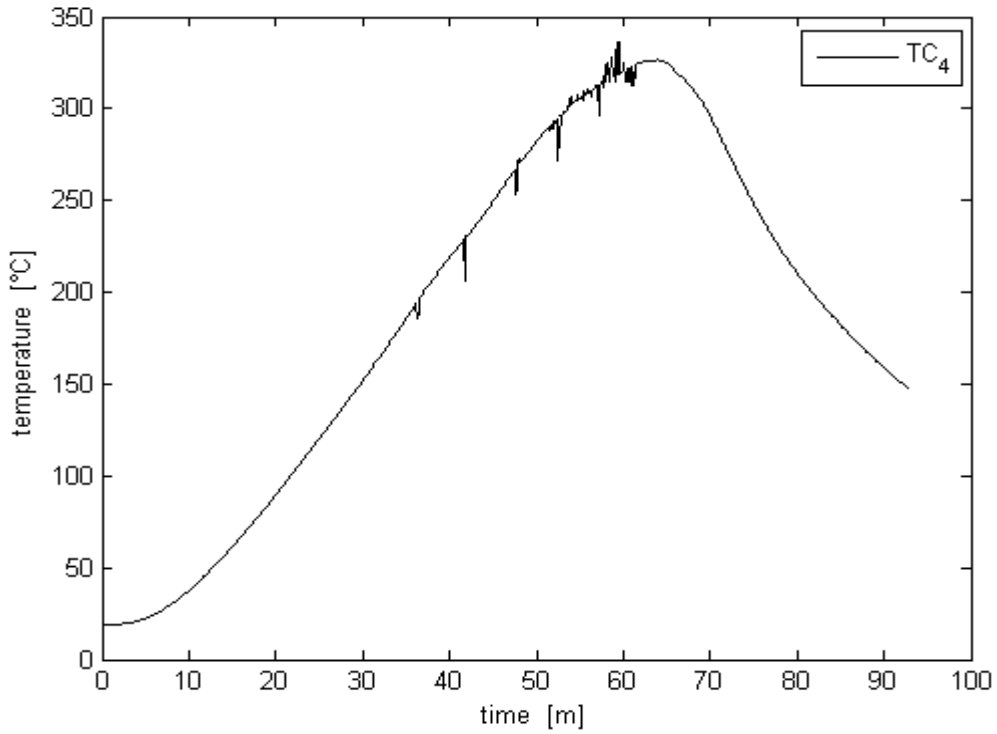

Figure 3.10 Temperature measured by thermocouple No. 4

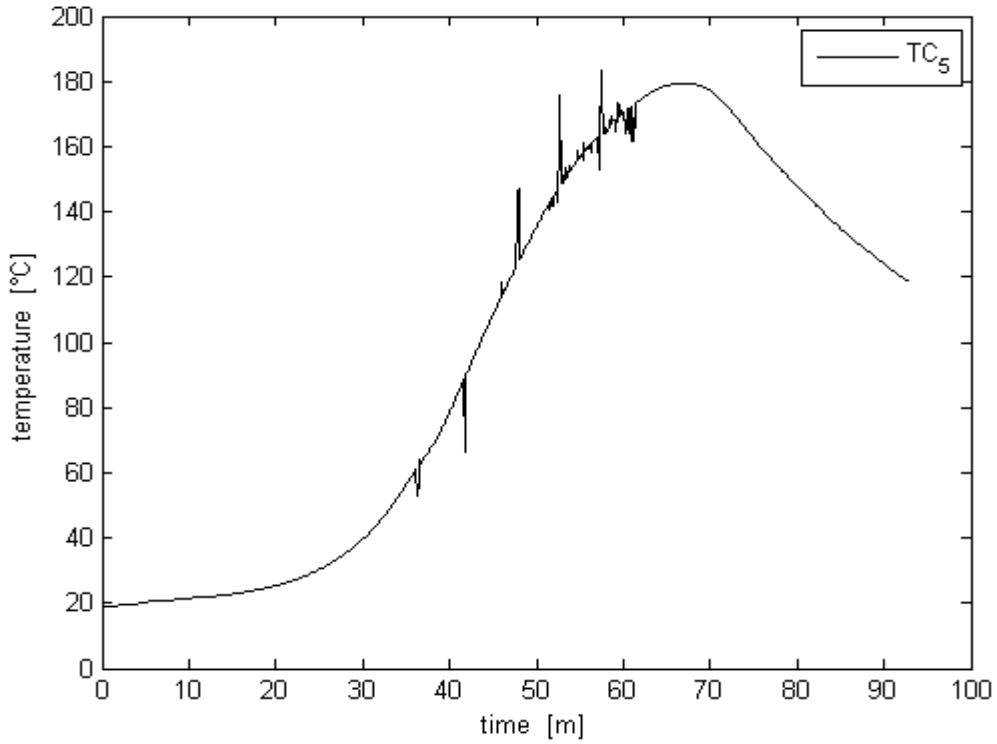

Figure 3.11 Temperature measured by thermocouple No. 5

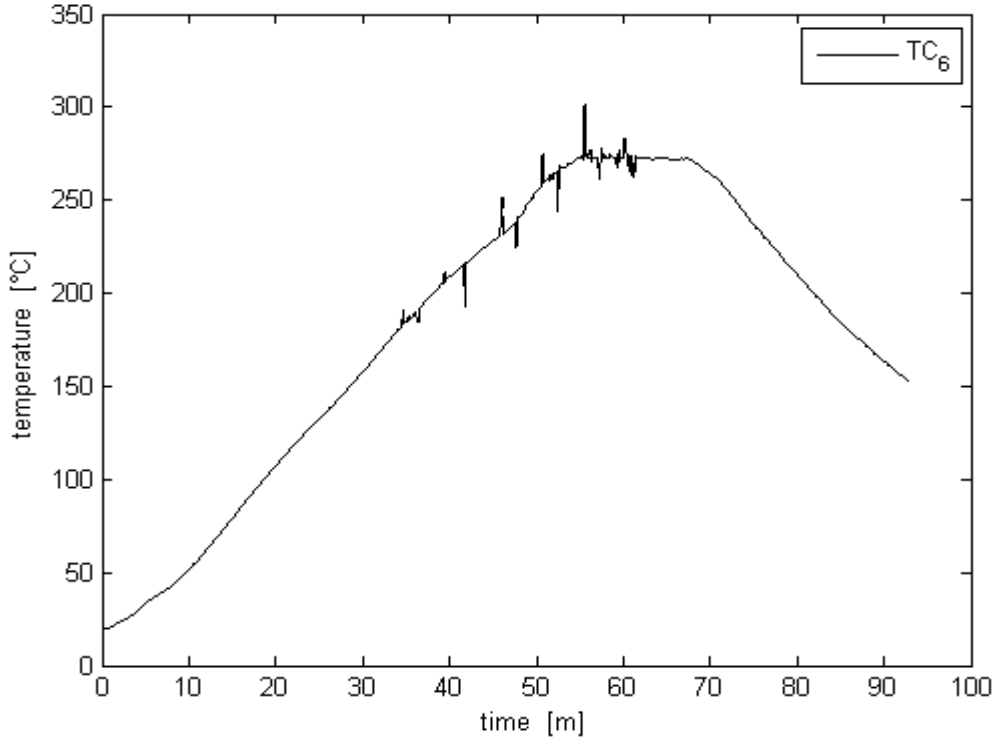

Figure 3.12 Temperature measured by thermocouple No. 6

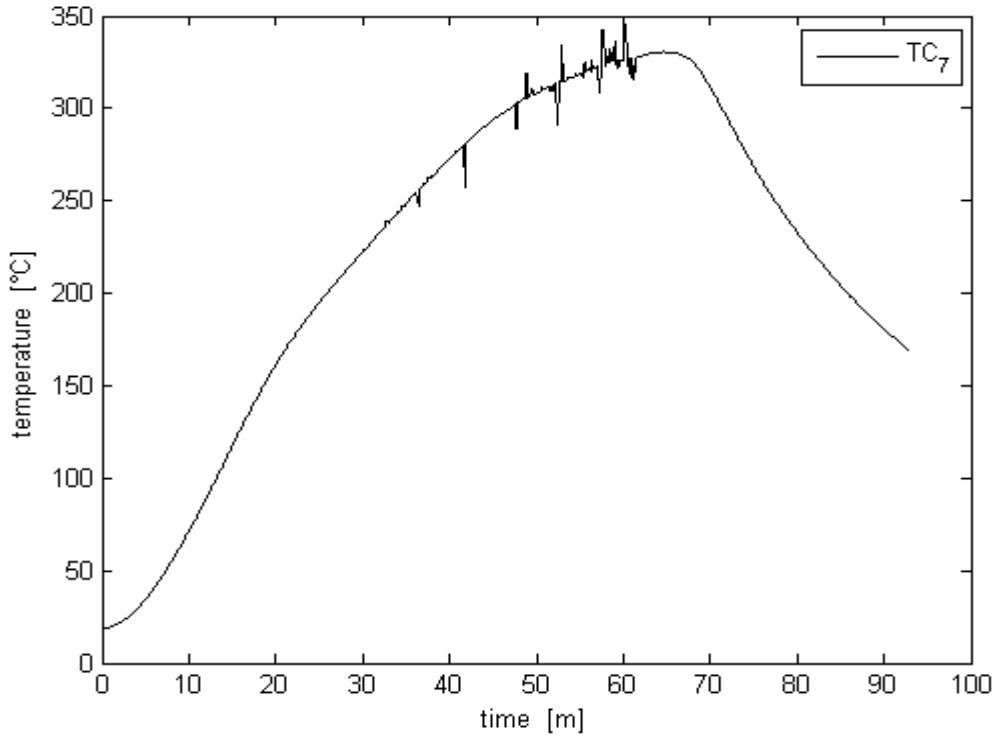

Figure 3.13 Temperature measured by thermocouple No. 7

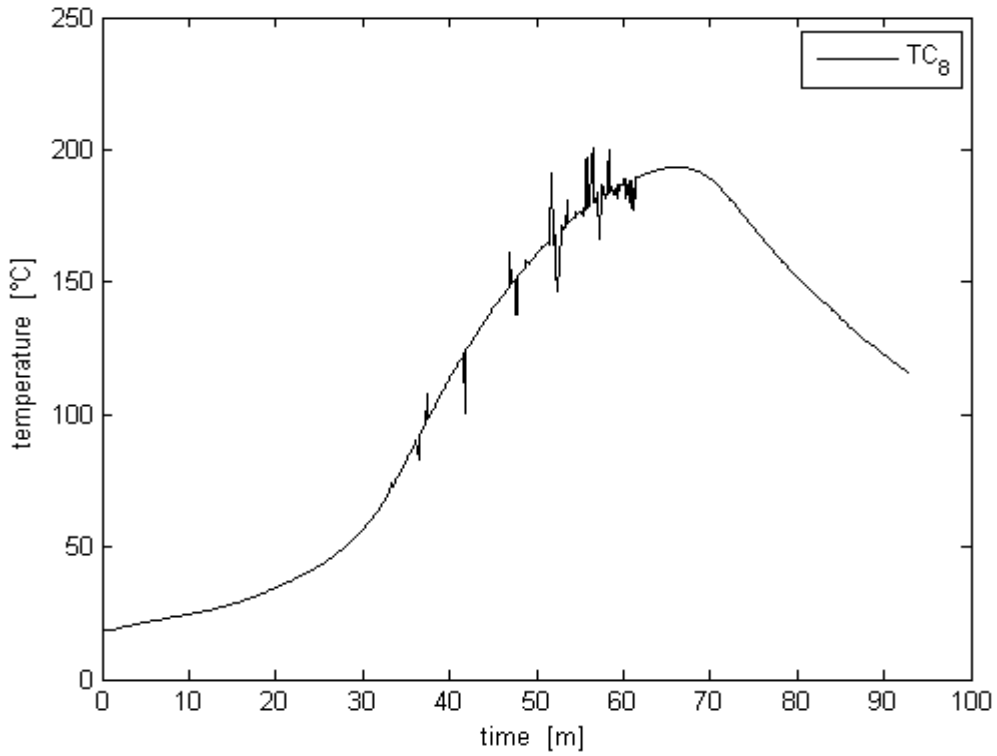

Figure 3.14 Temperature measured by thermocouple No. 8

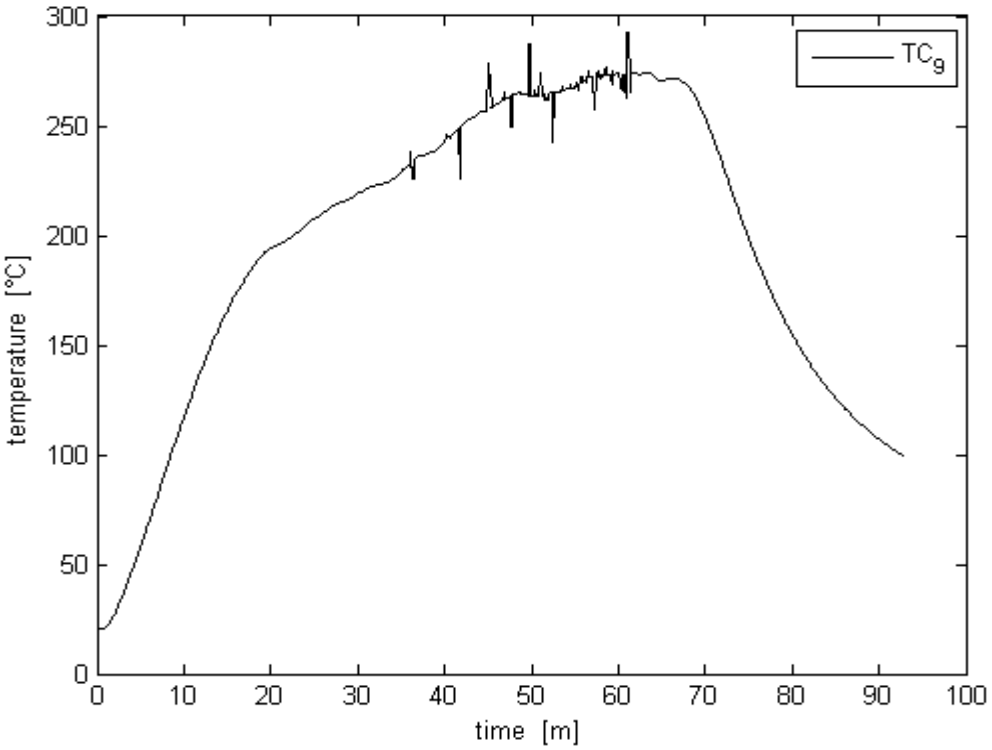

Figure 3.15 Temperature measured by thermocouple No. 9

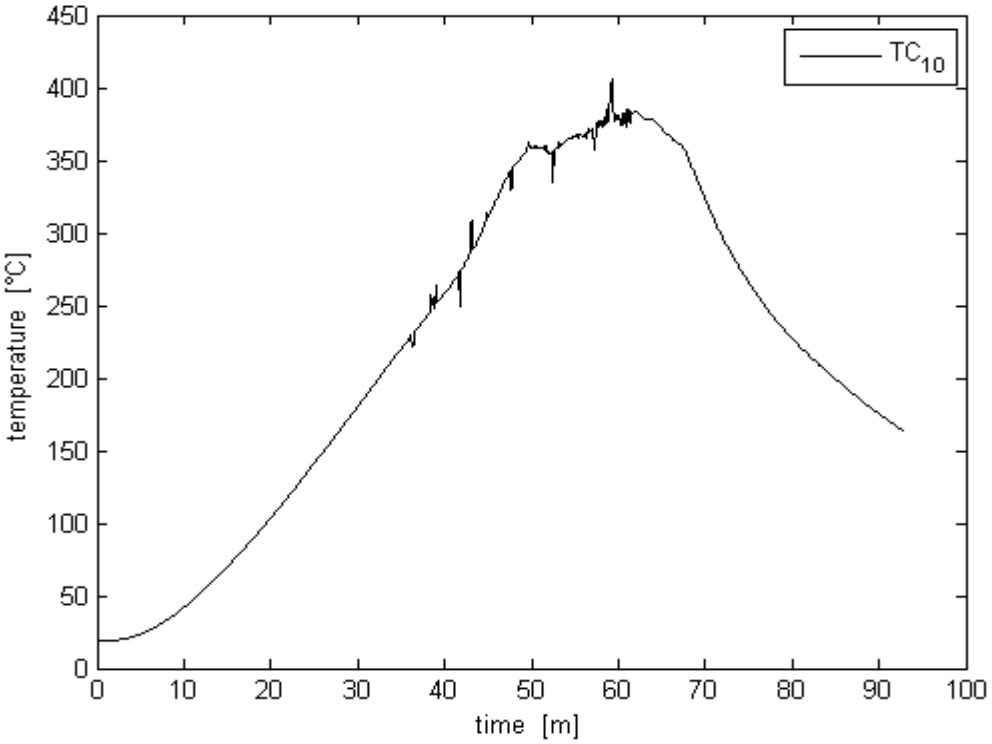

Figure 3.16 Temperature measured by thermocouple No. 10

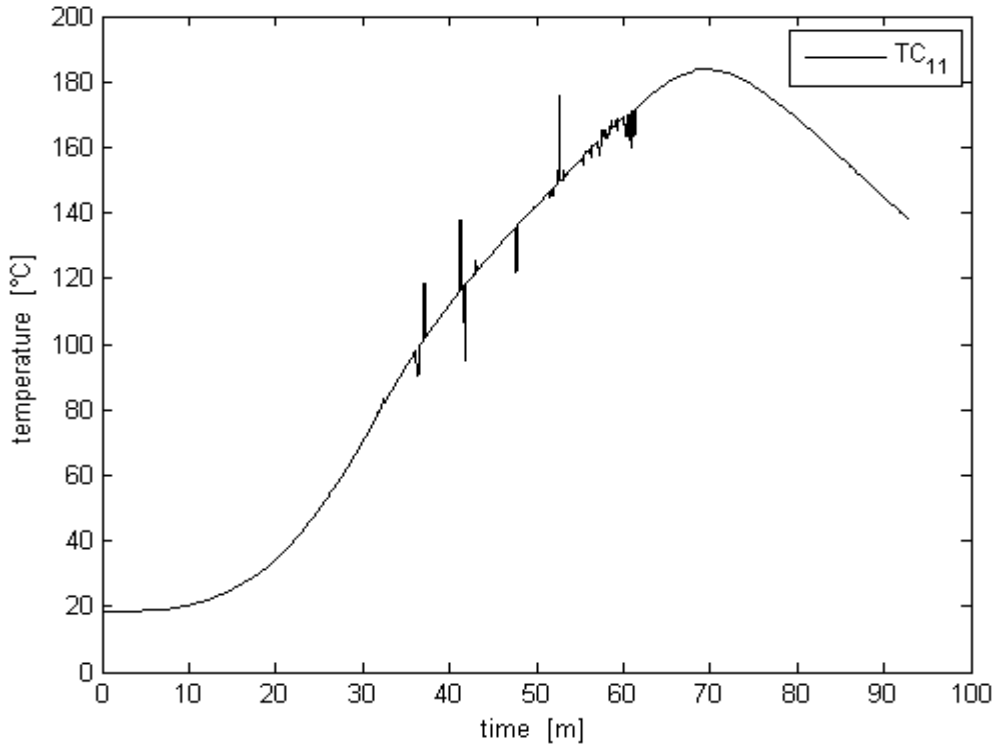

Figure 3.17 Temperature measured by thermocouple No. 11

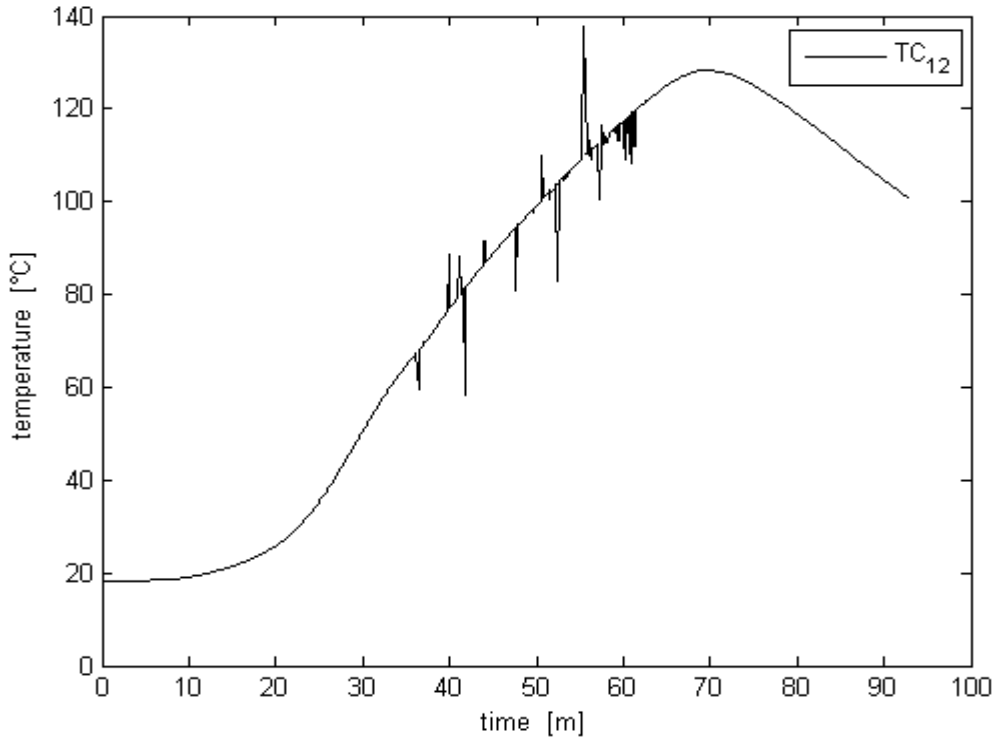

Figure 3.18 Temperature measured by thermocouple No. 12

The deformation of the door during the test was measured as shown in figure 3.20 and figure 3.19 shows the door at the end of fire test.

Figure 3.19 Fire door at the end of the test

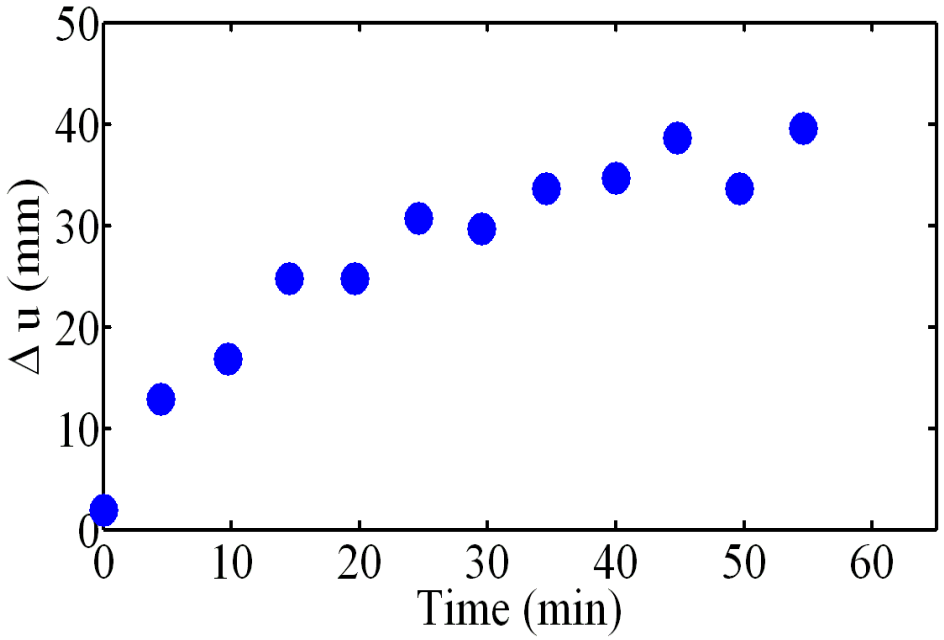

Figure 3.20 Deformation measured during the test

3.4 Finite Element Modeling

From the thermal point of view, the leaf can be considered as separated from the frame. Thus, heat flowing through the hinges can be neglected in calculations. In order to assess a reliable numerical strategy, only the leaf was modelled. The characteristics of this component (shown in Figure 3.1) are: 2m high, 1m wide and 60 mm thick. A mathematical model is developed by means of the Finite Element method.

3.4.1 Material Properties

The thermal properties of materials needed for the numerical analysis (thermal conductivity, density and specific heat capacity) are obtained from (Eurocode 3) for steel, assuming a constant density of 7800 kg/m3.

The filler insulation in the fire door consists of rock-wool as the main material. The manufacturer of the materials provides the material properties listed in Table 3.1, that were integrated with values available in (Hugi et. al. 2009) for higher temperatures.

TABLE3.1 Conductivity values for insulating material

Temperature(^{o}C)	Conductivity (W/mK)
10	0.035
100	0.043
300	0.073

3.4.2 Element type

Both the insulating material and steel plates are modelled by solid (SOLID70) elements.

SOLID70 has a 3-D thermal conduction capability. The element has eight nodes with a single degree of freedom, temperature, at each node. The element is applicable to a 3-D, steady-state or transient thermal analysis. The element also can compensate for mass transport heat flow from a constant velocity field. If the model containing the conducting solid element is also to be analysed structurally, the element should be replaced by an equivalent structural element (in this project SOLID45). An option exists that allows the element to model nonlinear steady-state fluid flow through a porous medium. With this option, the thermal parameters are interpreted as analogous fluid flow parameters. The geometry, node locations and the coordinate system for this element are shown in figure 3.21. This element is defined by eight nodes and the orthotropic material properties. A prism shaped element, a tetrahedral-shaped element and a pyramid-shaped element may also be formed as shown in figure 3.21.

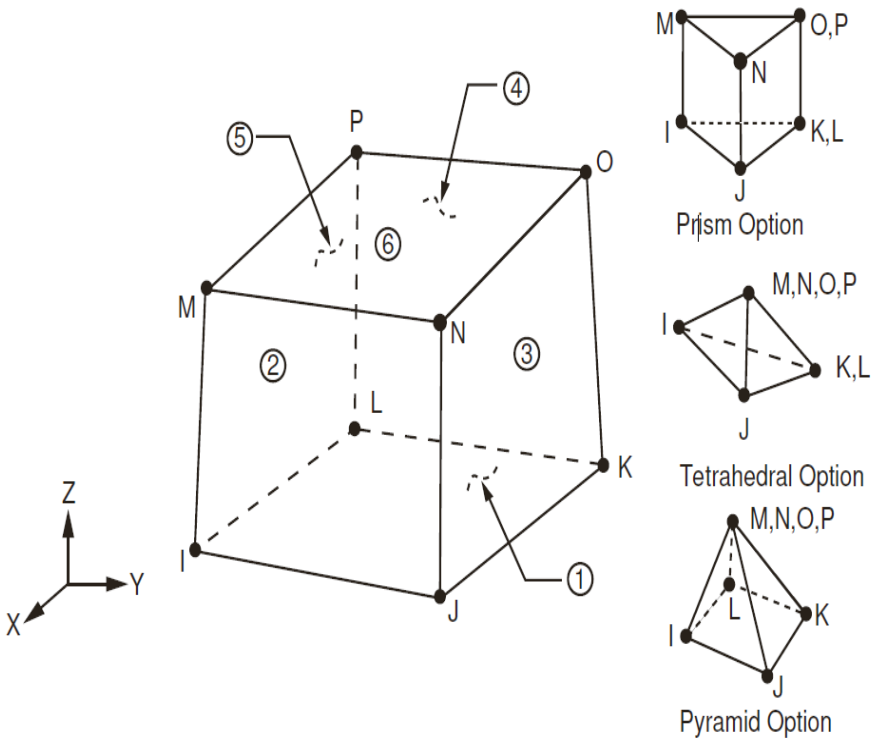

Figure 3.21 SOLID70 geometry

3.4.3 Modeling and Results

As mentioned in previous sections, the door modeled using solid elements. Figure 3.22 shows the door modeled by finite element modeling software (ANSYS).

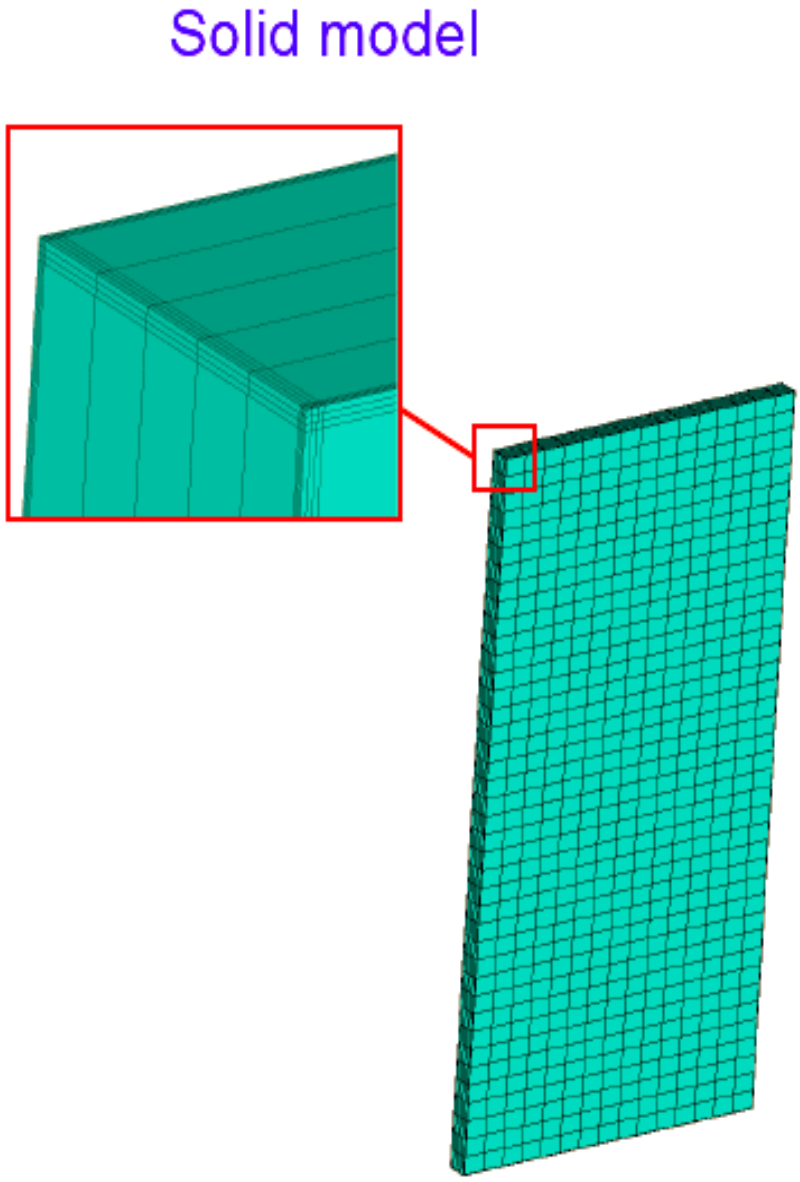

Figure 3.22 Finite element model of the door

The thermal analysis is performed taking into account radiative and convective heat exchange on the exposed side of the door, while only convection is considered on the unexposed side. The natural convection film coefficient was set to 10 W/(m2K), while the environmental temperature was set to 20 °C, according to standards provided in (Eurocode 3).

The theoretical temperature law of the furnace is considered performing a transient analysis, which implies an extra node representative of the hot ambient inside the furnace. Values of convective and radiative coefficients are imposed according to (Eurocode 3, Tabaddor et. al. 2009). This strategy thus considers the exposed surface as uniformly loaded by the heat coming from the furnace air.

The implemented analysis is therefore a non-linear transient one, and the resulting temperature distribution on the door is depicted in Figure 3.23.

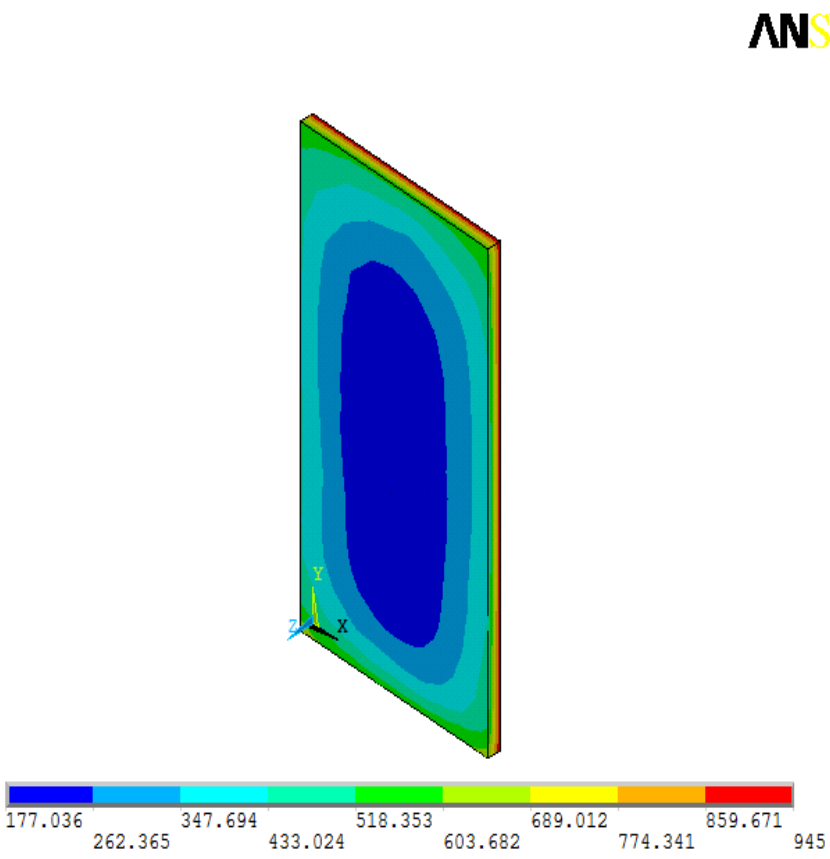

Figure 3.23 Numerical temperature distribution on the unexposed side of the door

It is possible to notice that, as depicted in Figure 3.24 , the temperature on the hot side reaches the simulated furnace temperature after only few minutes from the beginning of the heating process (time scale is limited to 10 minutes for the sake of clarity) and the final temperatures after 60 minutes are practically coincident. Since the slope of these curves, after the initial time interval, is not extremely high, a steady-state thermal analysis can be performed with a tolerable accuracy on the results.

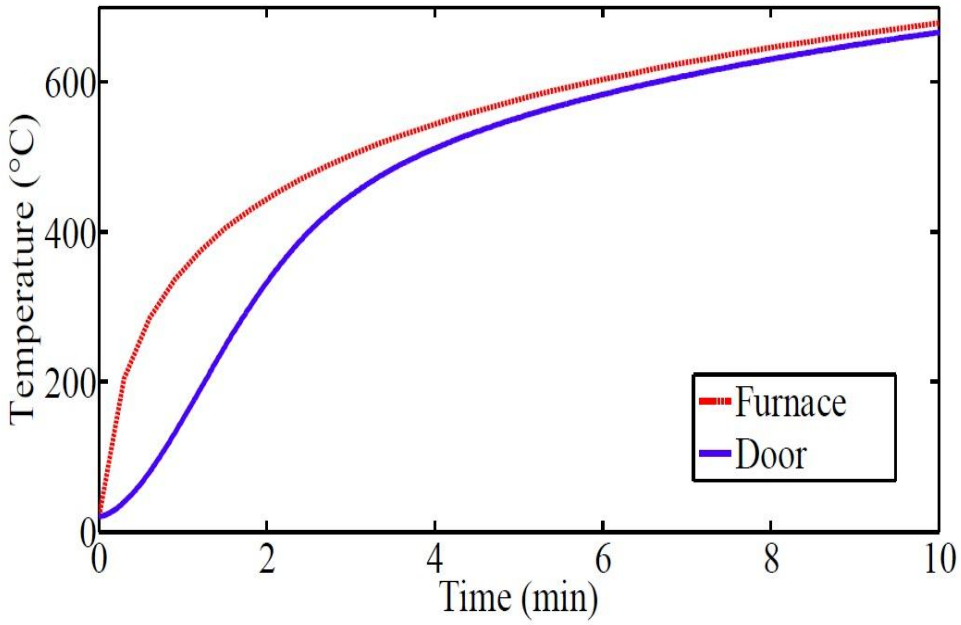

Figure 3.24 Temperature trend on the hot side

The transient analysis in which radiative and convective heat exchange are considered for the exposed side, can then be replaced in a satisfactory way by a steady-state analysis in which a fixed temperature (equal to the temperature after 60 minutes of the heating curve) is directly imposed on the hot side of the leaf. Figure 3.25 schematically represents the two implemented strategies.

The results obtained adopting the techniques with fixed temperatures are very similar to that shown in Figure 3.23. The only difference is due to the fact that absolute values are somewhat higher, suggesting that the transient state is not completely concluded.

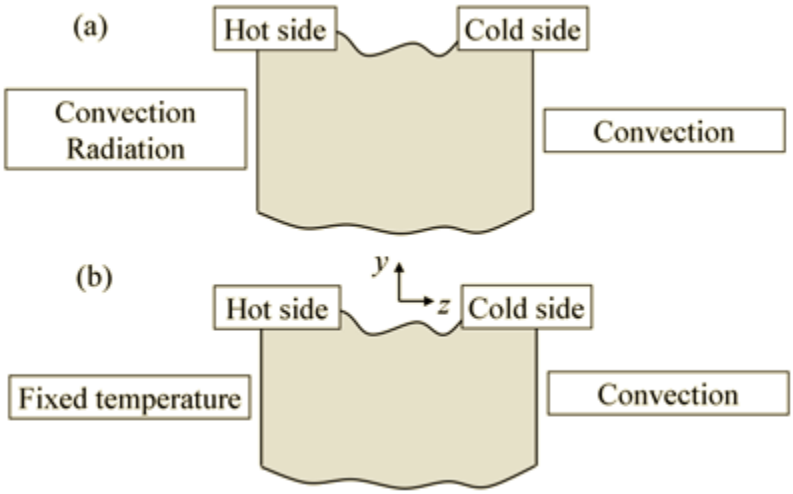

Figure 3.25 Strategies of implemented thermal analysis: (a) transient (b) steady state

As can be seen by comparing the experimental temperature distribution of Figure 3.6 and the numerical contour map of Figure 3.23, the model implemented can be considered adequate to accurately describe the thermal behavior of the leaf: the temperatures of lateral edges are higher than those in the central part for the presence of the thermal bridge, as experimentally observed. Furthermore, as shown in Figure 3.26, the evolution of temperatures at different levels on the unexposed side (with the transient analysis) is very close to the measured trend.

A numerical model that correctly evaluates the temperature distribution of the door can be of practical use to achieve sensitivity analysis on geometrical parameters and to implement strategies for reducing the temperature levels on the unexposed side of the door.

Furthermore, the thermal analysis represents the foundation for a subsequent structural analysis, in which the temperature distribution can be used as input to numerically evaluate the deformed shape of the door.

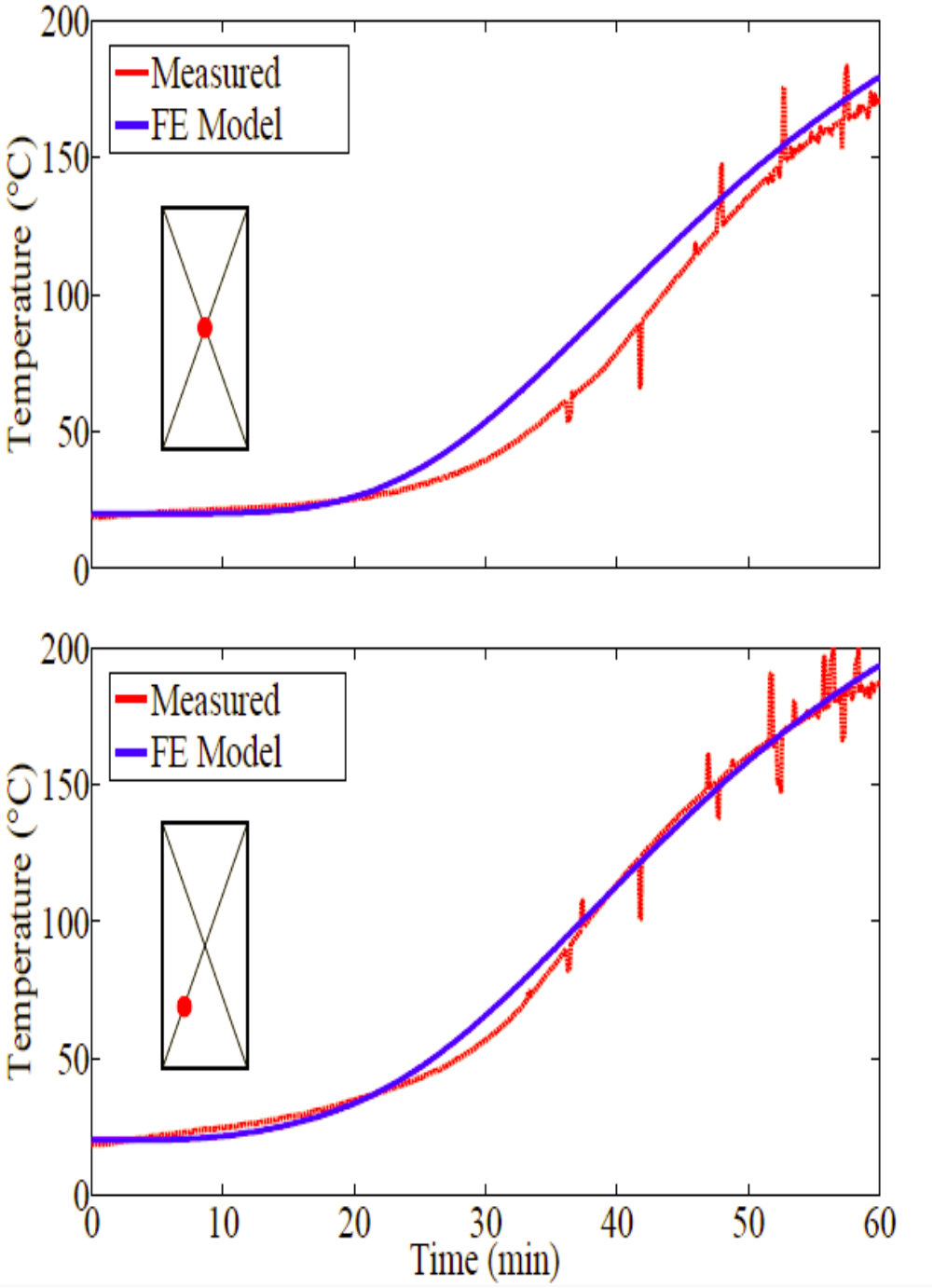

Figure 3.26 Temperature trends on the unexposed side of the door

In structural part, the structural properties of materials needed for the numerical analysis (modulus of elasticity and Poisson's ratio) are obtained from (Eurocode 3) for steel. While as mentioned before, the filler insulation in the fire door consists of rock-wool as the main material that the material properties provided by the manufacturer of the material.

The resulting deformation distribution on the door by implemented analysis is depicted in Figure 3.27.

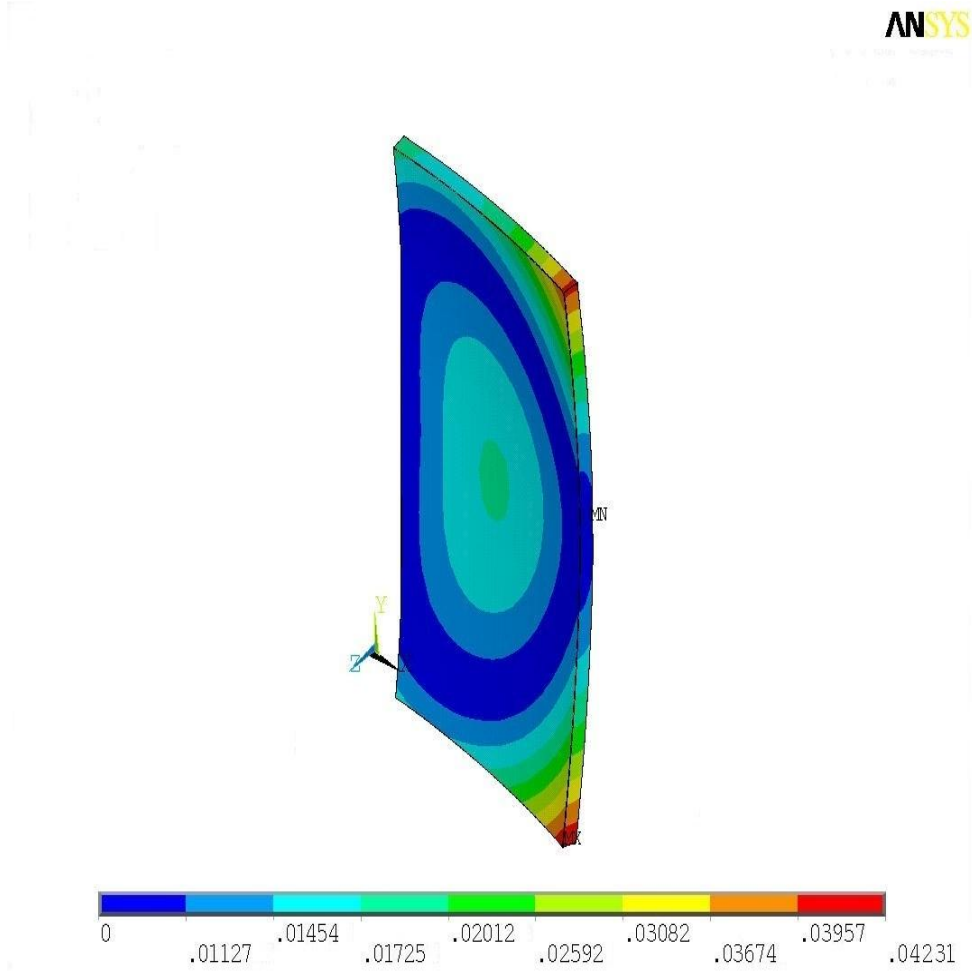

Figure 3.27 Numerical deformation distribution on the of the door

3.5 Conclusion

In this chapter the numerical simulation with FEM of the thermo-mechanical behavior of a fire door undergoing a fire test was performed. A measuring system was set up, in order to verify the numerical simulation. It consists of a temperature controlled furnace, a set of thermocouples and an infrared thermo camera. The experimental apparatus enables one to perform a fire test according to the standard codified procedure. The

obtained results show that the numerical model can predict the thermo-mechanical behavior of the door with good accuracy.

CONCLUSION

This thesis focused on application of finite element method to the design of innovative devices.

After a brief discussion of fundamentals of finite element method in the first chapter, the dynamic formulation for flexible-link mechanisms based on an ERLS approach, where the basic idea is to decompose the overall motion of the mechanism into the rigid motion of a suitably defined ERLS and an overlapped elastic motion, has been evaluated in the second chapter. After the kinematic formulation, the equations of motion for the flexible mechanism have been obtained by direct application of the virtual work principle.

A generic Matlab^{TM} software simulator that allows to simulate rigid-flexible link systems, based on ERLS approach, has been implemented and is presented in this thesis. Thanks to the ERLS based formulation, since it exploits the DH notation and the main concepts of the robotics kinematics, the approach to the flexible-link robots remains the same of the rigid ones allowing an easy approach. Then, in order to show the effectiveness of the method and of the simulator, different behaviors of specific robots with respect to different working conditions and mechanical parameters have been investigated.

The results have been compared with respect to Adams^{TM} showing a very good agreement (the small difference is because of defining ERLS) and, hence, the effectiveness of the method and the simulator.

In the third chapter the numerical simulation with FEM of the thermo-mechanical behavior of a fire door undergoing a fire test was performed. From the methodological point of view similar results could be achieved adopting solid elements. A strong reduction in computational time can be obtained referring to a steady state analysis. In this case, the obtained temperatures distribution shows only slight discrepancies with respect to that resulting from a transient analysis.

A measuring system was set up, in order to verify the numerical simulation. It consists of a temperature controlled furnace, a set of thermocouples and an infrared thermo camera. The experimental apparatus enables one to perform a fire test according to the standard codified procedure.

The obtained results show that the numerical model can predict the thermo-mechanical behavior of the door with good accuracy.

BIBLIOGRAPHY

[1] Shabana AA (1997), Flexible multibody dynamics: Review of past and recent developments, Multibody Syst. Dyn. **1**(2), 189–222.

[2] Bremer H (1999), On the dynamics of elastic multibody systems, Appl. Mech. Rev. **52**(9), 275–303.

[3] Huston RL (1981), Multibody dynamics including the effects of flexibility and compliance, Comput. Struct. **14**(5-6), 443–451.

[4] Huston RL (1991), Multibody dynamics: Modelling and analysis methods, Appl. Mech. Rev. **44**(3), 109–117.

[5] Huston RL (1991), Computer methods in flexible multibody dynamics, Int. J. Numer. Methods Eng. **32**, 1657–1668.

[6] Huston RL (1996), Multibody dynamics since 1990, Appl. Mech. Rev. **49**(10), S35–S40.

[7] Schiehlen W (1997), Multibody system dynamics: Roots and perspectives, Multibody Syst. Dyn. **1**, 149–188.

[8] Gaultier PE and Cleghorn WL (1989), Modelling flexible manipulator dynamics: A literature survey, Proc of 1st Natl App Mech and Robotics Conf, Paper No 89AMR-2C-3, Cincinnati OH.

[9] Erdman AG, Sandor GN, and Oakberg RG (1972), A general method for kineto elastodynamic analysis of mechanisms, ASME J. Eng. Ind. **94**, 1193–1205.

[10] Lowen GG and Jandrasits WG (1972), Survey of investigations into the dynamics behavior of mechanisms links with distributed mass and elasticity, Mech. Mach. Theory **7**, 3–17.

[11] Jandrasits WG and Lowen GG (1979), The elastic-dynamic behavior of a counter weighted rocker link with an overhanging endmass in a four-bar linkage, Part I: Theory; Part II: Application and experiment, ASME J. Mech. Des. **101**(1), 77–98.

[12] Lowen GG and Chassapis C (1986), The elastic behavior of linkages: An update, Mech. Mach. Theory **21**(1), 33–42.

[13] Thompson BS and Sung CK (1986), A survey of finite element techniques for mechanism design, Mech. Mach. Theory **21**, 351–359.

[14] Modi VJ (1974), Attitude dynamics of satellites with flexible appendages: A brief review, J. Spacecr. Rockets **11**, 743–751.

[15] Huston RL (1990), Multibody Dynamics, Butterworth-Heinemann, USA.

[16] Schiehlen W (1986), Technische Dynamik, Stuttgart, Teubner.
[17] Amirouche FML (1992), *Computational Methods in Flexible Multibody Dynamics*, Prentice Hall, Englewood Cliffs, NJ.

[18] Schiehlen W (ed) (1993), Advanced Multibody Systems Dynamics: Simulation and Software Tools, Kluwer Academic Publishing, Dordrecht.

[19] Pereira MF and Ambrosio JAC (1995), Computational Dynamics in Multibody Systems, Kluwer Academic Publishers.

[20] Xie M (1994), Flexible Multibody System Dynamics: Theory and Applications, Taylor and Francis, Washington.

[21] Shabana AA (1998), *Dynamics of Multibody Systems, 2nd Edition*, Cambridge Univ Press.

[22] Schwertassek R and Wallrapp O (1999), Dynamik Flexibler Mehrkvrpersysteme, Braunschweig, Vieweg.

[23] Geradin M and Cardona A (2001), Flexible Multibody Dynamics: A Finite Element Approach, John Wiley & Sons.

[24] Shabana AA and Pascal M (2001), Symposium on multibody dynamics and vibration, ASME 18th Biennial Conf on Mech Vib and Noise.

[25] Schiehlen W (ed) (1990), Multibody Systems Handbook, Springer-Verlag, New York.

[26] Likins PW (1967), Modal method for the analysis of free rotations of spacecraft, *AIAA J.* **5**(7), 1304–1308.

[27] Likins PW, Barbera FJ, and Baddeley V (1973), Mathematical modelling of spinning elastic bodies for modal analysis, *AIAA J.* **11**, 1251–1258.

[28] Imam I, Sandor GN, and Kramer SN (1973), Deflection and stress analysis in high speed planar mechanisms with elastic links, *ASME J. Eng. Ind.* **95**(2), 541–548.

[29] Craig RR (2000), Coupling of substructure for dynamic analysis: An overview, *41st AIAA/ASMA/ASCE/AHS/ASC Struct, Struct Dyn and Materials Conf*, AIAA-2000–1573.

[30] Craig RR and Bampton MC (1968), Coupling of sub-structures for dynamic analysis, *AIAA J.* **6**, 1313–1319.

[31] Argyris JH, Kelsey S, and Kaneel H [1964], Matrix Methods for Structural Analysis: A Precis of Recent Developments, MacMillan, New York.

[32] Belytschko T and Hsieh BJ (1973), Non-linear transient finite element analysis with convected co-ordinates, *Int. J. Numer. Methods Eng.* **7**, 255–271.

[33] Liou FW and Erdman AG (1989), Analysis of a high-speed flexible four-bar linkage, Part I: Formulation and solution, Part II: Analytical and experimental results on the Apollo, *ASME J. Vib., Acoust., Stress, Reliab. Des.* **111**, 35–47.

[34] Ambrosio JAC and Nikravesh PE (1992), Elastic-plastic deformation in multibody dynamics, Nonlinear Dyn. **3**, 85–104.

[35] Ambrosio JAC and Ravn P (1997), Elastodynamics of multibody systems using generalized inertial coordinates and structural damping, Mech. Struct. Mach. **25**(2), 201–219.

[36] Hsiao KM and Jang J (1991), Dynamic analysis of planar flexible mechanisms by corotational formulation, *Comput. Methods Appl. Mech. Eng.* **87**, 1–14.

[37] Iura M and Iwakuma T (1992), Dynamic analysis of the planar Timoshenko beam with finite displacement, *Comput. Struct.* **45**(1), 173–179.

[38] Elkaranshawy HA and Dokainish MA (1995), Corotational finite element analysis of planar flexible multibody systems, *Comput. Struct.* **54**(5), 881–890.

[39] Khulief YA (1992), On the finite element dynamic analysis of flexible mechanisms, *Comput. Methods Appl. Mech. Eng.* **97**, 23–32.

[40] Belytschko T, Schwer L, and Klein MJ (1977), Large displacement, transient analysis of space frames, *Int. J. for Numer. Methods in English*, **11**, 65–84.

[41] Simo JC and Vu-Quoc L (1988), On the dynamics in space of rods undergoing large motions: A geometrically exact approach, *Comput. Methods Appl. Mech. Eng.* **66**, 125–161.

[42] Cardona A and Geradin M (1988), A beam finite element non-linear theory with finite rotations, *Int. J. Numer. Methods Eng.* **26**, 2403–2438.

[43] Downer JD, Park KC, and Chiou JC (1992), Dynamics of flexible beams for multibody systems: A computational procedure, *Comput. Methods Appl. Mech. Eng.* **96**, 373–408.

[44] Ibrahimbegovic A and Al Mikdad M (1996), On dynamics of finite rotations of 3D beams, *Comput Methods in Appl Sci 96, Third ECCOMAS Comput Fluid Dyn Conf and the 2nd ECCOMAS Conf on Numer Methods in Eng* 447–453.

[45] Crisfield MA, Galvanetto U, and Jelenic G (1997), Dynamics of 3-D co-rotational beams, *Computational Mech., Berlin* **20**, 507–519.

[46] Avello A, Garcia de Jalon J, and Bayo E (1991), Dynamics of flexible multibody systems using Cartesian co-ordinates and large displacement theory, *Int. J. Numer. Methods Eng.* **32**(8), 1543–1563.

[47] Brenan KE, Campbell SL, and Petzold LR (1989), Numerical Solution of Initial-Value Problems in Differential-Algebraic Equations, North-Holland, New York.

[48] Haug EJ and Deyo R (1990), Real-Time Integration Methods for Mechanical System Simulation, Springer-Verlag, Berlin.

[49] Hairer E and Wanner G (1994), Solving Ordinary Differential Equations II. Stiff and Differential-Algebraic Problems, Springer, Berlin.

[50] Ryu J, Kim SS, and Kim SS (1994), A general approach to stress stiffening effects on flexible multibody systems, *Mech. Struct. Mach.* **22**(2), 157–180.

[51] Ryu J, Kim SS, and Kim SS (1997), A criterion on inclusion of stress stiffening effects in flexible multibody dynamic system simulation, *Comput. Struct.* **62**(6), 1035–1048.

[52] Housner J (1984), Convected transient analysis for large space structure maneuver and deployment, *Proc of 25th Struct, Struct Dyn and Materials Conf*, AIAA Paper No 84-1023, 616–629.

[53] Housner JM, Wu SC, and Chang CW (1988), A finite element method for time varying geometry in multibody structures, *Proc of 29th Struct, Struct Dyn and Materials Conf*, AIAA Paper No 88–2234.

[54] Iura M and Atluri SN (1988), Dynamic analysis of finitely stretched and rotated three-dimensional space-curved beams, *Comput. Struct.* **29**, 875–889.

[55] Simo JC and Vu-Quoc L (1986), A three dimensional finite strain rod model, Part II: Computational aspects, *Comput. Methods Appl. Mech. Eng.* **58**, 79–116.

[56] Simo JC and Vu-Quoc L (1986), On the dynamics of flexible beams under large overall motions—The plane case: Part I, Part II, *ASME J. Appl. Mech.* **53**, 849–863.

[57] Belytschko T, Lin JI, and Tsay C-S (1984), Explicit algorithms for the nonlinear dynamics of shells, *Comput. Methods Appl. Mech. Eng.* **42**, 225–251.

[58] Belytschko T and Glaum LW (1979), Applications of higher order corotational stretch theories to nonlinear finite element analysis, *Comput. Struct.* **10**, 175–182.

[59] Belytschko T, Stolarski H, Liu WK, Carptender N, and Ong JS (1985), Stress projection for membrane and shear locking in shell finite elements, *Comput. Methods Appl. Mech. Eng.* **51**, 221–258.

[60] Oden TD (1972), *Finite Elements of Nonlinear Continua*, McGraw- Hill, New York.

[61] Bathe KJ, Ramm E, and Wilson EL (1975), Finite element formulations for large deformation dynamic analysis, *Int. J. Numer. Methods Eng.* **9**, 353–386.

[62] W. Book (1974), Modeling, design and control of flexible manipulator arms, Massachusetts Institute of Technology.

[63] S. Dwivedy and P. Eberhard (2006), Dynamic analysis of flexible manipulators, a literature review, Mechanism and Machine Theory, **41** (7) 749–777.

[64] R. Theodore and A. Ghosal (1995), Comparison of the assumed modes and finite element models for flexible multilink manipulators, The International journal of robotics research, **14** (2) 91.

[65] R. Cannon and E. Schmitz (1984), Initial experiments on the end-point control of a flexible one-link robot, The International Journal of Robotics Research, **3** (3), 62.

[66] E. Bayo (1989), Timoshenko versus bernoulli-euler beam theories for the inverse dynamics of flexible robots, International Journal of Robotics & Automation, **4** (1), 53–56.

[67] P. Wang and J. Wei (1987), Vibrations in a moving flexible robot arm, Journal of sound and vibration, **116** (1), 149–160.

[68] V. Feliu, K. Rattan, and H. Brown Jr (1992), Modeling and control of single-link flexible arms with lumped masses, Journal of dynamic systems, measurement, and control, 114, 59.

[69] B. Nagaraj, B. Nataraju, and D. Chandrasekhar (2001), Nondimensional parameters for the dynamics of a single flexible link, in International Conference on Theoretical, Applied, Computational and Experimental Mechanics (ICTACEM).

[70] S. Tso, T. Yang, W. Xu, and Z. Sun (2003), Vibration control for a flexible-link robot arm with deflection feedback, International journal of non-linear mechanics, **38** (1), 51–62.

[71] F. Rakhsha and A. Goldenberg (1985), Dynamics modelling of a single-link flexible robot, in Robotics and Automation. Proceedings IEEE International Conference on, 2, 984–989.

[72] E. Barbieri and U. Ozguner (1988), Unconstrained and constrained mode expansions for a flexible slewing link, in American Control Conference, 83–88, IEEE.

[73] B. Tabarrok (1974), C. Leech, and Y. Kim, On the dynamics of an axially moving beam, Journal of the Franklin Institute, **297** (3), 201–220.

[74] K. Buffinton (1992), Dynamics of elastic manipulators with prismatic joints, Journal of dynamic systems, measurement and control, 114, 41.

[75] S. Tadikonda and H. Baruh (1992), Dynamics and control of a translating flexible beam with a prismatic joint, Journal of dynamic systems, measurement and control, 114, 422.

[76] S. Nagarajan and D. Turcic (1990), Lagrangian Formulation of the Equations of Motion for Elastic Mechanisms With Mutual Dependence Between Rigid Body and Elastic Motions: Part II - System Equations, Journal of dynamic systems, measurement and control, 112, 215.

[77] S. Nagarajan and D. Turcic (1990), Lagrangian formulation of the equations of motion for elastic mechanisms with mutual dependence between rigid body and elastic motions: Part I - element level equations, ASME J. Dynamic Systems, Measurement and Control.

[78] J. Bricout, J. Debus, and P. Micheau (1990), A finite element model for the dynamics of flexible manipulators, Mechanism and Machine Theory, **25** (1), 119–128.

[79] L. Chang and K. Gannon (1990), A dynamic model on a single-link flexible manipulator, Journal of Vibration and Acoustics, 112, 138.

[80] M. Giovagnoni (1993), Linear decoupled models for a slewing beam undergoing large rotations, Journal of sound and vibration, **164** (3), 485–501.

[81] M. Giovagnoni (1994), A numerical and experimental analysis of a chain of flexible bodies, Journal of Dynamic Systems, Measurement and Control, 116, 73–80.

[82] M. Tokhi, A. Azad, H. Poerwanto, S. Kourtis, and M. Baxter (1996), A Simulink environment for simulation and control of flexible manipulator systems, in Control'96, UKACC International Conference on (Conf. Publ. No. 427), 1, 210–215, IET.

[83] M. Tokhi, Z. Mohamed, S. Amin, and R. Mamat (2000), Dynamic characterisation of a flexible manipulator system: theory and experiments, in TENCON 2000. Proceedings, 3, 167–172, IEEE.

[84] J. Martins, M. Ayala Botto, and J. S´a da Costa (2002), Modeling of flexible beams for robotic manipulators, Multibody System Dynamics, **7** (1), 79–100.

[85] J. Martins, Z. Mohamed, M. Tokhi, J. S´a da Costa, and M. Botto (2003), Approaches for dynamic modelling of flexible manipulator systems, in Control Theory and Applications, IEE Proceedings, 150, 401–411, IET.

[86] J. Lee and B. Wang (1988), Optimal control of a flexible robot arm, Computers & structures, **29** (3), 459–467.

[87] Q. Liu (1993), Dynamic analysis of a spatial robot manipulator with a flexible prismatic link.

[88] G. Zhu, S. Ge, and T. Lee (1999), Simulation studies of tip tracking control of a single-link flexible robot based on a lumped model, Robotica, **17** (1), 71–78.

[89] W. Khalil and M. Gautier (2000), Modeling of mechanical systems with lumped elasticity, in Robotics and Automation, Proceedings. ICRA'00. IEEE International Conference, 4, 3964–3969.

[90] S. Megahed and K. Hamza (2004), Modeling and simulation of planar flexible link manipulators with rigid tip connections to revolute joints, Robotica, **22** (3), 285–300.

[91] R. Milford and S. Asokanthan (1999), Configuration dependent eigenfrequencies for a two-link flexible manipulator: Experimental verification, Journal of sound and vibration, **222** (2), 191–207.

[92] A. De Luca and B. Siciliano (1990), Explicit dynamic modeling of a planar twolink flexible manipulator, in Decision and Control, Proceedings of the 29th IEEE Conference, 528–530.

[93] W. Sunada and S. Dubowsky (1982), On the dynamic analysis and behavior of industrial robotic manipulators with elastic members, in American Society of Mechanical Engineers, Design and Production Engineering Technical Conference, Washington DC.

[94] A. Morris and A. Madani (1996), Static and dynamic modelling of a two-flexiblelink robot manipulator, Robotica, **14** (3), 289–300.

[95] A. Morris and A. Madani 1997, Computed torque control applied to a simulated two-flexible-link robot, Transactions of the Institute of Measurement and Control, **19** (1), 50.

[96] A. Morris and A. Madani (1998), Quadratic optimal control of a two flexible link robot manipulator, Robotica, **16** (1), 97–108.

[97] H. Lee (2005), New dynamic modeling of flexible-link robots, Journal of dynamic systems, measurement and control, 127, 307.

[98] V. Gamarra-Rosado and E. Yuhara (1999), Dynamic modelling and simulation of a flexible robotic manipulator, Robotica, **17** (5), 523–528.

[99] V. Gamarra-Rosado (2000), A planar flexible robotic manipulator, Kybernetes, **29** (5), 787–797.

[100] W. Book (1984), Recursive lagrangian dynamics of flexible manipulator arms, The International Journal of Robotics Research, **3** (3), 87.

[101] B. Siciliano and W. Book (1988), A singular perturbation approach to control of lightweight flexible manipulators, The International Journal of Robotics Research, **7** (4), 79.

[102] P. Chedmail, Y. Aoustin, and C. Chevallereau (1991), Modelling and control of flexible robots, International journal for numerical methods in engineering, **32** (8), 1595–1619.

[103] M. Arteaga (1998), On the properties of a dynamic model of flexible robot manipulators, Journal of dynamic systems, measurement and control, 120, 8.

[104] H. Asada, Z. Ma, and H. Tokumaru (1990), Inverse dynamics of flexible robot arms: modeling and computation for trajectory control, Journal of dynamic systems, Measurement and Control, 112, 177.

[105] R. Vidoni, A. Gasparetto, M. Giovagnoni, and P. Boscariol (2011), A novel 3D equivalent rigid link system approach for flexible-link mechanisms: formulation and comparison with the floating frame of reference approach, in Multibody dynamics, ECCOMAS thematic conference, Brussels, Belgium.

[106] W. Beres and J. Sasiadek (1995), Finite element dynamic model of multilink flexible manipulators, Applied Mathematics and Computer Science, **5** (2), 231–262.

[107] W. Beres, J. Sasiadek, and G. Vukovich (1993), Control and dynamic analysis of multilink flexible manipulator, in Robotics and Automation, Proceedings, IEEE International Conference, 478–483.

[108] A. Gasparetto (2004), On the modeling of flexible-link planar mechanisms: Experimental validation of an accurate dynamic model, Journal of dynamic systems, measurement and control, 126, 365.

[109] J. Denavit and R.S. Hartenberg (1955), A kinematic notation for lower-pair mechanisms based on matrices, ASME Journal of Applied Mechanics, 23, 215-221.

[110] A.A. Shabana (2005), Dynamics of Multibody systems, 3rd ed, Cambridge University press.

[111] MSC, 2010, http://www.mscsoftware.com

[112] Iwankiw, N (2007), Fire Resistance Design, Practice Periodical on Structural Design and Construction, **12** (1), 3-8.

[113] International Maritime Organisation (2012), FTP code International Code for Application of Fire Test Procedures.

[114] Thomson, G, and Preston, RR (1996), Towards Harmonized Standard Fire Resistance Testing, Fire Safety Journal, 27, 91-112.

[115] Sultan, MA (2006), Fire Resistance Furnace Temperature Measurements: Plate Thermometers vs. Shielded Thermocouples, Fire Technology, 42, 253-267.

[116] Chow, WK, and Chan, YY (1996), Computer Simulation of the Thermal Fire Resistance of Building Materials and Structural Elements, Construction and Building Materials, **10** (2), 131-140.

[117] Wang L and G. Quintiere J (2009), An Analysis of Compartment Fire Doorway Flows, Fire Safety Journal, 44, 718-731.

[118] Hugi, E, Ghazi Wakili, K and Wullschleger, L (2009), Measured and Calculated Temperature Evaluation on the Room Side of the Butted Steel

Door Frame Subjected to the Standard Fire of ISO 834, Fire Safety Journal, 44, 808-812.

[119] Tabaddor, M, D. Gandhi P, and Jones G (2009), Thermo-Mechanical Analysis of Fire Doors Subjected to a Fire Endurance Test, Journal of Fire Protection Engineering, 19, 51-71.

[120] Bisby, LA, Kodur, VKR, and Green, MF (2004), Numerical Parametric Studies on the Fire Endurance of Fibre-Reinforced-Polymer-Confined Columns, Canadian Journal of Civil Engineering, **31** (6), 1090-1100.

[121] Gardner, L (2007), Stainless Steel Structures in Fire, Proceedings of the Institution of Civil Engineers: Structures and Buildings, **160** (3), 129-138.

[122] Kodur, VK and Dwaikat, M (2007), Performance-Based Fire Safety Design of Reinforced Concrete Beams, Journal of Fire Protection Engineering, **17** (4), 293-320.

[123] Franssen, JM, Pineta, D and Dotreppe, JC (2007), Considering the Effects of Localized Fires in the Numerical Analysis of a Building Structure, Fire Safety Journal, **42** (6), 473-481.

[124] Beyler, C, Beitel, J, Iwankiw, N and Lattimer, B (2007), Fire Resistance Testing for Performance-Based Fire Design of Buildings, Final Report, Quincy, MA, USA, The Fire Protection Research Foundation.

[125] Purkiss, JA (2007), Fire safety engineering, Elsevier, 2nd edition.

[126] Harmathy, TZ (1981), The Fire Resistance Test and its Relation to Real-world Fires, Fire and Materials, 5, 112-122.

[127] Joyeux, D (2002), Experimental investigation of fire door behaviour during a natural fire, Fire Safety Journal, 37, 605-614.

[128] Moaveni, Saeed (1999), Finite Element Analysis, PRENTICE HALL.